The Flow and Variability of Sea-ice in the Canadian Arctic Archipelago: modelling the past (1950-2004) and the future (2041-2060)

by

Theressa Vanessa Sou

B.Sc. (Honours), University of Victoria, 1992

A Thesis Submitted in Partial Fulfillment of the
Requirements for the Degree of

Master of Science

in the School of Earth and Ocean Sciences

The Flow and Variability of Sea-ice in the Canadian Arctic Archipelago: modelling the past (1950-2004) and the future (2041-2060)

by

Theressa Vanessa Sou
BSc, University of Victoria, 1992

Supervisory Committee

Dr. Gregory M. Flato, Co-supervisor (Canadian Centre for Climate Modelling and Analysis)

Dr. Andrew J. Weaver, Co-supervisor (School of Earth and Ocean Sciences)

Dr. Katrin J. Meissner, Member (School of Earth and Ocean Sciences)

Supervisory Committee

Dr. Gregory M. Flato, Co-supervisor (Canadian Centre for Climate Modelling and Analysis)

Dr. Andrew J. Weaver, Co-supervisor (School of Earth and Ocean Sciences)

Dr. Katrin J. Meissner, Member (School of Earth and Ocean Sciences)

Abstract

Considering the recent losses observed in Arctic sea-ice and the anticipated future warming due to anthropogenic greenhouse gas emissions, sea-ice retreat in the Canadian Arctic Archipelago (CAA) is expected. As most global climate models do not resolve the CAA region, a fine-resolution regional model is developed to provide a sense of possible changes in the CAA sea-ice. This ice-ocean coupled model is forced with atmospheric data for two time-periods. Results from a historical run (1950-2004) are used to validate the model. The model does well in representing observed sea-ice spatial and seasonal variability, but tends to underestimate summertime ice cover. In the future run (2041-2060), wintertime ice concentrations change little, but the summertime ice concentrations decrease by 45%. The ice thickness also decreases, by 17% in the winter, and by 36% in summer. Based on this study, a completely ice-free CAA is unlikely by the year 2050, but the region could support some commercial shipping.

Table of Contents

List of Tables

List of Figures

Acknowledgements

My thanks to all who helped me complete this M.Sc. program, and my special gratitude to:

G. Flato, for your guidance and constructive feedback,

A. Tivy, for your idea to do graduate work,

N. Steiner and J. Dumas, for encouraging me throughout the process, and

D. Sou, for all of your support, love and kindness.

This research was supported by Arctic Net and the Polar Climate Stability Network.

Chapter 1

Introduction

1.1 Global warming and polar amplification

The earth is warming faster than ever before in human history. Global land air temperatures have increased 0.70°C over the last century (*Jones and Moberg* 2003), with the warmest years occurring most recently (Fig. 1.1). The report of the International Panel for Climate Change (IPCC) states that the warming since the 1950's is 'very likely' caused by an anthropogenically forced increase in greenhouse gases (*IPCC* 2007). Climate models are only able to reproduce this amount of warming when forced with increased greenhouse gas concentrations. Natural forcing of climate change, such as solar radiation and volcanic activity, do not explain the observed warming (*IPCC* 2001, 2007). On the other hand, human activities such as the burning of fossil fuels, deforestation and agriculture, have supplied the atmosphere with additional sources of carbon dioxide, methane and nitrous oxide. These greenhouse gases act to retain heat near the earth's surface. The climate response to such unprecedented forcing is of significant concern to the human population. In addition to global warming, there is evidence of more frequent and more extreme weather events, such as droughts and floods. The melting of sea-ice and glaciers is also expected, and has been observed.

The melt of sea-ice is a concern for several reasons. Firstly, the loss of sea-ice will

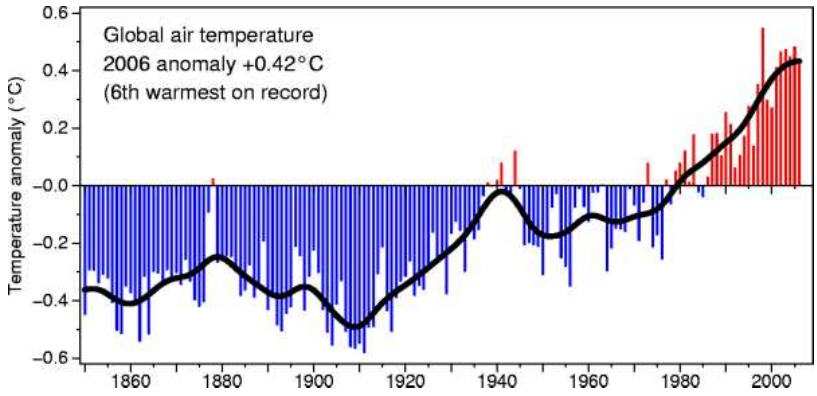

Figure 1.1: Global (land and marine surface) temperature record (*Brohan et al.* 2006)

negatively impact cultures and habitats dependent on ice cover. Secondly, the retreat of sea-ice will result in enhanced warming, due to the removal of the its insulating effect and an associated increased oceanic heat loss to the atmosphere, and due to a positive ice-albedo feedback (*Holland et al.* 2001): with less ice cover, the earth's surface is darker and absorbs more solar radiation, which warms the surface and melts more ice. As most of the world's ice is located at the poles, this positive feedback contributes to the polar amplification of global warming. Polar amplification is evident in climate models and observations (*Flato and Boer* 2001, *Moritz et al.* 2002, *Holland and Bitz* 2003, *Johannessen et al.* 2004). For example, observed Arctic land air temperatures from $60 - 90°$N have increased by 0.80°C over the last 100 years (*Jones and Moberg* 2003), at a faster rate than global air temperatures. However, a clear attribution of air temperatures changes to anthropogenic forcing in the Arctic remains elusive because datasets are limited and there is high inter-annual variability (*Polyakov et al.* 2003b). Nevertheless, the sea-ice cover of the Arctic Ocean is currently undergoing loss rates not previously seen during the observed record.

1.2 Arctic sea-ice retreat

The warming in the Arctic has occurred faster in the spring, summer and fall (*Comiso* 2003), and has resulted in longer open water seasons, a warmer ocean and thinner

ice. Sea-ice extent[1], concentration[2], and thickness have decreased over the last 30 years. The summer minimum ice extents (Fig. 1.2), as measured by satellite from 1979-2005, have decreased by 7.4% per decade, with record low minimum extents occurring recently. On the other hand, the wintertime ice extents are changing more slowly. The trend of the annual mean is -2.7% per decade (*IPCC* 2007, *Stroeve et al.* 2005). Ice has also thinned (*Rothrock et al.* 1999, *Wadhams and Davis* 2000) and there is less perennial[3] ice (*Comiso* 2002). However, measuring trends in ice thickness is difficult; data is limited, and ice is mobile. Consequently, the reasons for ice loss remain unclear (*Stroeve et al.* 2005). For example, changes in wind patterns may be as important as increases in air temperature (*Melling* 2001, *Holloway and Sou* 2002, *Polyakov et al.* 2003b, *Belchansky et al.* 2004).

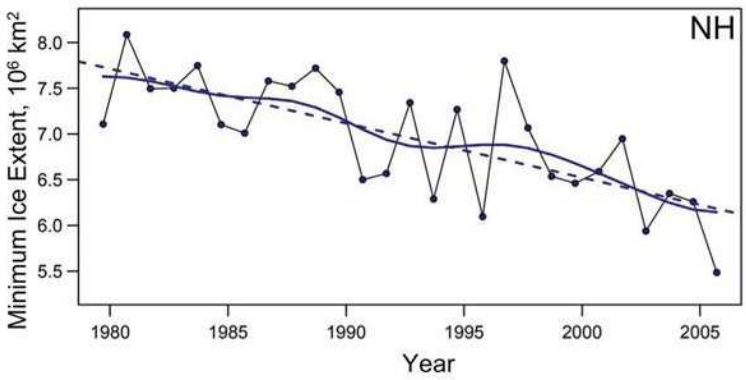

Figure 1.2: Summer minimum arctic sea-ice extent from 1979-2005 (*IPCC* 2007). The blue curve shows decadal variations, and the dashed line indicates the linear trend of 7.4% per decade.

During the 1990's, wind patterns played an important role in affecting ice loss. A shift in atmospheric circulation modified the wind and air temperature patterns and resulted in less ice in the Arctic. The atmospheric variability over the Arctic Ocean is

[1]Ice extent is the total area (in km^2) delineated by the ice edge, as defined by ice with concentrations greater than 15%.

[2]Ice concentration is defined as the fraction of the ocean surface covered by ice (%). Ice area is the area (in km^2) covered by ice.

[3]Perennial ice survives the summer. Seasonal ice does not.

partially captured by the Arctic Oscillation (AO) Index (Fig. 1.3)[4]. It was extremely positive during the 1990's, during which time the low pressure system centred over Iceland was anomalously strong. This resulted in the intensification of the south-westerlies that move across the northern North Atlantic and into the Arctic Ocean, as well as the northerlies over northern Canada. As a consequence, more warm North Atlantic air (and water) entered the Arctic and increased ice melt (*McLaughlin et al.* 2002, *ACIA* 2005). Simultaneously, air temperatures over the northeastern Canadian Arctic became cooler. Mean ice circulation (as shown in Fig. 1.4) shifted so that the Beaufort Gyre became weaker and smaller than before. Less ice was able to recirculate and grow within the gyre, resulting in reduced ice thicknesses and increased export through Fram Strait. Although new ice formed in regions that had lost ice to export, it was usually thinner than the exported ice. Also, under these cyclonic (anti-clockwise) conditions, the ice circulation is more divergent, with more leads and less ice ridging. Less ice ridging results in thinner ice, as compression thickens the ice (*Rigor et al.* 2002).

Even though ice loss under a positive AO can be explained, the minimum ice extents have occurred after 1996 when the AO index was in a neutral state. This more recent loss of Arctic ice may be a combination of warmer air temperatures, a dynamically preconditioned ice cover resulting in a thinner state, and increased oceanic heat flux (*Stroeve et al.* 2005). Several researchers have recently hypothesized that the ice regime has reached a point in which internal ice mechanisms (e.g. ice-albedo or growth-thickness feedbacks[5]) have more influence than the wind or air temperature forcing (*Bitz and Roe* 2004, *Lindsay and Zhang* 2005).

The recent reduction of sea-ice is also attributed to warming from anthropogenic

[4]The AO index is the first empirical orthogonal function of wintertime sea-level pressure poleward of 20°N (*Thompson and Wallace* 1998). Another index, the North Atlantic Oscillation (NAO) (*Hurrell* 1995), has patterns of variability closely connected to the AO; the AO will be used for this discussion.

[5]Ice growth stabilizes ice thickness and results in a negative feedback, which is dependent on ice thickness. Thinner ice returns to an equilibrium thickness faster than thicker ice.

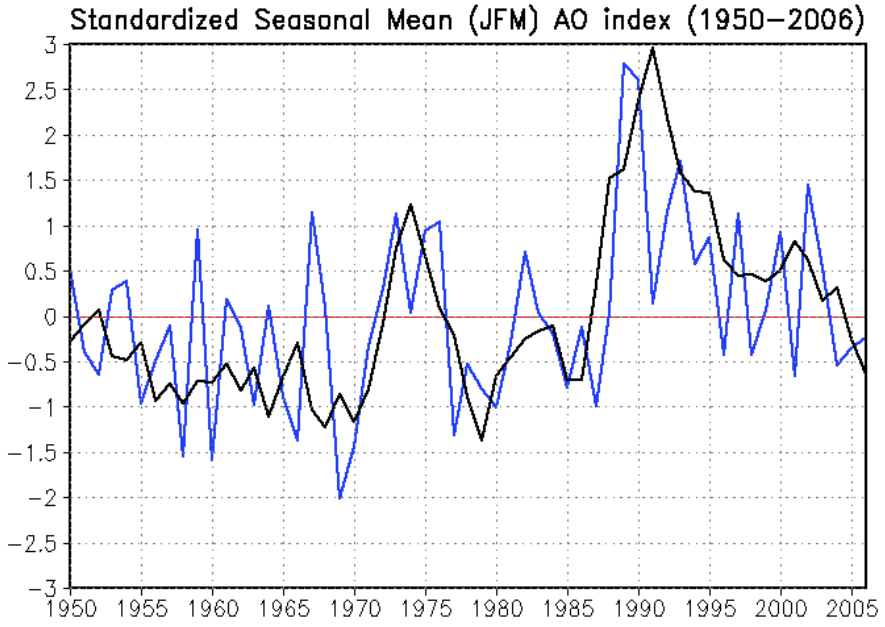

Figure 1.3: The standardized seasonal mean Arctic Oscillation index during cold season (blue line) is constructed by averaging the daily AO index for January, February and March for each year. The black line denotes the standardized five-year running mean of the index. Bith curves are standardized using 1950-2000 base period statistics. Taken from: www.cpc.ncep.noaa.gov

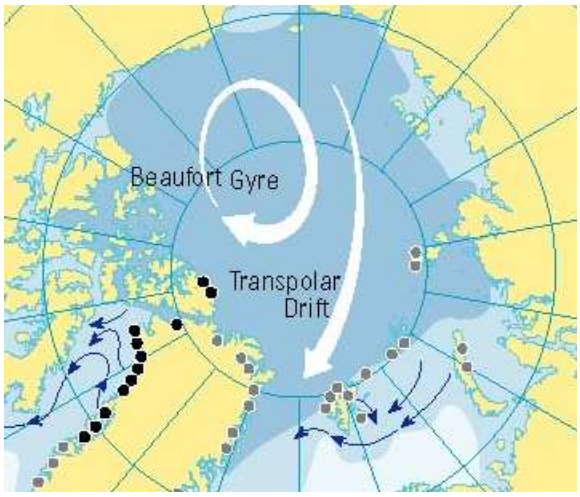

Figure 1.4: Map of mean ice circulation (www.amap.no). White arrows indicate ice movement.

forcing of greenhouse gases. Global climate models show that sea-ice loss is more rapid under greater emissions forcing, and observations and models indicate that natural variability, while a factor in changing sea-ice cover, is dominated by anthropogenic-induced warming (*Zhang and Walsh* 2006). A modelling study by *Rothrock and Zhang* (2005) indicated that the decreasing trend in Arctic ice volume is caused by air temperature changes more than wind induced changes. *Stroeve et al.* (2007) suggested that the acceleration of observed and modelled September ice extent trends over the last half century reflect increasing GHG impacts, and they estimated that more than a third of the observed trend is externally forced (e.g. by GHG loading). *Vinnikov et al.* (2006) agreed that the recent ice retreat reflects a change in climate, but noted that the reasons behind the acceleration of sea-ice retreat require more consideration.

1.3 Sea-ice of the Canadian Arctic Archipelago (CAA)

With the sea-ice in the Arctic Ocean showing evidence of overall retreat, changes of sea-ice cover in the northern Canadian islands have been of intense political and economic interest, for reasons described later. Currently, there is very little evidence of ice retreat in the northern Canadian Islands (referred to as the Canadian Arctic Archipelago (CAA), shown in Fig. 1.5). While sea-ice extent in the eastern Arctic (e.g. Barents and Kara Sea) has decreased, the trends in the CAA (and central Arctic) were statistically insignificant (*Parkinson and Cavalieri* 2002). The regional trends are partially explained by atmospheric variability (*Parkinson* 2000), but additional factors influence the regional response.

Unique characteristics of the CAA contribute to a slower response of sea-ice to climate change. First, the continental influence of the large number of islands and the nearby mainland, as well as the Arctic ice pack and Greenland glacier, results in a larger range of air temperatures, allowing ice to quickly recover during winter.

Second, the continued import of thick Arctic ice into the northern CAA contributes to retaining sea-ice. Third, the CAA sea-ice response to the dynamic forcing, such as associated with the AO index, is severely limited because the region is covered mostly by landfast ice (immobile ice fastened to land) during winter when the AO effect is most dominant. Even in summer, ice movement is restricted by narrow channels and consolidated[6] ice. Finally, multi-year ice, which exists in the central and northern regions, responds more slowly to changes in air temperature compared to thinner, seasonal ice (*Stroeve et al.* 2005). Other regions of landfast ice in the Arctic Ocean, such as the marginal seas from the Chukchi to Kara Sea, also do not show statistically significant change in thickness (*Polyakov et al.* 2003a).

The persistence of CAA ice is also seen in the future scenarios of global climate models, where summertime ice is retained in the north CAA and Central Arctic Ocean (*IPCC* 2001, *Walsh and Timlin* 2003, *Holland et al.* 2006, *IPCC* 2007).

1.4 Project motivation

Although there is little evidence of sea-ice retreat in the CAA, continued warming is anticipated by climate models (*IPCC* 2007). If the region does warm, the loss of sea-ice will be inevitable. Predicting when and how the ice will retreat in the CAA is important to local residents whose culture is integrated to their environment, including the use of sea-ice for transportation, hunting and fishing. Changes in sea-ice cover will affect the northern ecosystems, negatively impacting wildlife, such as polar bears and bowhead whales. Issues related to resource management of oil and natural gas reserves off the Canadian coast, as well as sovereignty and commercial shipping through the CAA, are also of great concern. For example, there is strong international political and economic interest in the 'Northwest Passage'; a route from Asia to Europe via the CAA is half the distance of the route currently used through the Suez or Panama Canals. Presently, access to the region is limited by ice.

[6]Consolidated ice has concentrations of 100% and is immobile.

Understanding key processes and predicting possible changes in ice cover are important for adaptation planning and resource management. Currently, the collection of in-situ data is limited due to severe working conditions. The cold temperatures, summer fog, winter darkness, and the remote location contribute to difficult and expensive field work conditions. As a result, in-situ measurements of ice thickness are sparse in time and do not have uniform coverage. A small number of ice cores, moorings and submarine transects provide ice thickness (or draft) data (*Melling* 2002). Ice thickness measurements also exist at coastal stations. Ice cover is better observed; the Canadian Ice Service has provided ice analysis charts since the late 1950s (*CIS* 2002), and ice extent and ice concentration has been available via satellite since 1978 (*Parkinson et al.* 1999). Estimating CAA ice area fluxes using satellite data, however, has only been possible during the last decade (*Agnew and Vandeweghe* 2005, *Kwok* 2005, 2006).

Modelling work supplements these limited observations of sea-ice in the CAA region, and provides a sense of what ice conditions may be possible in the future. The driving force behind this thesis is to provide regional climate change information. To date, there have been very few modelling studies of the CAA. Global climate models with resolutions of 200-300 km do not resolve channels of the CAA or the local-scale sea-ice processes. Pan-Arctic regional models have higher horizontal resolution, ranging from 9-50 km grid spacing (*ACIA* 2005, *Maslowski and Lipscomb* 2003), but there is very little focus on the CAA region. A regional model of the CAA was constructed by *Kliem and Greenberg* (2003), who modelled summer time conditions and focused on tides. *Dumas et al.* (2006a) simulated historical and future sea-ice at selected coastal stations in the CAA, but with a 1-d model. To my knowledge, there are not any published studies regarding the CAA response to future climate scenarios based on a regional model of the CAA.

1.5 Project description

In the current work, I provide atmospheric historical and future scenario forcing as done by *Dumas et al.* (2006a), but employ a more sophisticated model. I expand the investigation from a 1-d site specific analysis to a spatially complete analysis in a 3-d ocean-ice coupled model. The model domain consists of the northern islands of the Canadian Arctic above 70°N, as shown in Fig. 1.5.

The coupled ice-ocean model is integrated for two time-periods, 1950-2004 and 2041-2060. Details of the model set-up and forcing is provided in Chapter 3, following a description of the observed sea-ice conditions of the CAA (Chapter 2). In Chapter 4, model results from the historical run are used to assess the model's skill by comparing its representation of sea-ice to observations. Changes in sea-ice between the historical and the future simulation provide information about possible future ice conditions (and are shown in Chapter 5).

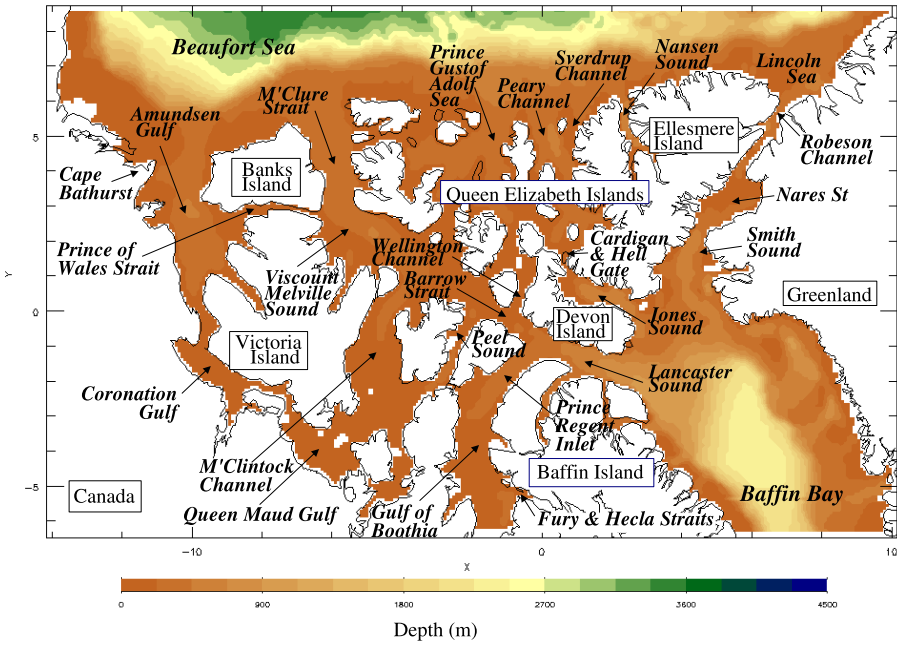

Figure 1.5: Domain and bathymetry of the model, as well as selected names of the CAA.

Chapter 2

Observed sea-ice conditions of the CAA

This chapter provides an overview of the observed sea-ice regime of the CAA. It includes the presentation of the climatological seasonal patterns, inter-annual variability and trends, and related sea-ice processes. The information here will be used as a basis for the model evaluation in Chapter 4.

2.1 Climatology

2.1.1 Seasonal cycle of extent and concentration

During the winter months, from November to May, the entire CAA region is completely ice covered with very little ice movement (*Parkinson et al.* 1999). Within the CAA, ice concentrations remain high all winter, but reach their maximum in early May (*CIS* 2002).

In May, while most of the region remains densely ice covered, polynyas[1] start to form (Fig. 2.1). The North Water Polynya (NOW), a recurring polynya in Smith Sound, opens up in early May (with ice concentrations ranging from 10-60%), as do nearby polynyas in Jones Sound and Lancaster Sound. Also at this time, a polynya in Amundsen Gulf (Bathurst polynya) opens. Smaller polynyas, such as Hell's Gate and Cardigan Strait, also exist (Fig. 2.2).

[1]Polynyas are regions of open water or thinner, less concentrated ice relative to the surrounding ice cover.

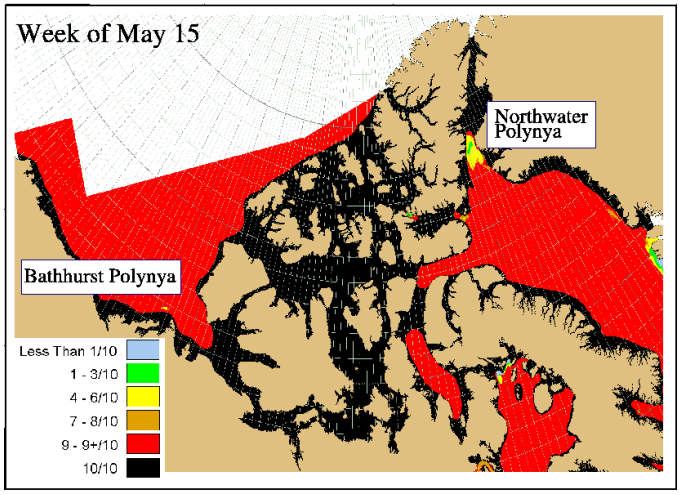

Figure 2.1: Observed median ice concentrations (1971-2000) for the week of May 15 (*CIS* 2002). Black represents landfast ice.

By mid-July, Smith Sound and Lancaster Sound are ice free (i.e. less than 10% ice concentrations). Ice along the Alaskan coast and within Amundsen Gulf retreats, retaining ice concentrations of about 10-60%. Open water is evident in Coronation Gulf. In early August, the western channel from Amundsen Gulf to Queen Maud Gulf is ice free, as is northern Baffin Bay. Wellington Channel, Jones Sound and Prince Regent Inlet are open by mid- August, while Peel Sound opens later in the month.

The minimum ice cover occurs in early September (Fig. 2.3), and the ice extent is about half of the wintertime extent (*Agnew et al.* 2006, *Parkinson and Cavalieri* 2002). Open water extends into the eastern and southern channels, while ice is less concentrated (10-60%) around Ellesmere Island and Devon Island, as well as in Nares Strait (40-60%). Densely concentrated ice remains in the central CAA, including the southern regions of M'Clintock Channel and the Gulf of Boothia. These channels act like cul-de-sacs which trap ice. M'Clintock Channel retains ice concentrations of mostly 90+%, while the ice in the southern Gulf of Boothia usually has lighter ice cover (10-30%). Depending on the year, Peel Sound alternates between ice-free years and years of thick multi-year ice with concentrations up to 50% (H.Melling, Pers. Comm.). Although ice remains densely packed in some regions, it is more mobile in

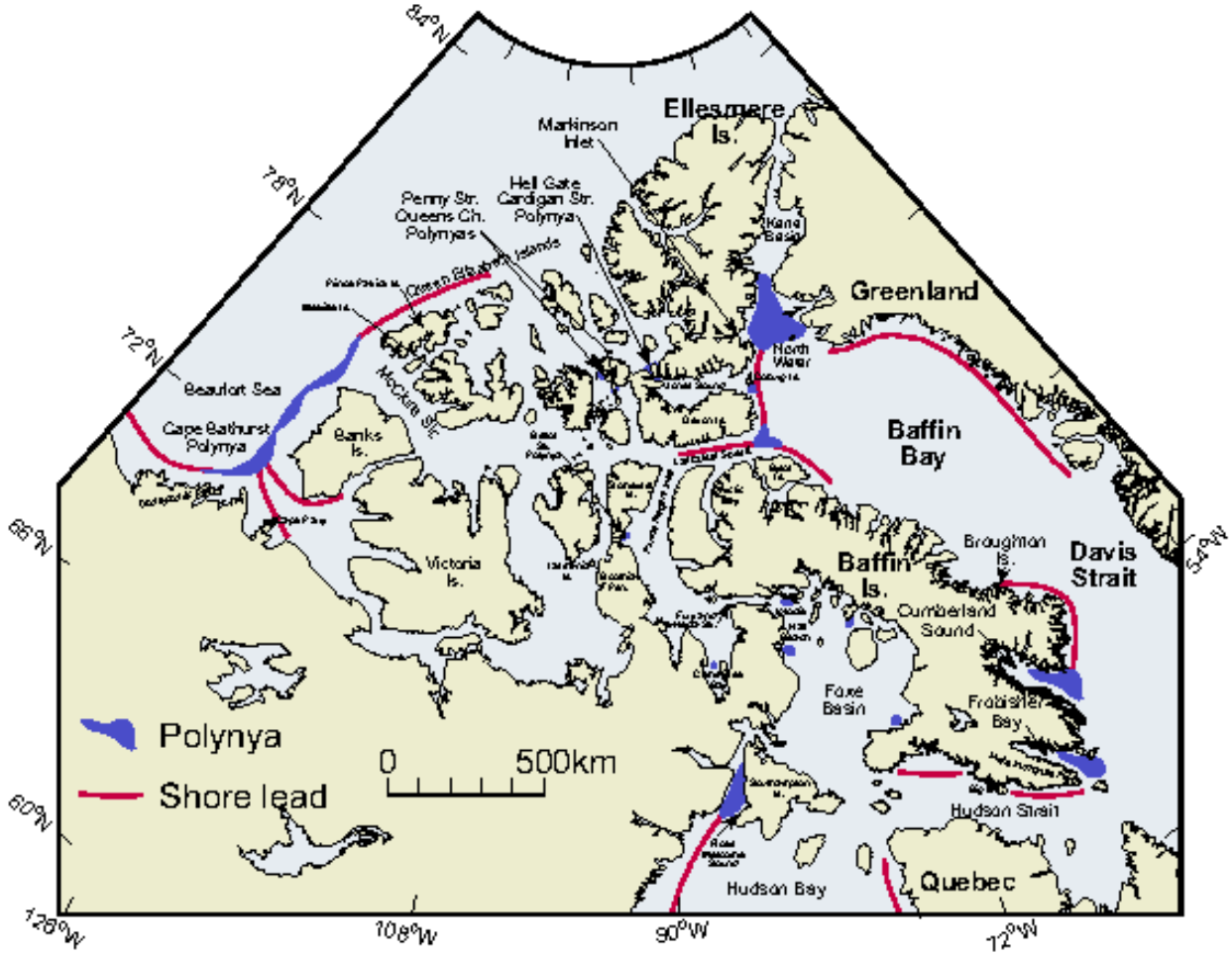

Figure 2.2: A map of polynya and shorelead locations (*Dunphy et al.* 2005), based on *Stirling* (1981)

summer, with the exception of perennial ice plugs[2] that exist along the northern edge of the Queen Elizabeth Islands (QEI) (black regions in Fig. 2.3).

Freeze up begins in mid September. Those regions which open up last tend to freeze first (e.g. central channels), and have the shortest open water durations. Lancaster Sound, Jones Sound and Gulf of Boothia (north part) are ice covered by late September, while Amundsen Gulf, Queen Maud Channel and eastern Smith Sound remain ice free. Wintertime ice plugs and ice arches form in Nares Strait and in the northern channels of the QEI, as well as in Amundsen Gulf, Barrow Strait, Lancaster Sound (*Melling* 2000), and contribute to ice consolidation. By early November, the entire CAA region is covered with 90% ice concentrations, and most of the QEI is landfast (*CIS* 2002).

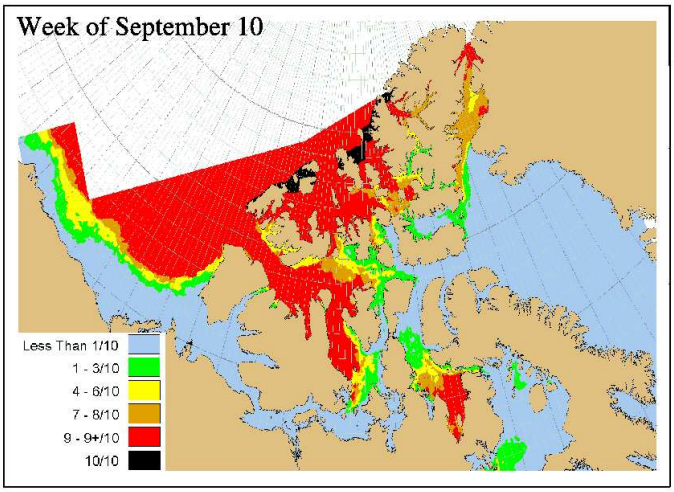

Figure 2.3: Observed median ice concentrations (1971-2000) for the week of September 10 (*CIS* 2002).

2.1.2 Spatial distribution of ice thickness

The ice thickness spatial distribution in the CAA is similar to patterns of extent. Regions with seasonal ice cover have dominantly first year ice, which grows to 1-2 m within a winter season, and is prevalent in the western and southern channels of the

[2]An ice plug is consolidated immobile ice that forms within a narrow channel.

CAA. Perennial, multi-year ice, on the other hand, occurs in the central and northern CAA, with thicknesses greater than 3 m. The average wintertime thickness is 3-4 m in the QEI (*Melling* 2000), 2.5 m in M'Clure Strait (*Bourke and Garrett* 1987, *Agnew et al.* 2006) and 2-6 m in northern Nares Strait (*Kwok* 2006).

2.1.3 Sea-ice motion

Generally, ice moves in a south and eastward direction, but is affected by wintertime consolidated ice, summertime ice plugs, and narrow channels. The length of time for ice transport through the CAA (i.e. from the Arctic to the Baffin Bay) depends on ice mobility. For example, ice can transit Nares Strait within a few months, especially during winters when ice plugs form later than usual. In comparison, ice may take up to a decade to travel through the northwestern channels of the CAA as ice is immobile 6-8 months of the year (*Melling* 2001).

Typical speeds of the mobile ice pack are estimated from a few observations: 8.5-17 km day^{-1} through Nares Strait; 8.5-12 km day^{-1} in the eastern and central channels of the QEI; and 4-8.5 km day^{-1} in M'Clure Strait and north QEI (*Melling* 2000). It is hypothesized that the topography of the eastern QEI intensifies the wind and increases ice velocities (H.Melling, Pers. Comm.), as evidenced in Nares Strait (*Samelson et al.* 2006).

2.1.4 Observed ice fluxes

Ice fluxes through the CAA are largely unknown. A comprehensive net of simultaneous in situ observations within the CAA does not exist due to the number of small channels. Recently, ice movement data has become available using satellite data with adequate resolution. It has provided information about the timing of ice consolidation as well as ice area fluxes. However, measuring the associated ice thickness is not currently possible via satellite. Ice volume fluxes are estimated using a representative ice thickness and observed area fluxes. In addition to ice concentration, thickness and

speed, ice volume fluxes are dependent on the direction and duration of ice movement, and the width of the channel.

The sea-ice area fluxes of the northern channels of the CAA are estimated by *Kwok* (2006) and *Agnew et al.* (2006) using satellite data for 1998-2002 and 2003-2006, respectively. These datasets represent the first baseline estimates of ice area exchange between the CAA and the Arctic Ocean. The fluxes are computed across 'gates' shown in Fig. 2.4.

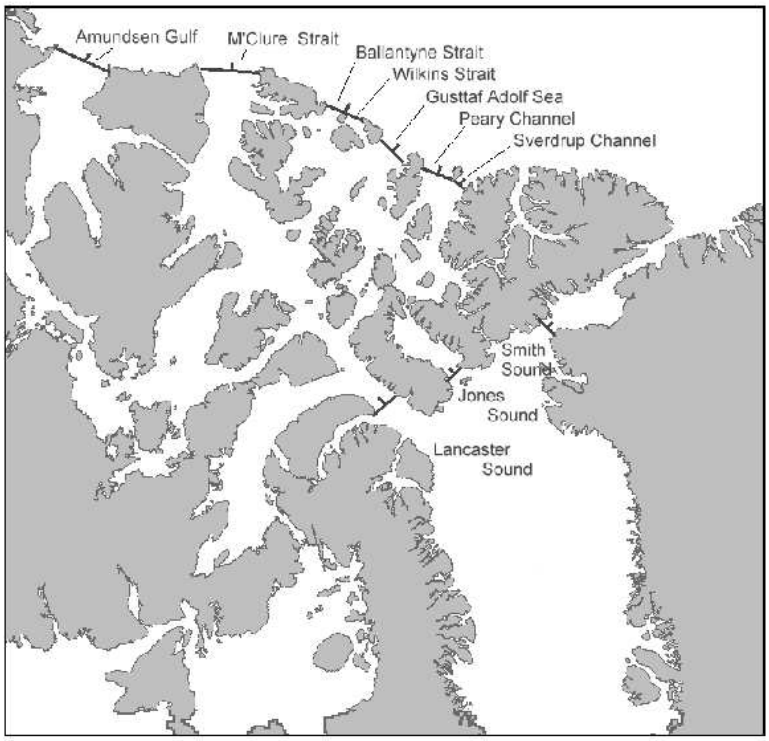

Figure 2.4: Location of gates used to estimated ice fluxes in the CAA by *Agnew et al.* (2006)

Based on the annually averaged fluxes from 1998-2002 (Table 2.1) estimated by *Kwok* (2006), ice consistently moves northward from Amundsen Gulf and M'Clure Strait, and southward into QEI. However, the fluxes vary seasonally; monthly climatologies by *Kwok* (2006) show that all three gates experience import during the summer. Of the three straits, Amundsen Gulf gate has the largest area fluxes, but the estimated ice volume fluxes are more similar as both M'Clure Strait and QEI

Source	*Kwok* (2006)							
	Area flux						Thickness	Volume flux
	(10^3 km^2 yr^{-1})						(m)	(km^3 yr^{-1})
Year	1998	1999	2000	2001	2002	Mean		
Amundsen Gulf	-113	-86	-44	-108	-71	-85	1	-85
M'Clure	-55	-37	14	-22	-9	-20	4	-80
QEI	5	8	29	4	5	8	3.4	27
Net	-163	-115	-1	-126	-75	-97		-138

Table 2.1: Observed (annually averaged) ice fluxes through northern CAA 'gates' from *Kwok* (2006) (1998-2002). Positive values represent import to the CAA and negative values represent export.

Source	*Agnew et al.* (2006)						
	Area flux					Thickness	Volume flux
	(10^3 km^2 yr^{-1})					(m)	(km^3 yr^{-1})
Year	2003	2004	2005	2006	Mean		
Amundsen Gulf	-41	2	-8	-8	-14	1.0	-14
M'Clure	-16	-15	-4	14	-5	2.5	-13
QEI	42	24	30	48	36	3.4	120
Net	-15	11	18	54	17		94

Table 2.2: Observed (wintertime) ice fluxes through northern CAA 'gates' from *Agnew et al.* (2006) (2003-2006), where fluxes represents winter (Sept-June) only. Positive values represent import to the CAA and negative values represent export.

have much thicker ice. It is also observed that the southern QEI channels (i.e. Ballantyne Strait, Wilkins Strait and Prince Gustaf Adolf Sea) have a larger net import and higher inter-annual variability than the remaining QEI channels (Peary Channel and Sverdrup Channel), probably because ice plugs are more common in the more northern straits (*Kwok* 2006, *Agnew et al.* 2006). The light ice conditions of the 1998 summer were very unusual, and resulted in low import through the QEI and high exports from M'Clure Strait and Amundsen Gulf. Consequently, the net (annual) volume flux as estimated by *Kwok* (2006) of -137 km^3 yr^{-1} is biased by this extreme year and the following time of ice recovery.

Kwok's (2006) data from RADARSAT had year-round coverage, but the data used by *Agnew et al.* (2006) was from the Advanced Microwave Scanning Radiometer Sensor (AMSR-E) and was unable to detect ice motion in summer (July and August); his values therefore represent winter (September to June). The direction of ice fluxes are similar to *Kwok* (2006), as ice is exported from Amundsen Gulf and M'Clure Strait and imported into QEI. The lack of summer data significantly impacts the average ice flux, especially at the QEI and M'Clure gates as this is when the ice is the most mobile. Estimates for Amundsen Gulf may be more like annually averaged estimates as the region is usually ice free from July to August. With these factors in mind, and noting that the time period of observations are different, Agnew et al.'s (2006) wintertime estimate for the northern boundary was 94 km^3 yr^{-1} (net import), and was dominated by the QEI-S gates (see Table 2.2). *Agnew et al.* (2006) attributes the difference from Kwok's (2006) results to changes in atmospheric circulation and an easier import of Arctic Ocean ice after 1998.

An additional northern gate exists at Nares Strait (Robeson Channel), and fluxes were provided by *Kwok* (2005) for the years 1996-2002. An ice plug forms in Robeson Channel sometime between November and March, which prevents the import of Arctic ice from the Lincoln Sea and allowing ice south of the arch to consolidate. This plug

usually breaks up by July and August. Ice area export is estimated to be 33 x 10^3 km^2 yr^{-1}. The inter-annual variability is high, and ranges from 16 to 48 x 10^3 km^2 yr^{-1}. Based on 4m thick ice, the ice volume flux is estimated to be 130 km^3 yr^{-1} (*Kwok* 2005).

Observations of sea-ice area fluxes are also available at Barrow Strait and Lancaster Sound (*Agnew and Vandeweghe* 2005) for 2002-2004. Although a very short time-series, the results provide a sense of local ice conditions and associated winter export from October to May (8 months). Barrow and Lancaster Straits are usually ice free in October. An ice plug forms in Barrow Strait by late fall, and affects the winter time export. For example, the winter export flux was 12 x 10^3 km^2 during 2002/3 when ice consolidation occurred in early November but was 20 x 10^3 km^2 the next year when the ice plug formed further west in December. Regions of new ice production can be identified using ice flux observations, as in Lancaster Sound where the wintertime flux through a gate in western Lancaster Sound (27 x 10^3 km^2) is much less than through a gate at Barrow Strait to the east (69 x 10^3 km^2).

The net wintertime ice flux through the southern boundary of the CAA, including Lancaster Sound, Jones Sound and Smith Sound, is estimated to be 110 km^3 yr^{-1}, with the largest exports being from Lancaster Sound (*Agnew et al.* 2006). Previous estimates of (annual) ice export into Baffin Bay range from 655 km^3 yr^{-1} (*Dey* 1981) and 220 km^3 yr^{-1} (*Sadler* 1976), but are based on very limited datasets (e.g. over several weeks).

By considering 2003-2006 data for both the northern and southern boundaries of the CAA, excluding Nares Strait, *Agnew et al.* (2006) estimates the net wintertime flux to be -42 x 10^3 km^2. This implies that the CAA is a region of ice generation. The net fluxes show that the CAA provides ice to both the Arctic Ocean and the Labrador Sea.

Even though recent satellite technology contributes to a better understanding of

CAA ice fluxes, many uncertainties remain, including the choice of representational ice thickness and inability of short time-series to represent a region with high inter-annual variability. However, the data does help in providing a sense of the CAA ice flux contribution to surrounding regions, i.e. the Arctic Ocean and Baffin Bay.

2.1.5 Estimates of freshwater fluxes

The movement of ice in the CAA affects both the local ice-ocean processes, as well as the freshwater budgets of the Arctic Ocean and the Labrador Sea. As part of a Arctic Ocean freshwater budget, *Serreze et al.* (2006) estimated that the ice freshwater flux into the CAA was 160 km^3 yr^{-1}, based on observations from Lancaster Sound (*Prinsenberg and Hamilton* 2005). This value is similar to the crude estimate[3] of 155 km^3 yr^{-1} made by *Aagaard and Carmack* (1989). The more recent observations by *Kwok* (2006) and *Agnew et al.* (2006) are in rough agreement, as *Kwok* (2006) estimated the ice volume flux to be 138 km^3 yr^{-1}. The freshwater budget of *Serreze et al.* (2006) shows that the freshwater ice flux through the CAA region is very small compared to the oceanic freshwater flux through the CAA (3200 km^3 yr^{-1}), and to the freshwater exiting through Fram Strait, both in solid (ice) form (2300 km^3 yr^{-1}) and liquid form (2400 km^3 yr^{-1}).

The influence of the CAA freshwater export on the buoyancy fluxes of Baffin Bay and Labrador Sea remains unclear; modelling studies are contradictory. For example, in a high resolution model, *Williams* (2004) found that the oceanic freshwater from the CAA is a major contributor to the freshening of the Labrador Sea. In contrast, a modelling study done by *Myers* (2005) found that the CAA water exited along the Newfoundland coast and was not entrained into the Labrador Sea Gyre at all. In another study, *Komuro and Hasumi* (2005) agreed with *Myers* (2005), but argued that the Arctic Ocean's loss of freshwater to the CAA increased the salinity of the

[3]The CAA ice flux estimate is based on a thickness of 2 m with a velocity of 5 cm s^{-1} transecting a total crossectional area of 34 km^2 for 3 months.

Fram Strait export water, indirectly affecting the Labrador Sea convection.

The contribution of ice exports to Baffin Bay is considered to be small. However, *Williams* (2004) noted that ice exports do play a role in seasonal variability. Summer ice melt increased the freshwater flux while the timing of fall ice formation (salt rejection) was associated with minimum freshwater fluxes.

2.2 Inter-annual variability and trends

2.2.1 Inter-annual variability

As the CAA is completely ice-covered every winter, the maximum ice extent is nearly constant from year to year. In contrast, the minimum (summertime) ice extent has high inter-annual variability. September, usually the month of minimum ice extent, has the most variability, followed by August and October (*Parkinson and Cavalieri* 2002). Normalized ice coverage[4] for Septembers from 1971-2006 ranged from .29 to .67 (Fig. 2.5). Also, light ice years followed heavy ice years. For example, the extremely light ice year of 1998 was preceded by an unusually heavy ice year, but ice cover returned to normal levels within 3-5 years (*Agnew et al.* 2001, *Dumas et al.* 2006b). A similar event occurred in 1981, and to a lesser degree in 1994. The summer of 1961 (not shown) also had relatively little ice cover. The recent light ice years of 1998, 1999, 2006 remain within the range of observed variability.

The 1970's had the most heavy ice years in the record (Fig. 2.5), which was confirmed by *Crocker et al.* (2005). They calculated an ice severity index using ice concentration from the weekly June to October 1968-2000 CIS navigational ice charts and concluded that the CAA region had more severe ice conditions in the 1970's, with decreasing severity during the 1980-1990's. The year of 1998 had the lowest ice severity.

Summertime semi-permanent ice plugs in the northern QEI straits show low inter-

[4]Normalized ice coverage is the ice area divided by the regional area.

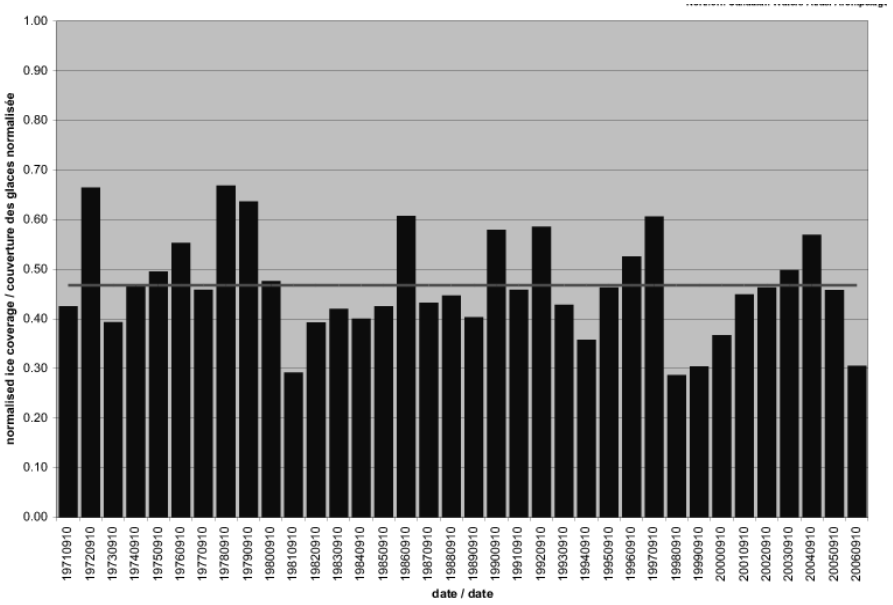

Figure 2.5: Time-series (1971-2006) of observed normalized ice coverage for the week of Sept 10 (*CIS* 2002)

annual variability and their loss indicates unusual conditions. The Sverdrup ice plug was present in every year of the navigational ice chart record except in 1962 and, unusually, in the consecutive years of 1998-2000. The ice plug in Nansen Strait was also lost in 1962 and 1998, as well as 1971 (*Brown and Alt* 2001). The loss of ice plugs may be an indicator of climate change in the future, but so far their loss appears to be primarily connected with years that experience anomalous air temperatures, storm events or wind direction.

2.2.2 Trends

Assessing the trends of ice cover in the CAA is difficult due to large scale variability and relatively short-term datasets. *Parkinson et al.* (1999) calculated trends of CAA ice extent and area for 1979-1996 using satellite-derived ice concentrations on a 25x25 km grid. The annually averaged and summer ice extent trends were -0.8 and -2.4% per decade, respectively. The associated ice area trends were greater, being -2.0 and -9.1% per decade. Excepting for trends related to ice area in winter and spring, none of the trends were statistically significant. Extended out to 1999, the annual trend

reflected the exceptionally light ice year of 1998 and was -1.6 (+/- 0.9)% per decade (*Parkinson and Cavalieri* 2002). Although trends of ice cover were mostly negative, they remain inconclusive.

Trends are also calculated using ice area data from the CIS charts. The trend in September ice coverage (area) was -4.3% per decade for 1971-2006. However, the trend depends significantly on the start and end point, eg. from 1979-2005 the trend was +0.15% per decade, and from 1971-2001 was -5.9% per decade. *Falkingham et al.* (2002) reported at rate of -8% per decade of minimum ice coverage from 1969-2001. Summer time coverage of multi-year ice can be another indicator of climate change, but data in the western channels of the CAA for 1968-2006 showed no significant change (*Howell et al.* 2007). In contrast, trends of landfast ice extent show decline and was -5.5% per decade within the CAA over 1976-2004, with less landfast ice cover in the Gulf of Boothia, Lancaster Sound and Amundsen Gulf. Landfast ice cover along the northern coast of the CAA is also experiencing a decline (-23% per decade) (*Yu et al.* 2006).

Trends of maximum landfast ice thickness, observed since the 1950's, vary spatially (*Brown and Cote* 1992, H.Melling, Pers. Comm.) and do not reflect large scale warming, but rather changes in snow cover. Ice thicknesses at Resolute (Barrow Strait) and Cape Parry (in Amundsen Gulf) have increased (slightly) while ice thicknesses at Mould Bay (northern QEI) and Cambridge Bay (southern coast) have decreased.

There is some evidence that the CAA ice cover is influenced by regionally varying atmospheric forcing. The 1979-1996 satellite data shows that the decreasing trend of ice in the western CAA is compensated by increasing ice cover in the eastern CAA (*Parkinson et al.* 1999). This spatial variability may be a result of a prolonged positive phase of the NAO/AO during the 1990's (*Melling* 2001). During this time, the intensified Icelandic Low advects cold air southward over Nares Strait and into

Baffin Bay, cooling the eastern CAA. Also, a weakened Beaufort High permits warm southerly air to extend into the western CAA, affecting the timing of snow melt and consequent ice melt (*Belchansky et al.* 2004, *Stone et al.* 2005).

Changes in the Aleutian Low of the North Pacific also affect the western Arctic, including the western CAA, and are partially represented by the Pacific Decadal Oscillation (PDO) (*Mantua et al.* 1997). The PDO is based on the first EOF of North Pacific Ocean sea surface temperatures, and is correlated with the North Pacific sea level pressure (SLP). A positive PDO is associated with a strengthened Aleutian Low and Beaufort High. A study by *Lindsay and Zhang* (2005) showed that simulated sea-ice thickness in the Beaufort Sea was positively correlated with the AO and negatively correlated with the PDO. The effect of the PDO index extends to the western CAA, but is poorly documented.

Presently, the available data does not indicate significant sea-ice retreat, but other indicators do suggest a changing cryosphere in the CAA region. Reports from indigenous people of the CAA provide another source of data regarding changes in weather and ice cover. Their culture has remained connected with the environment and their survival, while hunting, fishing, and travelling on the sea-ice, requires a precise understanding of their environment and the ability to assess weather conditions. Although many factors influence the perception of climate change, there is a consensus among the indigenous people: weather of this decade has become more unpredictable and its variability is more extreme (*ACIA* 2005). People have observed changes in wind (direction, intensity, and timing), sea-ice (thickness, extent, and decay) and snow (strength). At Iqaluit (southern Baffin Island), Sachs Harbour (Banks Island) and Clyde (eastern Baffin Island), ice breakup was earlier. Off the coast of Igloolik (Foxe Basin), the wind played a larger role in ice break up than previously, when melt was the primary source of decay. Unusually thin ice has turned into a hazard for ice fishing and travel, resulting in more people falling through the ice. Landfast ice had

weakened and thinned, or had disappeared, and resulted in more shoreline erosion during winter storms. Also, flooding and permafrost loss had increased, making water quality an issue. There is also evidence of loss of snow cover, glaciers, and lake ice (*Brown and Alt* 2001), as well as the thinning and fracturing of the Ward Hunt ice shelf (northern Ellesmere Island) (*Mueller et al.* 2003).

2.3 Sea-ice processes of the CAA

Anticipating the sea-ice response to climate change requires an understanding of sea-ice behaviour, which is affected by two main processes: thermodynamics (i.e. growth and melt) and dynamics (deformation and advection).

Thermodynamics

The melt of sea-ice at its surface depends on net radiation, turbulent heat exchange (sensible and latent heat fluxes), heat conduction, and snow cover. Basal freeze and melt is determined by oceanic temperatures and heat conduction, which is dependent on ice thickness. Solar radiation and air temperatures vary seasonally and regionally, and directly influence patterns of sea-ice cover. In the winter, the CAA is dark (polar night) and cold and results in a complete and thick ice cover, while summertime conditions are sunlit and warm and are associated with minimum ice cover. The southern regions receive more solar radiation than the northern regions, with partial daylight in spring and fall. Air temperatures are also warmer in the southwestern CAA. The annual mean air temperature (1950-2004) is shown in Fig. 2.6. Solar radiation and air temperatures contribute to observed regional variability of ice cover.

In the spring, warming air temperatures melt the snow cover and form melt ponds on the surface. This significantly reduces the surface albedo from snow (80%) and ice (70%) to that of water (10%), and increases the amount of solar radiation absorbed by the surface. With the removal of the overlying snow cover, ice is able to melt, resulting in more open water and absorption of solar radiation. Seasonal ice melts

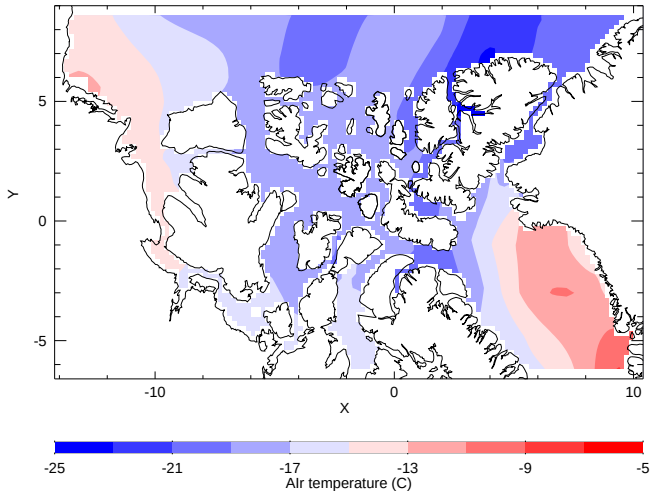

Figure 2.6: Annually averaged air temperature (1950-2004), taken from the CAA model forcing as described in Chapter 3.

completely during the summer. Perennial ice, which survives the summer season, loses its snow cover by June and partially melts during July and August. Freeze up occurs in fall as air temperatures cool and solar radiation decreases. Air temperature plays a key role in the formation of seasonal or perennial ice and determines the open water duration (as it controls freeze up as well as spring melt of snow) (*Flato and Brown* 1996). Warmer air temperatures result in a shorter ice cover duration and will tend to reduce maximum ice thicknesses, but the ice response is weak as winter thicknesses depend mostly on snow cover. Warmer fall temperatures (e.g. October) will have a greater effect, as delayed fall ice formation will result in a warmer ocean and less ice growth before snow fall.

Air temperatures of the CAA have increased since the 1950's (Fig. 2.7). Although the years of 1981 and 1998 were anomalously warm in all seasons, the winter months (October to March) show the most warming and inter-annual variability.

Summertime cloud and fog strongly influences the amount of net solar radiation and the rate of ice and snow melt. For example, the northern QEI experiences dense fog from moisture coming off melt ponds and open leads in the Arctic Ocean pack ice. Fog blocks solar radiation and delays ice melt. Eureka receives an unusual

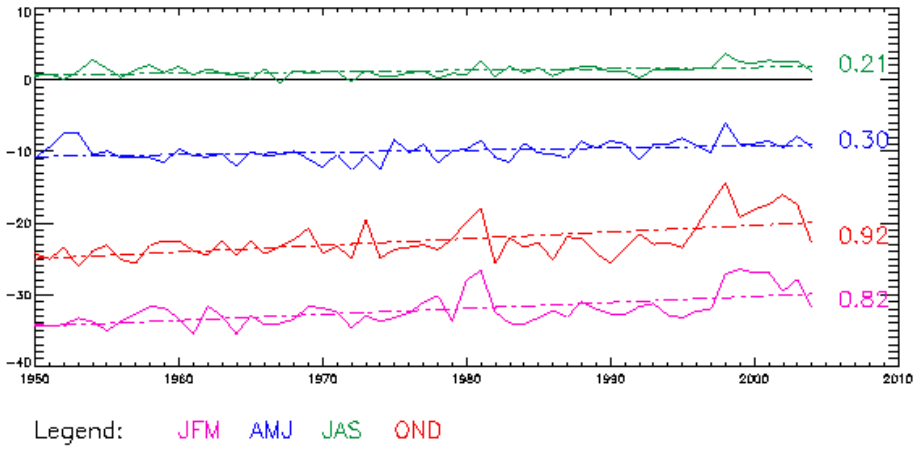

Figure 2.7: Seasonally averaged air temperature for the CAA region. Data is from the regional CAA model forcing, which is based on adjusted values from the NCEP/NCAR Reanalysis. Trends are in °C per decade

amount of net radiation for its latitude because of clear skies, resulting from the rain shadow effect of surrounding mountains. Consequently, spring breakup of streams at Eureka occurs earlier than at Resolute further south (*Maxwell* 1981). The presence of land (or perennial ice cover) also modifies the local conditions, creating a continental climate with larger seasonal extremes compared to a maritime climate. Compared to the Arctic Ocean, the CAA climate is more continental with the presence of large islands, narrow channels and close proximity to mainland Canada and the perennial ice pack (*Maxwell* 1981).

Snow cover plays an important role in determining ice thickness: the inter-annual variability of maximum ice thickness is strongly influenced by seasonal variations in snow cover (*Flato and Brown* 1996), while landfast ice thickness trends at Alert and Resolute are found to be negatively associated with snow depth (*Brown and Cote* 1992). Snow cover has a lower thermal conductivity than ice and insulates ice from overlying air temperatures; it retards ice melt during spring warming and slows ice growth during fall cooling. The loss of snow cover in the spring and summer signals the initiation of ice melt. Consequently, thinner snow cover and warmer spring air temperatures result in an earlier ice melt (*Stone et al.* 2005, *Belchansky et al.* 2004).

Snow thickness depends on many factors: the snowfall rate, which is dependent on precipitation and air temperature; snow advection by wind and ice; and snow melt from air temperatures. There is large spatial and seasonal variability in snow cover, and coverage on sea-ice is poorly known. From data on landfast ice (coastal stations of the CIS observational network) snow thicknesses range from wintertime maximum average of 0.10 m at Cambridge Bay to 0.80 m at Resolute. Observations of on-land snow cover, as shown in Fig 2.8, provide a sense of the spatial distribution but also reflect the topography, with thicker snow in mountainous regions (e.g. eastern Ellesmere Island and Baffin Island). The maximum depth for most of the CAA is less than 1.0 m, excluding the mountainous regions. There is very little data for mobile sea-ice (e.g. in regions of Lancaster Sound or Nares Strait).

At low-lying elevations on-land snow melts completely in summer. The QEI has the longest snow cover duration, being snow free only during late July and early August. The southern and western regions are snow free much longer, from early June to late September (*Brown et al.* 2003).

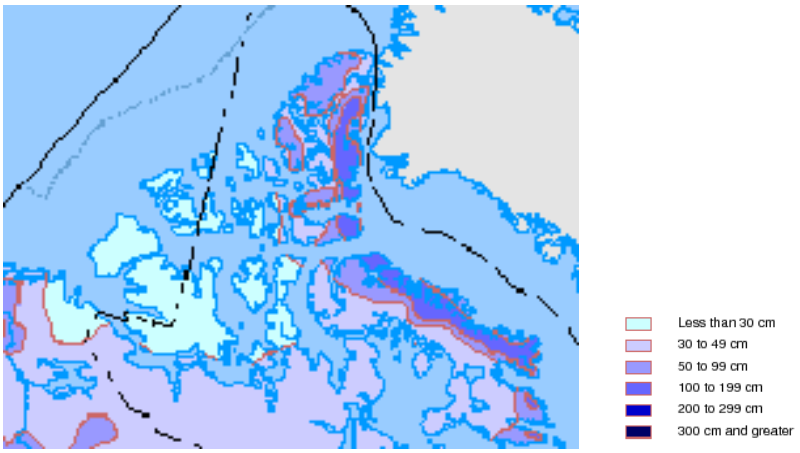

Figure 2.8: Average maximum snow depth 1979-1997 (*Brown et al.* 2003)

The insulating role of snow may be lost in a warmer and wetter climate if snow is partially replaced by slush ice. Slush ice is formed when the weight of snow pushes ice and snow under water and freezes. The thermal conductivity of slush-ice is much

greater than snow, and results in more ice growth in winter. Slushing provides a negative feedback, where a warmer climate with more snow precipitation may result in thicker ice (*Brown and Cote* 1992). Currently, slushing is not very common in the CAA.

The oceanic heat flux plays a key role in melting the keels of imported ridged ice in the northern QEI, where the heat from the Atlantic-derived water is mixed upwards against the continental shelf. Also, due to mixing within the channels, the CAA halocline is warmer compared to the Arctic Ocean, and results in more basal ice melt (*Melling* 2002).

Dynamics

In regions of mobile ice, dynamics modify ice thickness. Under convergent forces, ice is compressed or pushed up over other ice floes, becoming thicker. Alternatively, ice divergence reduces the ice concentration, resulting in increased wintertime growth or summertime melt. Advection also changes a region's ice thickness by exporting ice (e.g. thinning) or by importing relatively thinner or thicker ice. Generally, ice movement is caused by wind and oceanic currents, and is resisted by consolidated ice and narrow channels.

The wind pattern over the CAA is part of the larger atmospheric circulation seen in the Arctic. In the winter, there is a high pressure system over the continents and the Beaufort Sea, and a low pressure system over the northern Pacific and Atlantic oceans, extending into the eastern Arctic. In the summer, the winds are much weaker; the high pressure system over the land dissipates and the oceanic low pressure systems weaken (*ACIA* 2005). In the NCEP/NCAR Reanalysis, north-westerlies exist over the CAA, with the exception of Amundsen Gulf which experiences south-easterlies (Fig. 2.9). North of the CAA, the wind direction is westward in the Beaufort Sea, southward towards the QEI, and is eastward above Ellesmere Island and in the Lincoln Sea. Baffin Bay to the south consistently experiences cyclonic circulation. The wind

patterns remain similar all year, except over the Beaufort Sea and Amundsen Gulf, which vary seasonally. In spring, the annual mean westward wind direction reverses in both regions, and continues to be eastward in the Amundsen Gulf into summer. Daily, the wind is highly variable in direction and intensity through out the CAA region, which can result in large ice fluxes when the ice is mobile.

Topography modifies local wind patterns, which affect the ice cover. For example, the steep sides of Nares Strait constrain the wind to an along-channel direction (*Samelson et al.* 2006). Also, the mountain range on Ellesmere Island and surrounding islands help protect the ice from intense storm activity, and associated ridging. In-situ ice of the QEI and the interior of M'Clure Strait are relatively undeformed.

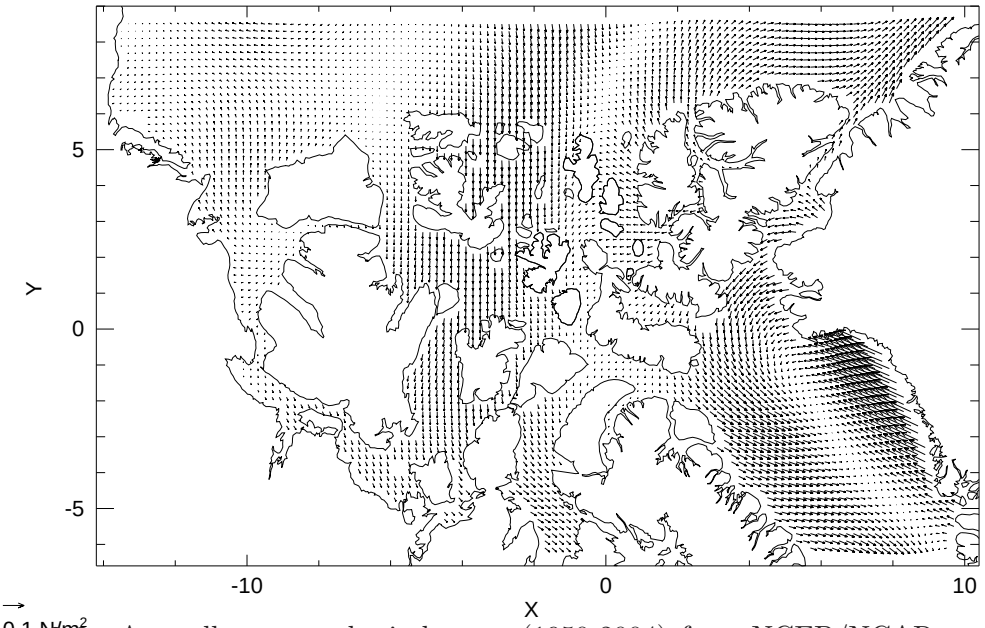

Figure 2.9: Annually averaged wind-stress (1950-2004) from NCEP/NCAR, as interpolated to the model

Although the sea-ice responds to wind over short periods (a few days), the wind variability tends to average out over time (i.e. weeks) and the oceanic current and sea-surface tilt effects become more significant in controlling net ice movement (*Thorndike and Colony* 1992). The mean direction of the ocean currents through the CAA is southward, in part due to the sea level difference between the Arctic Ocean and

Baffin Bay (*Melling* 2000, *Kwok* 2005). Due to the combination of wind and oceanic currents, sea-ice generally moves southward, as observed in the QEI (*Melling* 2002) and Nares Strait (*Kwok* 2005).

Advection plays an important role in defining sea-ice characteristics in the CAA and modifies regional ice thickness. The northern channels of the QEI and M'Clure Strait are dominated by exceptionally thick ice, ranging from 6-7 m in winter, and 4-5 m in summer, resulting from import of heavily ridged, multi-year ice from the Arctic ice pack. Due to prevailing winds and ice circulation, the Arctic ice is pushed up against the coast and into the CAA (*Bourke and Garrett* 1987). However, the upwelled oceanic heat flux along the northern CAA coast melts the incoming ice keels, reducing the ice thickness within the CAA interior (*Melling* 2002). Ice is also exported from the QEI and M'Clure Straits into more southerly channels, resulting in a mixture of imported multi-year ice and dominantly in-situ first year ice. In some years, there is a large export of sea-ice from the QEI, which permits a compensating influx of Arctic Ocean ice, and is usually followed by several years of stable, limited export from the QEI (*Melling* 2002).

Ice islands and icebergs are also present within the CAA, and travel southward. Ice islands are large blocks of ice that can be over 50 m thick and 40 km in diameter, and are formed from ice that has broken away from ice shelves. They mostly originate from northern Ellesmere Island. Icebergs also form in this region, and calve off the glaciers on Northern Ellesmere Island, Devon Island and Axel Hieberg Island. They are commonly found in Nansen Sound and Jones Sound (*Sanderson* 1988).

Tides and polynyas: a combination of dynamics and thermodynamics

Tides affect the ice dynamically, via daily shifting, as well as contributing to the mean oceanic flow. Thermodynamically, they increase the heat flux to the ice via oceanic mixing, resulting in more wintertime leads and reduced ice growth. Tides and intense storms loosen up ice, break up ice plugs and inhibit ice consolidation.

For example, uplift from strong spring tides break up ice, and tidal mixing advects warmer water from below. Smaller polynyas in Hell Gate and Cardigan Strait exist as a result of vertical mixing from tides and channel restriction which provides oceanic heat (*Dunphy et al.* 2005, *Smith et al.* 1990) as well as wind advection of ice away from the narrow opening.

Based on a barotropic inverse tidal model of the Arctic by *Padman and Erofeeva* (2004), the CAA tides are strongest in Nares Strait and the Gulf of Boothia, where both regions experience amplitudes of 1.2 m (M2) and mean tidal current speeds of 16+ cm s^{-1}. Tidal currents are also strong in Barrow Strait and Lancaster Sound (10-15 cm s^{-1}), and to a lesser degree the Mackenzie Shelf region (7 cm s^{-1}). Simulations by *Dunphy et al.* (2005) done specifically for the tides of the CAA region, using the Webtide prediction package, show similar results. Tides are not included in this study, so these affects will be missing, but are considered to be negligible for long term (annually averaged) ice studies.

Polynyas are caused by advective and thermodynamic processes or both, as is in the case of the North water polynya (NOW). The NOW is formed as wind pushes ice away from both the Greenland coast and an ice plug in northern Smith Sound, while the warm west Greenland current melts the ice from below (*Smith et al.* 1990, *Yao and Tang* 2003). The Bathurst Polynya in Amundsen Gulf is created in a similar way; the Beaufort ice pack moves away from the landfast ice in the Amundsen Gulf and results in leads which induce oceanic mixing and increase surface heat flux (*Barber and Hanesiak* 2004).

Chapter 3

Methodology

With the intent to model the sensitivity of CAA sea-ice to climate change, two experiments are conducted using a regional ice-ocean model of the Canadian Arctic Archipelago with 0.2° horizontal resolution. Firstly, the model is forced with observationally-based atmospheric data from 1950-2004. Secondly, a future scenario is run under atmospheric forcing derived from observed data and climate model output. Most of the observationally-based data is taken from the Reanalysis Project of the National Center for Environmental Prediction and the National Centre for Atmospheric Research (NCEP/NCAR) (*Kalnay et al.* 1996). The climate model output is provided by the Canadian Centre for Climate Modelling and Analysis (CCCma) model, CGCM2 (Coupled Global Climate model, version 2) (*Flato and Boer* 2001). This chapter describes, in more detail, the model and then the forcing.

3.1 Model Description

The model employed here is comprised of a sea-ice component, described below, coupled to an ocean component (Modular Ocean Model, version 2) (*Pacanowski* 1995) and forced with atmospheric data. A simple snow model, similar to that described by *Walsh et al.* (1985), is also included. The setup for this model follows previous studies by *Nazarenko et al.* (1998), *Holloway and Sou* (2002) and *Tivy et al.* (2004).

Albedo	Open water	Melting Ice	Dry Ice	Melting Snow	Dry Snow
This study	0.1	0.5	0.6	0.7	0.8
Parkinson & Washington (1979)	0.1		0.5		0.75

Table 3.1: Albedo values chosen for different states of open water and ice and snow conditions, as suggested by G. Holloway (Pers.Comm.). Values used by *Parkinson and Washington* (1979) are included for comparison

3.1.1 Model physics

Ice and snow model: thermodynamics

Sea-ice is represented by a single layer with a linear temperature profile and no heat capacity. The surface ice temperature is determined by the surface energy balance:

$$H\downarrow + LE\downarrow + netLW + (1-I_o)(1-\alpha_I)SW\downarrow + (k_I/h_I)(T_B - T_{sfc}) = 0 \qquad (3.1)$$

where: H, LE, LW, SW represent sensible heat, latent heat, longwave and shortwave radiation respectively; I_o is the fraction of the net incident shortwave which penetrates the upper surface, and is set to 0.17; α is ice albedo; k_I is the ice conductivity, h_I is the ice thickness; T_B is the ice bottom temperature and T_{sfc} is the ice surface temperature. The term $(1-I_o)(1-\alpha_I)SW\downarrow$ represents the shortwave radiation absorbed by the ice surface, and $(k_I/h_I)(T_B - T_{sfc})$ is the conductive heat flux. A similar surface energy budget is applied over snow, except I_o is set to zero, and the albedo also varies. There is a lot of uncertainty regarding the albedo of the ice and snow surfaces, and generic values are chosen to represent a range of observations (see Table 3.1). The bottom energy balance included the conduction of heat through the ice, the transfer of heat from the ocean, and bottom growth and melt.

Methods to calculate the sensible and latent heat fluxes, shortwave radiation, and conduction through the ice, are from *Parkinson and Washington* (1979). As there is no heat storage in this model, the penetrating shortwave radiation either melts the

Month	Jan	Feb	Mar	Apr	May	Jun	Jul	Aug	Sep	Oct	Nov	Dec
Cloud Fraction	0.50	0.50	0.50	0.55	0.70	0.75	0.75	0.80	0.80	0.70	0.60	0.50

Table 3.2: Monthly cloud fraction (*Parkinson and Washington* 1979)

ice bottom or is transmitted through the ice to heat the underlying ocean[1]. The rate of attenuation is calculated by:

$$I_o(1-\alpha_I)SW\downarrow(1.0-e^{1.5*h_I}) \tag{3.2}$$

The calculation for net longwave is from *Rosati and Miyakoda* (1998):

$$LW=\epsilon\sigma T_{sfc}^4(0.39-0.05e_a^{1/2})(1-BC)+4\epsilon\sigma T_{sfc}^3(T_{sfc}-T_a) \tag{3.3}$$

where: ϵ is the emissivity of the surface; σ is the Stefan-Boltzman number; T_{sfc} is the surface temperature and T_a is the air temperature; e_a is the atmospheric vapour pressure; B is 0.8 is linear correction factor; and C is fraction of cloud cover. The *Rosati and Miyakoda* (1998) longwave scheme considers the difference between the surface and air temperatures and is well suited for models with both ice and open water regions. Cloud cover is taken from *Parkinson and Washington* (1979), in which spatially constant monthly climatological values are assigned as shown in Table 3.2.

Similar to the ice model, snow is represented by a single layer. Snow cover increases the surface albedo, blocks penetration of shortwave into the surface, prevents surface ice melt, and modifies the thermal conductivity. The thermal conductivity of the combined snow and ice layer is the weighted sum of the conductivities of ice and snow. In this model, heavy snow cover can submerge the ice[2] and the flooded snow

[1]In comparison, *Parkinson and Washington* (1979) neglect the penetrating shortwave in order to represent heat lost to the underlying ocean and to melt brine pockets, two processes which are not included in their model.

[2]The draft associated with the combined weight of the snow and ice is calculated, and if it is greater than the ice thickness, the snow is flooded by the difference between the draft and ice thickness.

is converted to ice. Sublimation of snow and ice to the atmosphere and frost are included. There is no parameterization for melt ponds on the ice or snow surface, other than as represented by the surface albedo.

The rate of snow fall depends on precipitation rates and air temperature. Precipitation falls as snow when the air temperature is colder than -5° and as rain when the air temperature is above 5°. When the air temperature is between -5 to +5°, the ratio of snow to rain decreases linearly as the air warms.

Ice and snow model: dynamics

The dynamic component of the ice model includes a momentum balance, a constitutive law, and equations for ice thickness distribution, and ice strength.

The momentum balance is given as:

$$mD\mathbf{u}/Dt = mf\mathbf{k} \times \mathbf{u} + \tau_{\mathbf{a}} + \tau_{\mathbf{w}} - mg\nabla H + \mathbf{F} \tag{3.4}$$

where m is the mass of ice per unit area; $\mathbf{u}$ represents ice velocity; τ_a and τ_w are air and water stresses; $mf\mathbf{k} \times \mathbf{u}$ is the Coriolis force, with the Coriolis parameter f and vertical unit vector $\mathbf{k}$; $mg\nabla H$ represents sea surface tilt, where H is the sea surface elevation and g is the gravitational constant; and $\mathbf{F}$ is the force due to gradient of internal ice stress.

The ice state is represented by the area mean thickness (h) and ice concentration (A). The ice thickness distribution is approximated by two-categories. The 'thin ice/open water' thickness category includes ice thinner than a cutoff thickness (h_o) and open water. The 'thick' category ice includes ice thicker than h_o. The cutoff thickness defining the ice thickness distribution categories, h_o, has been changed from 0.5 (*Hibler* 1979) to 0.2 to represent a faster lead closing, which is considered to be more realistic (H. Melling, Pers. Comm). Ridging is represented by an increase in ice thickness when ice is advected into a cell with 100% ice concentration. An upstream

advection scheme is applied for this study.

The internal ice stress ($\mathbf{F}$) depends on the rheology scheme. Ice interaction is represented by a viscous-plastic rheology, following *Hibler* (1979), where the stress state is proportional to the strain rate for very small deformation (i.e. nearly rigid behaviour) and is independent of strain rate for large plastic deformation.

The constitutive law connects ice stress with strain rate and ice strength. Ice strength (P), as parameterized by *Hibler* (1979) is strongly dependent on the amount of thin ice and open water ($1 - A$), and is also dependent on (cell-averaged) ice thickness (h) as follows:

$$P = P^* \; h \; exp[-C(1 - A)] \tag{3.5}$$

where P^* and C are constants and A is the ice covered fraction of the grid cell. The thicker the ice, the stronger (more resistant) the ice is to deformation. The ice strength parameter, P^*, is set to 15,000 Nm^{-2} following *Kreyscher et al.* (2000). The constant C is kept at 20 after *Hibler* (1979) and is based on the observation that pack ice with more than 10% open water exhibits little resistance to convergence.

Snow is advected with the ice velocities.

Ocean model

MOM is a three dimensional primitive equation ocean model (*Pacanowski* 1995), based on the work of *Bryan* (1969). The model consists of the Navier-Stokes equation which is subject to the Boussinesq and hydrostatic approximations. The non-linear equation of state relates density to temperature, salinity, and pressure. Temperature, salinity and velocity are prognostic variables. In this application, there is no restoring to observed ocean temperature or salinity values, and the fluxes are completely dependent on the atmospheric forcing and surface energy budget. Lateral boundaries are considered solid walls, except where open boundaries are assigned as a special condition. Convection occurs using a 'full convect' method (*Pacanowski* 1995), where

all static instabilities are removed from the water column with one pass. The ocean model assumes a rigid lid, in which the ocean volume does not change. The tracer timestep is set to 4 hours, while the momentum timestep is 15 minutes.

The subgrid scale mixing terms for the diffusion and viscosity are set to constant values. Vertical diffusion is 10^{-6} m^2 s^{-1}, while vertical and horizontal viscosities are 10^{-3} m^2 s^{-1} and 10^3 m^2 s^{-1} respectively. The explicit horizontal diffusion is set to nearly zero as dictated by the flux- corrected transport (FCT) advection scheme, which includes implicit diffusion. The FCT advection scheme for oceanic temperatures and salinities is an improvement over the centered difference scheme, which has more numerical dispersion. The FCT advection scheme was implemented into the MOM (version 2) model (*Nazarenko et al.* 1998), and is based on the same method as the MOM (version 3) FCT option.

Because eddies are not resolved by the CAA model, an eddy-topography interaction parameterization by *Holloway* (1992) is included. It represents the role of eddies interacting with the bottom topography, and results in a driving force. The parameterization depends on the bottom topography, the Coriolis parameter and an eddy length scale. The length scale is set to 4 km (substantially less than the model resolution) for this CAA domain. More details about the implementation are given by *Nazarenko et al.* (1998).

Atmosphere-Ocean-Ice Coupling

The coupling time-step of the atmosphere, ocean and ice modules is done at every tracer time-step (4 hours). The model is forced with atmospheric data; there is no feedback from the earth surface to the atmosphere. However, the coupling of the ocean and ice components does include an exchange of heat, salt and momentum. For example, when ice is present and the ocean temperature is above freezing, the oceanic heat flux (calculated as the difference between the ocean temperature and freezing temperature) melts the ice, with a relaxation timescale of one day. If all

the ice melts within one time-step, the heat surplus is returned to the ocean. Ocean temperatures are not permitted to go below freezing. Also, ice growth results in brine rejection (release of salt) into the ocean; the melt of ice freshens the ocean surface. In this case, the ocean model has a rigid lid, so adding or removing a volume of freshwater is not possible. Instead, any freshwater flux is converted to an equivalent salt flux, using a constant reference salinity of 34.8 ppt. The ice model requires information regarding sea surface tilt. As the ocean has a rigid lid, the surface tilt is calculated using the surface pressure gradients. Finally, the presence of ice modifies the momentum transfer to the ocean from wind-stress. Under ice, the stress to the ocean is equal to the water drag on the ice.

3.1.2 Model grid and bathymetry

The model grid is rotated[3] (*Eby and Holloway* 1994) so that the grid North Pole is 90° away from the area of interest. This moves the CAA region to lie over the grid equator. Rotation provides a nearly equidistant grid spacing and avoids meridian convergence at the pole. Geographic latitudes are provided for the calculation of the Coriolis term.

The horizontal grid spacing is 0.2°, with 24 fixed ocean depth levels[4]. The top six levels have a vertical resolution of 5m. Below 30 m, the vertical resolution linearly increases to a maximum of 140 m. The maximum depth is set at 1200 m, cutting off deeper regions in the Arctic Ocean and Baffin Bay to reduce integration time.

Bathymetry from the merged IBCAO_ETOPO5 (*Holland* 2000) is on a 10 km grid, and is interpolated to the CAA model grid using a cosine weighted average method. The method does not preserve narrow and deep passages, cutting off straits or shallowing sills. Consequently, changes were made manually to improve the topog-

[3]The grid North pole lies in the South China Sea (14°N, 114°E) and the grid prime meridian point falls within the CAA model domain (75°N, 90°W).

[4]The bottom of the levels (in m) are as follows: 5, 10, 15, 20, 25, 30, 40, 55, 75, 100, 130, 165, 205, 250, 300, 360, 430, 510, 600, 700, 810, 930, 1060, 1200.

raphy representation. For example, Nares Strait is widened slightly and deepened to better agree with navigational topographic charts. Similarly, narrow straits around Ellesmere and Victoria Islands were widened to a minimum of two tracers points (and one associated velocity point) to permit oceanic and ice transport.

3.2 Forcing data

3.2.1 Lateral open boundary forcing

Open boundaries exist in the CAA model, one in the Beaufort Sea, and the other in Baffin Bay (Fig. 3.1). Fury and Hecla Straits, which connect to Foxe Basin, are closed. In order to provide monthly varying lateral boundary conditions for the CAA regional model, a basin-wide model (of the Arctic Ocean) was constructed. It is set up similarly to the CAA model (see Appendix A for more details) and is run (offline) for both the historical (1950-2004) and the future (2041-60) runs. The lateral boundary forcing provided to the CAA regional model includes oceanic fields (temperature, salinity, velocity and streamfunction), ice fields (velocity, thickness and concentration) and snow fields (thickness). A 'free outflow' condition is applied in the regional model so that outflow oceanic temperatures and salinities are not reset to the boundary values.

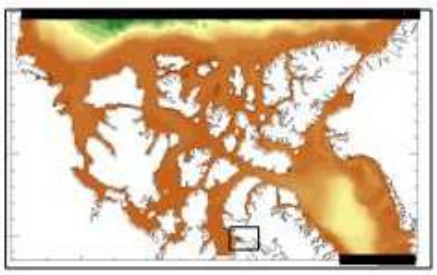

Figure 3.1: The location of the CAA model open boundary model is shown by thick black lines. The location of Fury and Hecla Straits are indicated by the black box.

Oceanic fluxes through the CAA are poorly observed but are of great interest in terms of freshwater budgets of both the Arctic Ocean and Labrador Sea. Although oceanic fluxes are not a primary focus of this thesis, the oceanic transport does affect

ice velocity, and is briefly discussed here. The oceanic volume transport through the CAA model is set by streamfunction data from the basin-wide model, and represents the flow through the passage between Greenland and Canada. The oceanic flow through the CAA varies monthly, ranging from 0.3 to 0.9 Sv (Fig. 3.2)

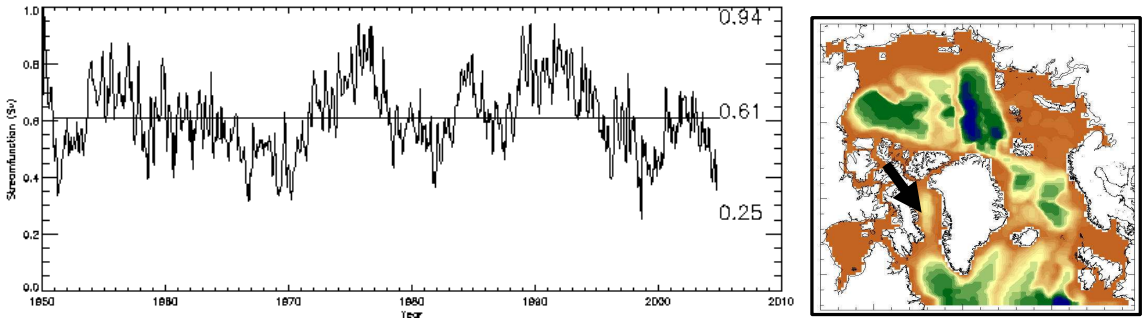

Figure 3.2: Oceanic transport through the CAA, as determined by the Arctic Ocean model

Observed estimates of oceanic volume fluxes through the CAA are limited, and simultaneous measurements in key straits do not exist. Consequently, volume transport estimates are uncertain, and annually averaged transports range from 0.7 to 2.0 Sv (*Melling* 2000, *Sadler* 1976, *Fissel et al.* 1998, *Prinsenberg and Hamilton* 2005), and mostly depend on assumptions made about the ratio of flow through the main straits. For example, the flow through Lancaster Sound is thought to be twice as big as through Jones Sound, and half of the total flow through the CAA. Nares Strait is usually assigned about a third of the total flow. Diagnostic modelling work by *Kliem and Greenberg* (2003) report of summer total transport of 0.9 Sv, with 34% of the flow through Barrow Strait (e.g. Lancaster Sound), 20% through Jones Strait, and 46% through Nares Strait. Observations indicate high interannual and seasonal flow variability. Based on three years of moored current meter data (1998-2001) in Lancaster Sound, the ocean transport ranged from -0.01 Sv to 1.3 Sv.

Compared to observations, the CAA model underestimates the oceanic transport through the straits of the CAA region, but does capture the range of flow, as well as the flow ratio through the straits (Table 3.3). The simulated transport does not

Channels	Ocean volume flux (Sv)	% of CAA total
Nares Strait	0.143	23%
Jones Sound	0.146	25%
Lancaster Sound	0.325	53%
Total	0.614	

Table 3.3: Simulated annually averaged ocean volume transports (1950-2004) into Baffin Bay from the CAA regional model. Positive means net southward flow.

have a strong seasonal cycle, with slightly less flow in the spring.

Initial conditions

For both the historical and future scenario runs, the initial ice concentration and thickness fields are taken from the end of a five year run (1950-1954) of the Arctic Ocean basin-wide model, initialized with zero ice. The resulting ice field is interpolated to the CAA grid. Although the initial ice cover conditions for the future 2041-60 (CAA model) period are taken from the end of the pan-Arctic 1950-1955, the model equilibrates within the first few years to the new climate conditions (Fig. 5.12).

In all cases, the three-dimensional ocean temperatures and salinities are initialized with climatological December values from the Polar Science Centre Hydrographic Climatology (PHC; *Steele et al.* 2001). Although initializing the future run with historical ocean conditions may bias the results due to a colder underlying ocean, it is expected that the effect on future ice conditions will be modest. The Arctic Ocean is currently highly stratified, and global climate models indicate that stratification will increase in the future (*Saenko* 2006). Therefore, it is expected that the CAA region will remain well-stratified, limiting the influence of a warming deeper ocean on the sea-ice. Also, the region retains winter ice cover in almost all global climate models and in the CAA model, as will be seen later. Further study is necessary to assess the simulated changes in CAA ocean conditions and its affect on the sea-ice.

3.2.2 Atmospheric forcing

Historical, 1950-2004

Monthly data from 1950 to 2004 for air temperature, specific humidity, and surface pressure is taken from the NCEP/NCAR Reanalysis (*Kalnay et al.* 1996). Daily wind-stress and wind-speed is taken from the NCEP/NCAR surface winds[5]. The NCEP/NCAR Reanalysis (*Kalnay et al.* 1996) generally agrees well with observations in the Arctic region, especially in terms of cyclonic activity (*Bromwich et al.* 2007). However, the reanlaysis over-estimates shortwave radiation and under-estimates cloud cover (*Curry et al.* 2002, *Bromwich et al.* 2007). Consequently, values for cloud cover are taken from *Parkinson and Washington* (1979) and shortwave radiation is parameterized within the model. Also, the NCEP/NCAR precipitation data is not used because precipitation rates are excessive in the CAA region (*Serreze and Hurst* 2000). Instead, a climatological precipitation dataset (1960-2002) is taken from *Serreze et al.* (2003), available on a 175 km grid of the Arctic (*Serreze et al.* 2003); although based on land observations, it is suited for this study as it includes data from coastal sites within the CAA. Specific humidity is taken from the NCEP/NCAR Reanalysis, but is modified so that the relative humidity used in the model never exceeds 95%.

The NCEP/NCAR air temperatures compare well at the SHEBA site in the Beaufort Sea, but are generally too cold (*Curry et al.* 2002). This is also the case over the CAA region, especially in summer. Because the NCEP/NCAR Reanalysis does not resolve the narrow channels of the CAA, the resulting air temperatures better represent high altitude glaciers of Greenland and Ellesmere Island than maritime conditions. This poses a problem as modelled ice thicknesses are very sensitive to summers that do not warm to above freezing (*Flato and Brown* 1996). Interpolated

[5]For the wind forcing, both the NCEP/NCAR land and ocean points are used, but due to problems mentioned later, only the ocean points are taken for the air temperature forcing.

to the CAA model grid, the summertime NCEP/NCAR (ocean) air temperatures were not high enough to permit snow (and thus ice) melt, especially in the eastern region (e.g. around Ellesmere Island). Without summertime melt, the simulated ice thickness was much larger than observed, in some places exceeding 10 m. This result is important to note when considering simulated CAA ice cover from models forced with NCEP/NCAR air temperatures.

To address this problem, a correction is applied to the NCEP/NCAR air temperatures using the IABP/POLES (International Arctic Buoy Program/ Polar Exchange at the Sea Surface) dataset (*Rigor et al.* 2000). The IABP/POLES dataset better represents the air temperatures over sea-ice and ocean in the CAA; it has a higher resolution than the NCEP/NCAR Reanalysis, and includes observations from local coastal sites. It is available from 1979-2003, which is not long enough to adopt the dataset for this study. To derive a correction for the NCEP/NCAR data, the difference between the NCEP/NCAR and IABP/POLES air temperatures is calculated for each grid point and for every month from 1979-2003[6]. The anomalies are averaged into a monthly climatology and added to the NCEP/NCAR monthly time-series data from 1950-2004. The adjustment is largest in summer, with temperatures increasing from 0.5 to 5.0°C depending on the region. The simulated ice thickness under the adjusted forcing is more like observed, both in terms of thickness and seasonal cycle.

Instead of adjusting the NCEP/NCAR air temperatures, replacing the reanalysis with data from the European Centre for Medium-Range Weather Forecast (ECMWF, *Uppala et al.* 2005) was considered. To evaluate the ERA-40 2m air temperatures, the data from NCEP/NCAR, IABP/POLES and observations are compared at six sites within the CAA region. It was found that the ERA-40 air temperatures would require a similar adjustment using the IABP/POLES dataset (but for different biases). Also, the ERA-40 is on a coarser grid (2.5°) and is available for a shorter length of

[6]Only the ocean points are considered from the NCEP/NCAR data, and the ocean and coastal points are included from the IABP/POLES data.

time (1958-2001) than the NCEP/NCAR model data. The ERA-40 dataset was not adopted here.

The climatological monthly river runoff for the Mackenzie and Peel Rivers is included in the CAA model. The total annually averaged river volume is about 300 km^3 yr^{-1} (9700 m^3 s^{-1}) and peaks in summer. The data is from R-ARCTICNET version 3 (*Lammers et al.* 2001) which incorporates data from 1970-2000.

Future scenario, 2041-2060

Future climate data is taken from the CGCM2 model (*Flato and Boer* 2001), which is run on an approximately 3.75° horizontal grid. Data is available from 1850-2100 for three different GHG scenarios: IS92a, SRES A2 and SRES B2, as defined in the Special Report on Emission Scenarios (*IPCC* 2000). The SRES A2 case was chosen for this study because it is more extreme in terms of population and levels of emissions, and would provide a large signal. It is forced with observed levels of equivalent CO2 concentrations up to 1990, after which the levels increase to reach 779 ppmv by 2050 and 1320 ppmv by 2100.

For this thesis, the objective is to provide an initial evaluation of the response of the CAA to a warming climate. Clearly the magnitude of the response will be directly related to the projected warming. The CGCM2 projections are generally well within the range of projections from other climate models and the CGCM2 model does well in representing historical climate changes (*Flato and Boer* 2001). The maximum Arctic ice cover in CGCM2 is only slightly underestimated by the model (14 instead of 15 x10^6 km^2) (*Kim et al.* 2002), and the amplification of future warming in the Arctic is substantial (*Holland and Bitz* 2003, *Flato and Boer* 2001).

The atmospheric forcing for the future run is calculated by applying the climatological anomalies between 1970-1989 and 2041-2060 as simulated in the CGCM2[7]

[7]Only the atmospheric variables over the ocean grid points inthe CGCM2 model are considered and interpolated to the CAA model grid.

to the historical forcing from 1970-1989. This method retains the variability of the historical forcing while imposing the change between the present and future CGCM2 climate. The present and future time-periods were chosen following *Dumas et al.* (2006a), with the intent to compare model results. A similar application of CGCM2 output has also been done by (*Saenko et al.* 2002, *Dumas et al.* 2006a) and is described by *Hulme et al.* (1999) as follows:

$$x_f(t) = x_p(t) + (c_f - c_p) \tag{3.6}$$

or

$$x_f(t) = x_p(t) \times c_f/c_p \tag{3.7}$$

where, c_p and c_f are the monthly climatological data from CGCM2 for the present day (1970-1989) and the future (2041-60), respectively; x_p is the 1970-1989 historical forcing; and x_f is the derived forcing for 2040-2061 applied to the future run. The difference method is used for air temperature (Equation 3.6). All other atmospheric variables are modified using the ratio method (Equation 3.7). For both the x_f and x_p fields, the wind-stress and wind-speed are daily time-series, air temperature, specific humidity and shortwave are monthly time-series, and precipitation is a monthly climatology. The future shortwave anomalies are taken from the CGCM2 data, and applied to the historical shortwave forcing, calculated offline using the NCEP/NCAR surface pressure and specific humidity after *Parkinson and Washington* (1979). Cloud cover is taken from *Parkinson and Washington* (1979).

Differences between the past and future forcing

The future atmospheric forcing (2041-2060) has warmer winters and wetter summers as compared to the historical forcing from 1970 to 1989 (Fig. 3.3). Air temperatures differ the most in October, November and December, warming by 10°C overall. Regionally, the central and northern CAA, as well as Amundsen Gulf, warm the most

(Fig. 3.4). This shift to warmer fall temperatures is also evident in the historical forcing, which experiences the most warming in October, November and December over the CAA study region (Fig. 2.7).

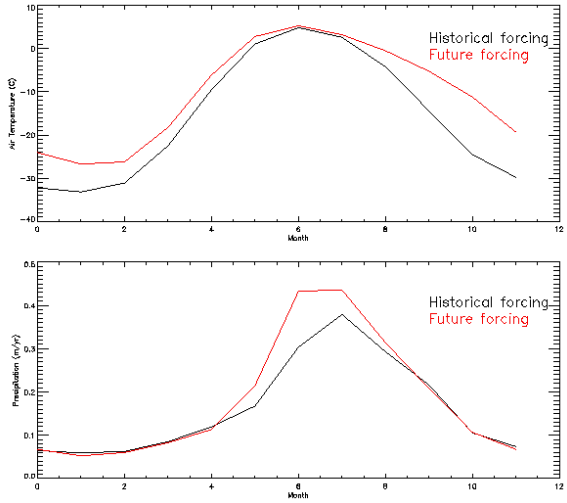

Figure 3.3: Comparison between past (1970-89) and future (2041-60) forcing: seasonal cycle of air temperature (upper panel) and precipitation (lower panel)

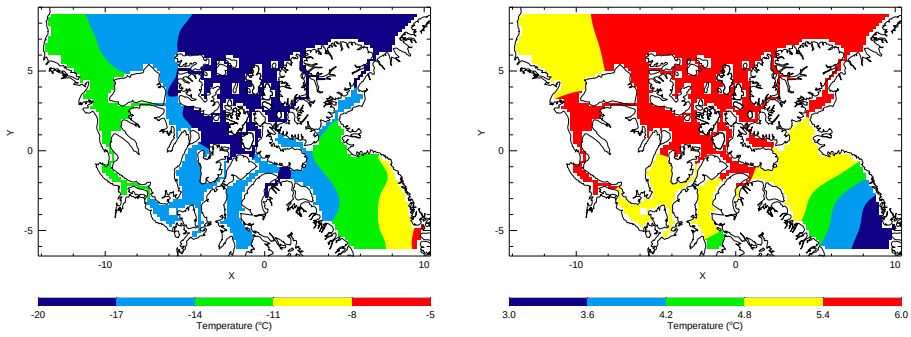

Figure 3.4: Annually averaged climatology of past (1970-1989) air temperature (left panel) and the difference between future (2041-2060) and past (right panel).

Summertime precipitation rates are larger in the future forcing, with little change during the rest of the year (Fig. 3.3). The domain averaged air temperatures remain below or close to 5°C, so precipitation will be a mix of snow and rain during summer. Regionally, Lancaster and Barrow Straits experience the largest increase in summer precipitation, where Smith Sound and the central CAA experience the most change annually (Fig. 3.5).

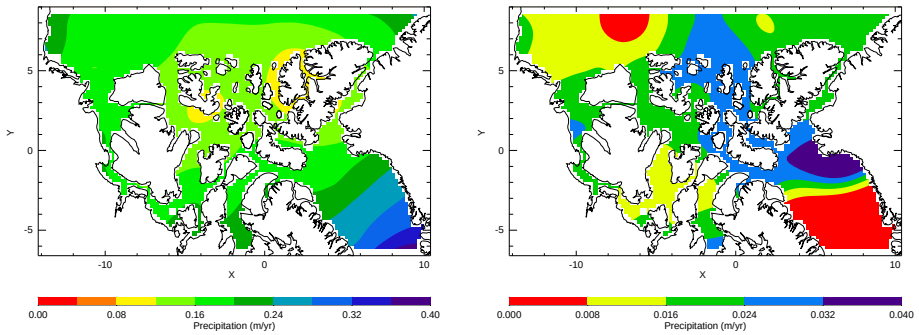

Figure 3.5: Annually averaged climatology of past (1970-89) precipitation (left panel) and the difference between future (2041-2060) and past (right panel)

The remaining atmospheric variables experience little change from the past to the future. The wind-stress magnitude is slightly lower all year, the specific humidity is larger in winter, and shortwave is slightly lower in summer.

Chapter 4

Modelled results, 1950-2004

4.1 Expectations of the model

Innately, models are unable to reproduce the real world with all of its complexities. Due to their sparsity, observations are also limited in representing the climate, and additional interpretation is required to understand physical processes and feedbacks of a natural system. Models play a key role in climate research, in terms of aiding in the interpretation, both via sensitivity studies and simulating future scenarios.

An open question in this study is whether or not a model with fine horizontal resolution (22 km), forced with coarse resolution atmospheric data (+200 km), can accurately reflect sea-ice conditions in the CAA. Global climate models (such as CGCM2 and NCEP/NCAR Reanalysis) do not resolve the CAA channels. Hence, the atmospheric forcing data taken from the GCMs will miss local details, such as the strong topographically channelled wind through Nares Strait or the topographic affects on precipitation.

In general, precipitation data is especially lacking, so this model employs a climatological mean, neglecting the associated inter-annual variability in rainfall and snowfall rates[1]. Due to the simplified cloud representation local effects are missing, such as the observed local maximum of net radiation at Eureka (*Maxwell* 1981).

[1]Snowfall will still vary as it is also dependent on air temperature.

Despite these limitations, I expect the model to reproduce a reasonable climatology, seasonal cycle and inter-annual variability. Wind forced advection and seasonal variability in air temperature are important processes influencing sea-ice. Of course, details in year to year variability or regional spatial regions may not be captured.

4.2 Model validation

The goal of this chapter is to present results from the historical run (1950-2004), and to assess the model's ability to represent observed sea-ice characteristics. Firstly, spatial patterns of climatological ice concentration, thickness and velocity are presented, followed by patterns of break up and freeze up dates, as well as summer duration. Secondly, inter-annual variability of the ice extent, concentration and thickness are considered. The contribution of advective and thermodynamic-derived change to the simulated ice volume is presented, including an analysis of associated ice fluxes through the CAA. Lastly, the ice thickness and summer duration at six sites are compared with observations and the results of a 1-d model (*Dumas et al.* 2006a).

4.2.1 Seasonal ice cover

Ice concentration and extent: comparison to CIS ice charts

The CAA regional model successfully represents observed seasonal patterns of ice extent and concentration. The simulated wintertime ice cover within the CAA is densely concentrated, opening in early May in Smith Sound and Amundsen Gulf, as seen in observations (Fig. 4.1). The simulated opening of the North Water Polynya and Bathurst Polynya, as well as the polynyas in Jones Sound and Lancaster Sound, has the same timing and spatial patterns as observed. The model also represents the opening of ice along the coast of Greenland to the south.

A direct comparison of the dense ice concentrations is not possible using the CIS ice charts. The model results are plotted using the same legend, as shown in Figures 4.1 and 4.2, except for the definition of the 10/10 ice category (shown in

black). While it represents regions with 10/10 type ice concentrations in both cases, the black regions in the observation data represent landfast ice. This landfast ice is identified by analysts, who consider evidence of ice motion. This process cannot be replicated using a model. For the model results, it represents ice with 10/10 ice concentrations, without considering ice movement. However, plots of modelled ice velocity show that the simulated ice in May is motionless within the CAA channels, and is mobile in the Beaufort Sea, Amundsen Gulf and in Baffin Bay, in agreement with the CIS ice charts.

Ice plugs play an important role in ice dynamics within the CAA, but validation of the model's ability to simulate the formation of ice plugs is not possible here. While the model has the physics required to simulate ice plugs, the resolution is not high enough for explicit representation. The channels of the northern QEI are represented by 2-3 velocity points, where 10-20 are needed to resolve the damming process. Also, observations of ice plugs are subjective: identifying compact immobile ice regimes, as is done for the ice charts, depends on various kinds of indirect evidence of motion. Direct comparison is difficult. Even so, observed wintertime ice plugs (arches) in Lancaster Sound and Nares Strait, seen in the ice charts for May and June, are well represented by dense ice in the model. Also, the model has regions of very dense ice concentrations in summer, as seen in Fig. 4.2, which coincide with areas of summertime ice plugs. A plot of ice duration based on simulated ice velocities (Fig. 4.6), discussed later, confirms these regions are immobile.

The model shows less skill in representing the summertime ice cover, and underestimates the minimum ice extent. Simulated ice concentrations within the central CAA are lower than observed, as shown for July and September (Fig. 4.2). Although the central regions retain ice, with dense ice remaining in the QEI as seen in observations, the southern regions of Nares Strait, Gulf of Boothia and M'Clintock Channels are ice free by September, unlike observed. Simulated ice concentrations are also too

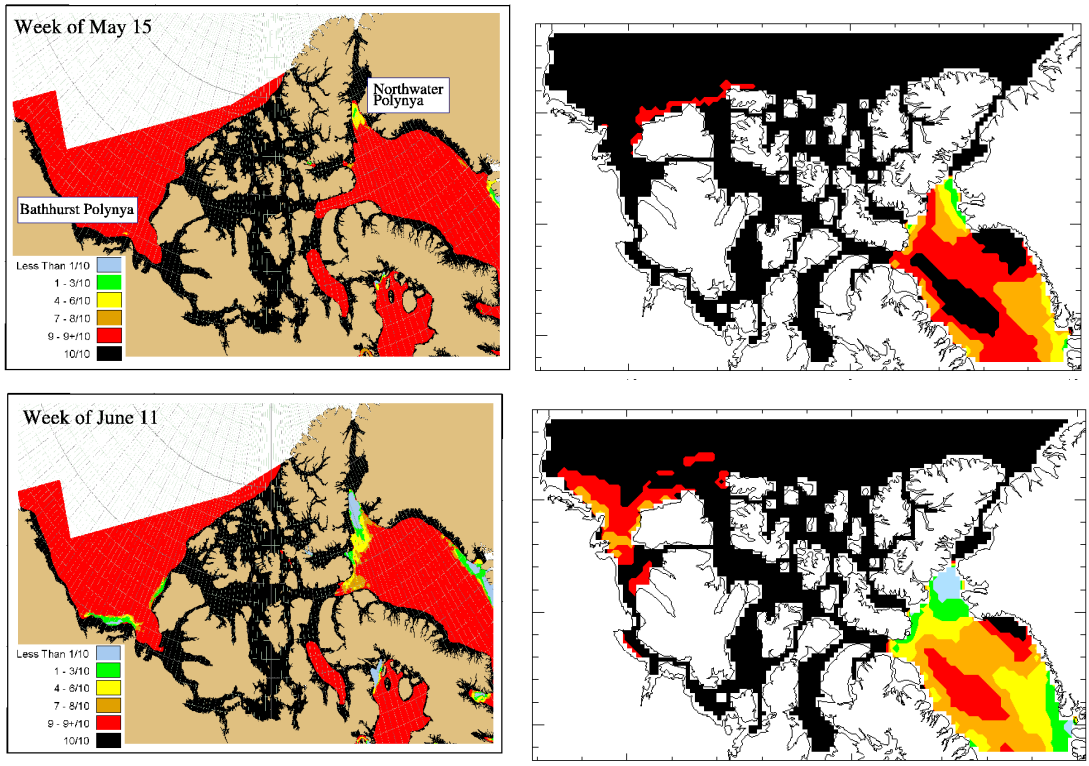

Figure 4.1: Observed (left) and modelled (right) springtime median ice concentrations (1971-2000)

low in M'Clure Strait Also, the simulated ice remains too close to the Alaskan coast, possibly resulting from model diffusion, or the lateral boundary conditions.

The discrepancies in summertime cover between observations and model results are reflected during fall freeze up (October, Fig. 4.2); in the model, the ice appears too soon along the Alaskan coast, and ice concentrations are lower in the southern channels compared to observed. Ice cover in Nares Strait has recovered to become more like observed. By November, both the observations and model have dense ice concentrations covering the CAA region as well as northern Baffin Bay. Coronation Gulf is the last region to freeze in both the model and in the CIS ice charts.

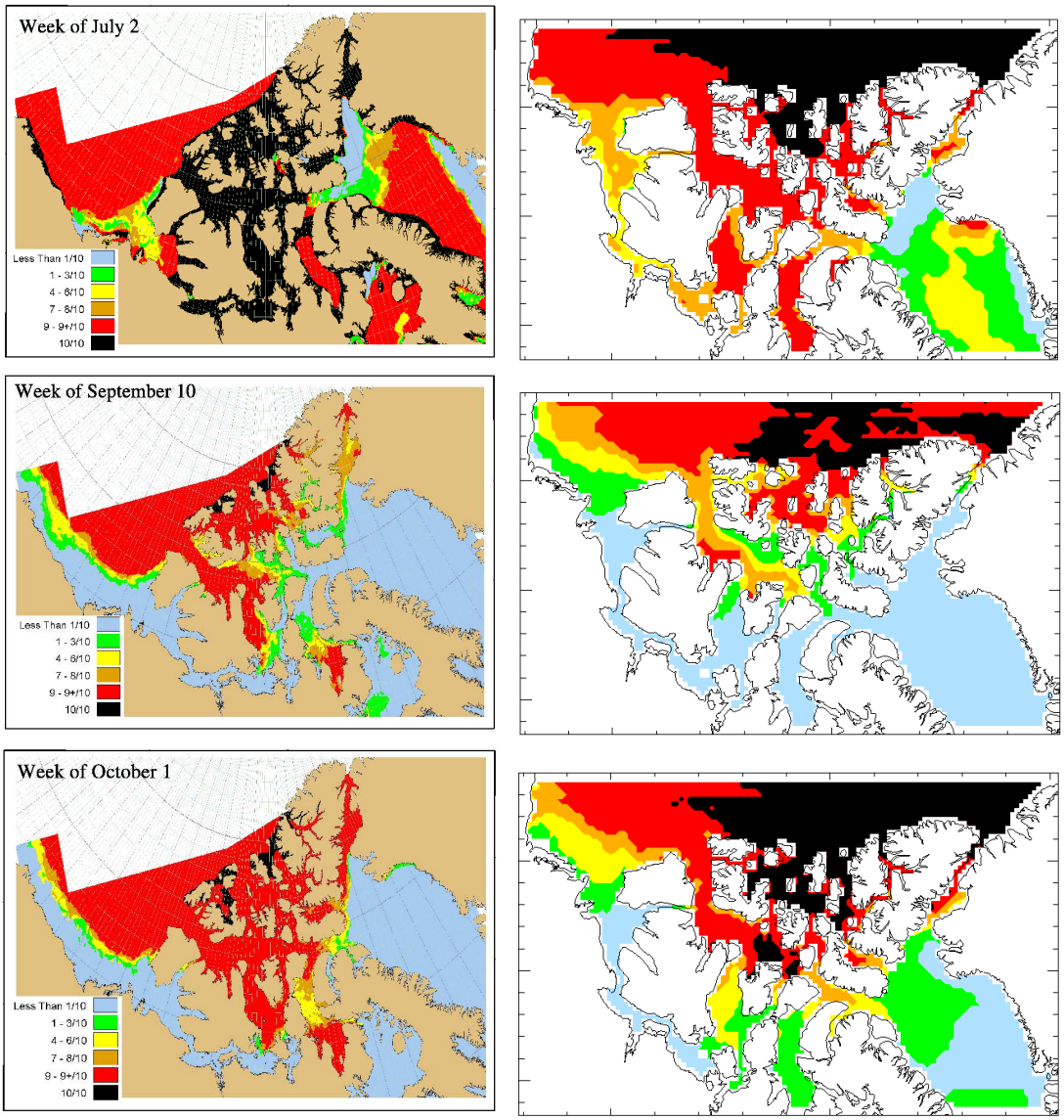

Figure 4.2: Observed (left) and modelled (right) summer and fall median ice concentrations (1971-2000)

Ice thickness and velocity

The simulated ice thickness and velocities follow the expected pattern, and are shown in Fig. 4.3. During winter, the simulated ice thickness along the northern CAA coast ranges from 4 m in the southern Beaufort Sea to 7-8 m north of Ellesmere Island, as observed (*Bourke and Garrett* 1987). The model also does well simulating ice thickness with the CAA region: ice in the QEI and M'Clure Strait is 3-4 m on average, and the southern channels have ice that is less than 2 m thick. Simulated ice is mostly immobile within the CAA, excepting Amundsen Gulf and Lancaster Sound, and mobile in the Beaufort Sea and Baffin Bay. The movement of the Arctic ice pack pushes ice into the QEI, dividing into a southwestward flow towards Alaska and a northeastward flow toward Fram Strait. Ice in Baffin Bay moves in a cyclonic gyre.

In summer, the observed ice along the northern CAA coast is thinner than in winter, ranging from 1 m in the southern Beaufort Sea to 6 m north of Greenland (*Bourke and Garrett* 1987), and is well represented by the model. The north and central regions of the CAA retain simulated ice thicknesses up to 3 m., with regions of open water in the south and east. Simulated ice velocities are largest in Amundsen Gulf, M'Clure Strait, and eastern QEI, while the central QEI has little ice motion. In early September, ice moves southward through M'Clure Strait, and the western QEI, but northward from Amundsen Gulf, eastern QEI and northern Nares Strait. The model poorly represents the ice direction in northern Nares Strait; although reversals are observed occasionally, the model indicates an average northward flow of ice where a southward flow of ice is observed. This discrepancy is a result of a coarse wind field.

Limited observations suggests that the mobile ice pack velocities within the north and central CAA ranges from 5 to 20 cm s^{-1} (4-17 km d^{-1}), with larger velocities in the east due to topographic channelling of wind. Observationally-based estimates of ice velocities do not exist for Amundsen Gulf (*Melling* 2000). The simulated ice velocities range from 3-12 cm s^{-1}, are largest in Amundsen Gulf and M'Clintock

Channel, and smallest in Nares Strait and the QEI. The spatial pattern diverges from the observations, which is expected as topographic wind channelling is missing in the model. The simulated motion of Arctic ice pack (north of the CAA) is northeastward, which is typical of summertime low conditions in the Arctic.

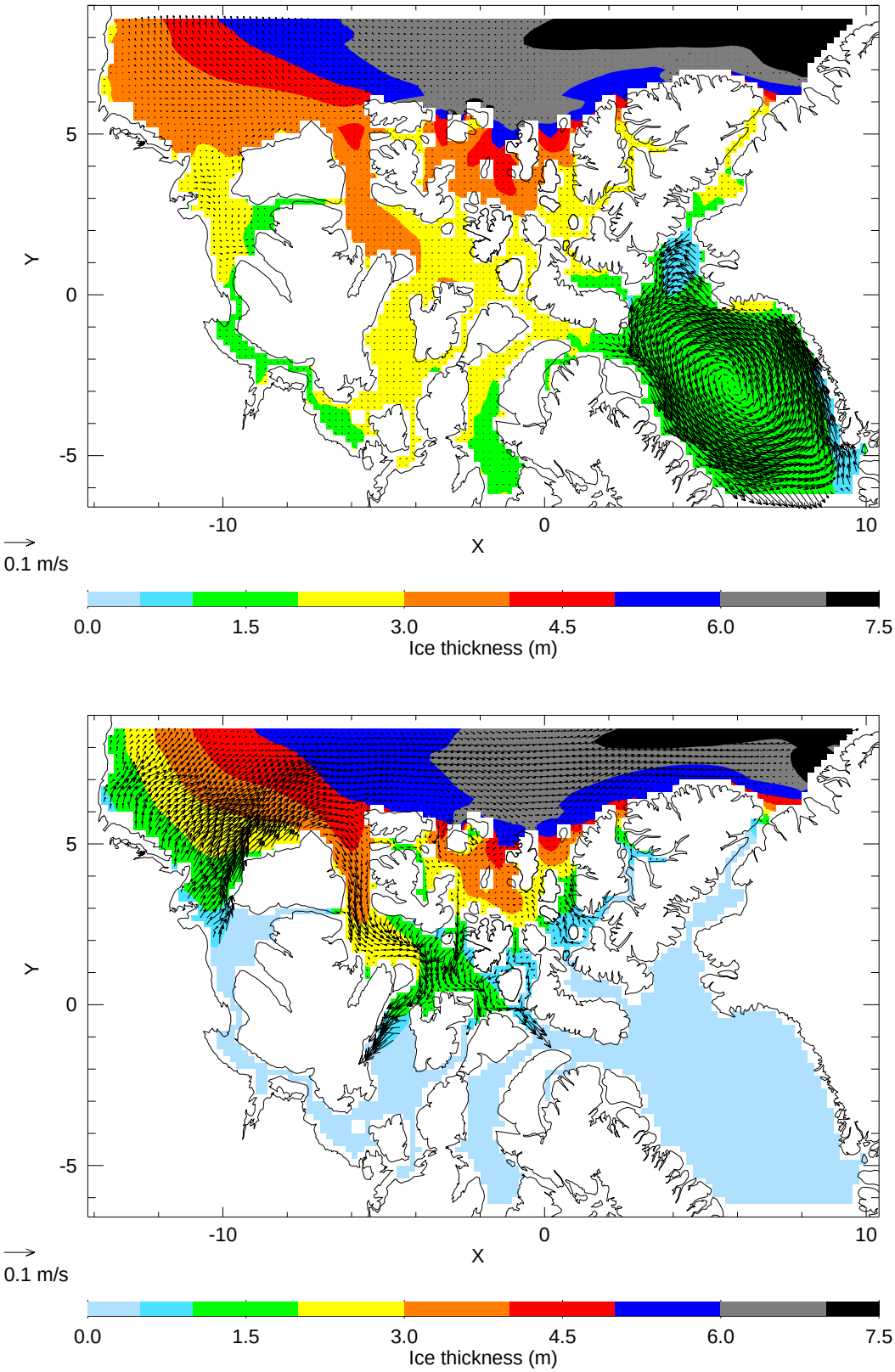

Figure 4.3: Modelled climatological (1971-2000) ice thickness and velocity for the week of May 15 (upper panel) and the week of September 10 (lower panel)

Modelled snow cover

Simulated winter snow cover within the CAA reaches 20 cm, and is thinner in north-west Baffin Bay (7 cm) and thicker on the Arctic ice pack (50 cm). The CAA snow cover melts quickly within 2 weeks in early July, with light snow cover remaining only in the central QEI. The entire CAA region has no snow cover for 5 weeks in the summer (mid-July to mid-August). The snow returns in the central regions by early September, and the entire CAA is completely snow covered by early November (1-10 cm). Although the timing and spatial patterns of seasonal snow cover is similar to observed, simulated snow thickness may be under-estimated in the eastern regions.

4.2.2 Summer duration

Predicting the length of time when the region is safe for navigation on or through the ice is important for resource planning. It is also an indicator of climate change. Recent observations suggest that the summer duration is increasing as break up is occurring earlier, and freeze up later. For indigenous people (and wildlife) this means less time spent on the ice, travelling and hunting. It could also mean more time for marine activities.

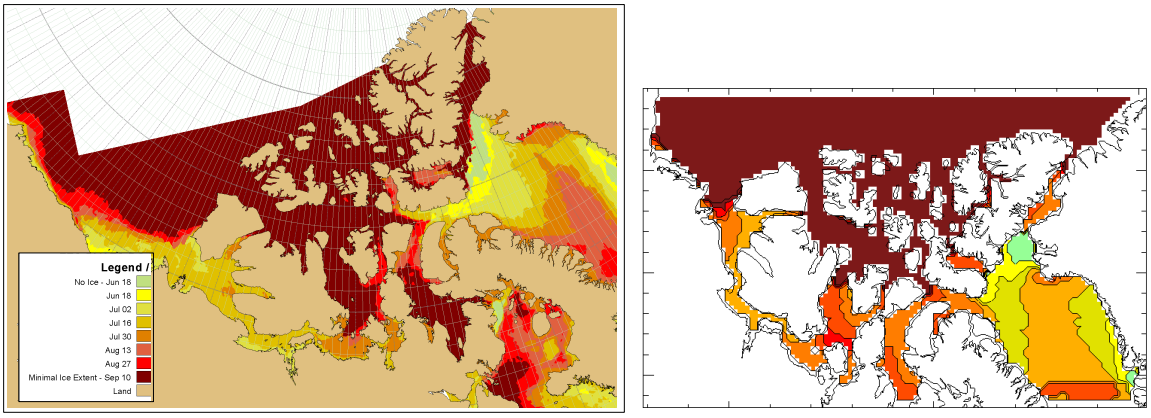

Figure 4.4: Break up dates for observed (left panel) and simulated (right panel), as based on median ice concentration of 1/10 for 1971-2000.

The measure of summer duration is dependent on the criteria used to define the

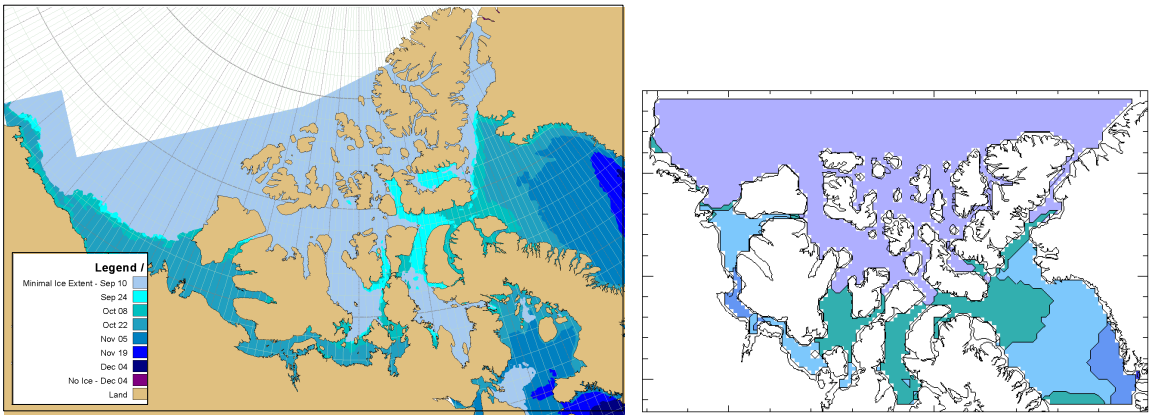

Figure 4.5: Freeze up dates for observed (left panel) and simulated (right panel), as based on median ice concentration of 1/10 for 1971-2000.

dates of break up and freeze up. To explore this dependence, summer duration is calculated three ways, based on ice concentration, ice thickness and ice velocity. Firstly, summer duration is calculated from the time the weekly median ice concentration is less than 1/10 for 1970-2001, as done for the CIS sea-ice analysis charts; associated break up and freeze up dates are shown in Fig. 4.4 and 4.5. The overall patterns agree reasonably well, although the simulated minimal ice extent (the region that does not experience break up or freeze up) extends too far south along the Alaskan coast, but not far enough in the Gulf of Boothia, M'Clintock Channel or Nares Strait. The timing of simulated break up and freeze up is similar in Amundsen Gulf, Jones Sound and northern Baffin Bay. The resulting summer duration (Fig. 4.6a) varies regionally within the model, and is less than a month in the northern interior, 2-3 months (8-12 weeks) in the south, and 4+months (16-18 weeks) in the NOW region and along the Greenland coast.

Secondly, summer duration, defined by the length of time ice thickness is less than 0.5 m, provides information about the length of time it is safe to be on the ice. It is generally longer, by up to 4 weeks in the southern interior and Baffin Bay (Fig. 4.6b), compared to the concentration based definition.

Lastly, a velocity-based definition (Fig. 4.6c) represents the duration of immobile

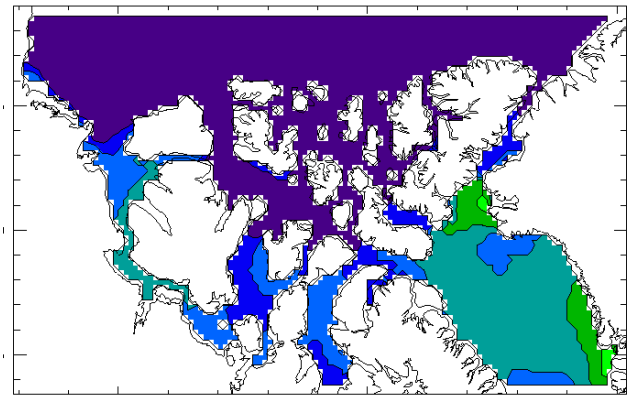

(a) Median concentration less than 1/10

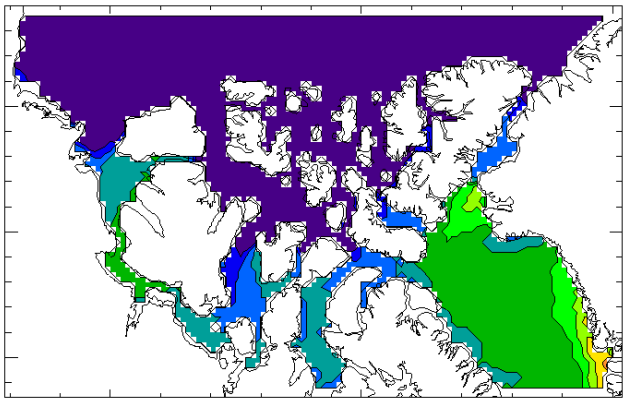

(b) Median thickness less than 0.5 m

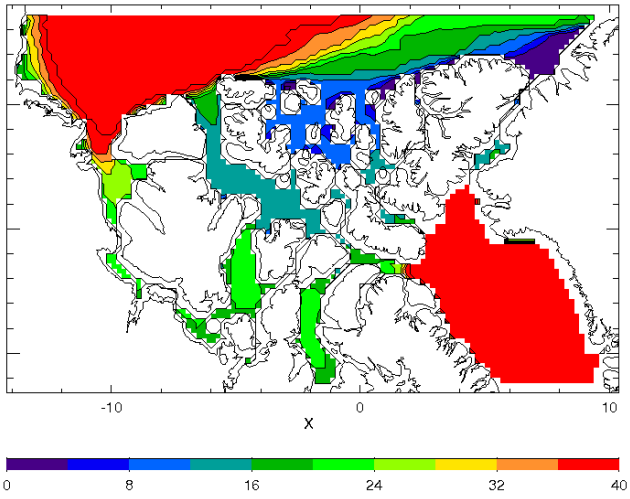

(c) Median velocity greater than 0.005 m s^{-1}

Figure 4.6: Simulated summer duration (in number of weeks) based on different criteria (1971-2000)

or landfast ice, which may be helpful to people working or travelling on the ice. For this study, an ice velocity threshold of 0.005 m/s (0.3 m/minute) is used. The simulated summer duration is very short in the northern channels with observed ice plugs, extending to several months within the QEI channels. Ice is mobile for 12-16 weeks in Viscount Melville Sound and Nares Strait, and for half the year in the southern interior channels. Ice in the Beaufort Sea and Baffin Bay, including parts of Lancaster Sound, is mobile all year.

4.2.3 Inter-annual variability in ice cover

Monthly ice extent: comparison to satellite data

The time-series of satellite-derived ice extent for each month (Fig. 4.7) provides information of seasonal variability in ice extent, as well as inter-annual variability from 1978-1999 (*Parkinson and Cavalieri* 2002). The observed ice extent remains at its maximum from November to May, after which the ice begins to retreat in June or July and continues until the time of minimum ice extent in September. October is a transitional month between minimum and maximum ice extents. The model also retains nearly complete ice cover from November to May, with ice extent decreasing in June or July. However, compared to the observations, the timing of simulated ice retreat and expansion is off slightly. The simulated ice extent suddenly drops to a minimum in August, increases slightly in September and advances to a near maximum extent in October. Although the observed minimum occurs in September, there have been two years in record (1980 and 1997) when the minimum occurred in August. The August and September extents are quite similar, in both the model and the observed.

Observed summertime inter-annual variability is captured by the model, which displays a similar range of September ice extent, as well as the early retreat and a minimum in 1998. As the winter ice cover is constant, the inter-annual variability and trends of the CAA ice extent is dominated by the summer values. All months experience a negative trend, with the largest losses observed in July and August. The annually averaged trend is -1.6%+/- 0.9 per decade (*Parkinson and Cavalieri* 2002). The comparable simulated trend is -1.23% per decade.

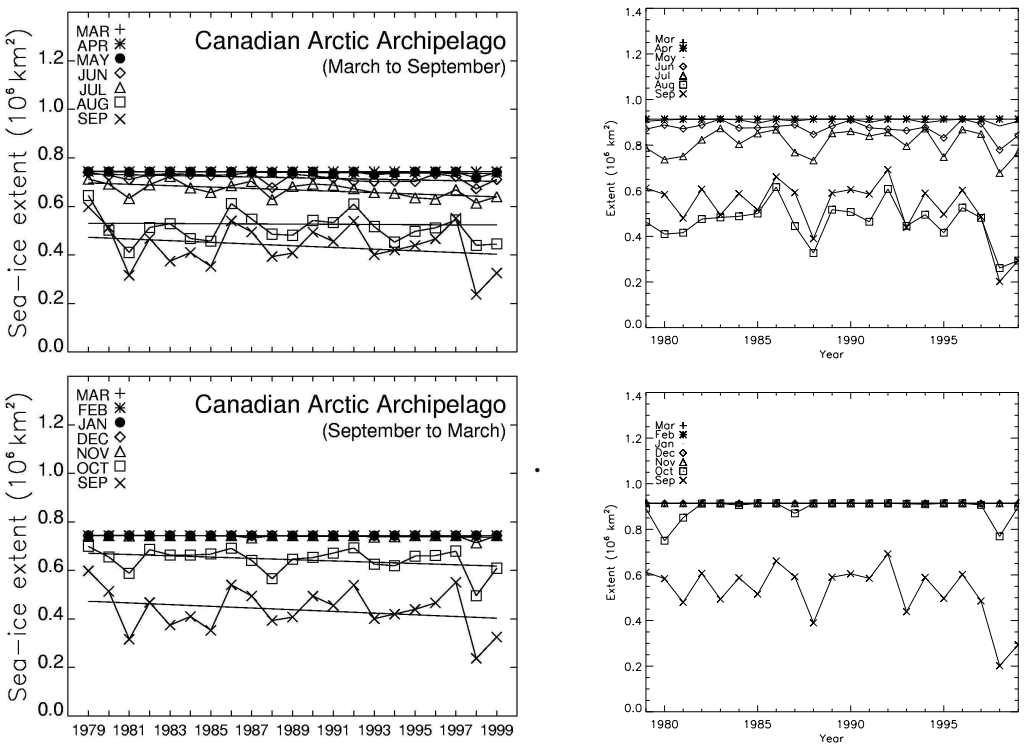

Figure 4.7: Time-series of monthly ice extents for observed (left panel) from *Parkinson and Cavalieri* (2002) and modelled (right panel) from 1979 to 1999. The ice extents from *Parkinson and Cavalieri* (2002) do not include Nares Strait.

Summertime ice cover: comparison to CIS ice charts

The model's ability to represent the summertime minimum ice cover[2] is also evident when compared to the CIS ice coverage data from 1971-2004 (Fig. 4.8). There is a strong correlation (0.71) between the model results and observations (and is statistically significant at more than the 99% level). However, the simulated trend (-10.9% per decade) is larger than observed (-3.4% per decade); this difference is significant at the 90% confidence level. Unfortunately, the time-series is relatively short and the trends are dependent on the chosen time-period. For example, the simulated trend for 1950-2004 is negative (-2.0% per decade), while both the simulated and observed ice cover trends from 1979-1997 are positive (1.1 and 7.2% per decade, respectively).

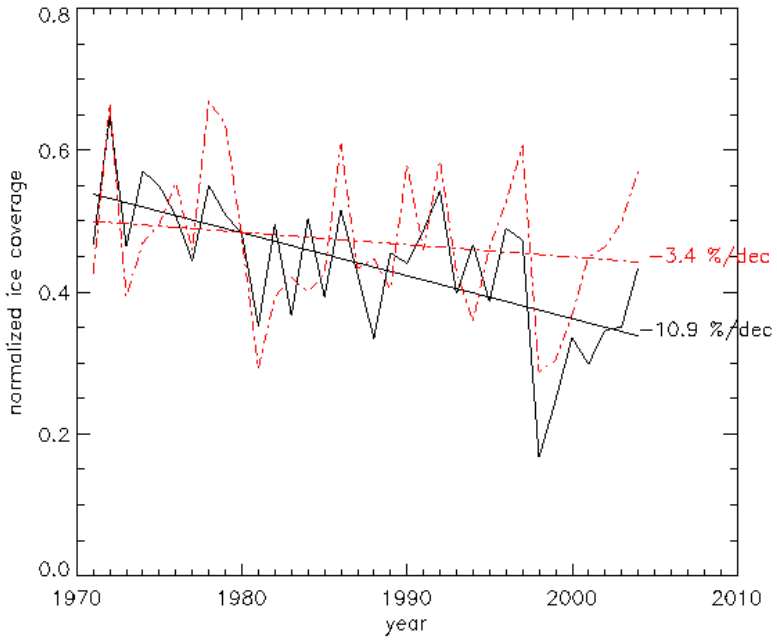

Figure 4.8: Normalized ice coverage from 1971-2004, simulated (solid line) and observed (dashed line).

The model also captures a similar range of ice coverage and timing of extreme years (e.g. light ice years of 1998 and 1981 and heavy ice years of 1997 and 1972).

[2]The week of September 10 represents the yearly minimum.

Figs. 4.9a and b illustrate the spatial variability in the simulated ice cover; ice concentrations from a heavy ice year are compared to a light ice year. Even in an extremely light year, such as 1998, ice remains in the QEI. Compared to observations (Figs. 4.9c and d), the model does well, in that 1997 has much more summertime ice cover than 1998. However, the simulated ice cover is under-represented in both years. During the heavy ice year of 1997, open water penetrates into the simulated ice cover of the central CAA, as far north as M'Clure Strait and the QEI; in comparison, the observations retain 95%+ ice cover. Similarily, most of the CAA is ice free in the model results for the light year of 1998, where more ice is retained in the observations. The model's tendency to underestimate summertime ice cover possibly increases its sensitivity to anomalously warm years, like 1998 (Fig. 4.8).

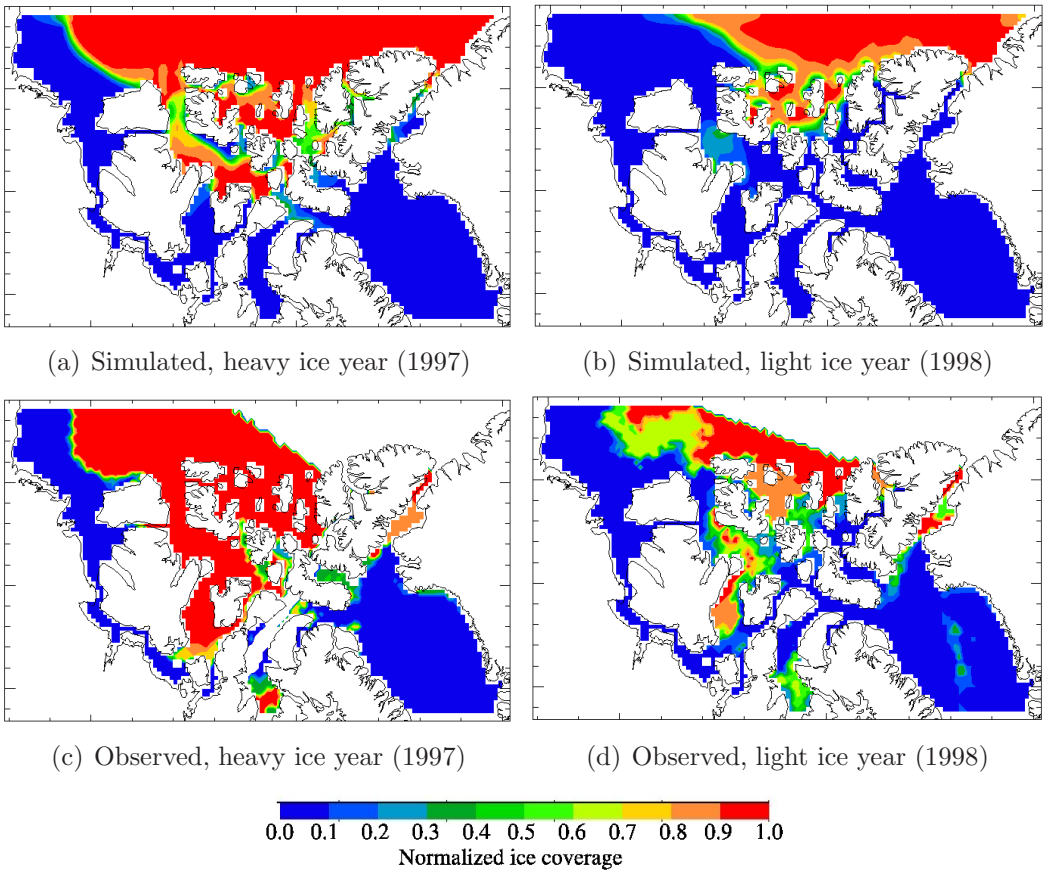

(a) Simulated, heavy ice year (1997)

(b) Simulated, light ice year (1998)

(c) Observed, heavy ice year (1997)

(d) Observed, light ice year (1998)

Figure 4.9: Normalized ice coverage for the week of September 10. White represents regions without observations.

Timing of the minimum ice cover

The timing of the observed minimum ice cover, both in concentration and extent, occurs in September. The CIS charts use the week of September 10 to represent the minimum ice cover week for their 1971-2000 climatology. From 1950-1997, the simulated minimum occurred at the end of August (Fig 4.10), but since 1998 the timing has shifted to early September. This shift is in agreement with observations, where 1998 was observed to have the latest minimum (1961-2000), which occurred the week of September 28 (*Brown and Alt* 2001).

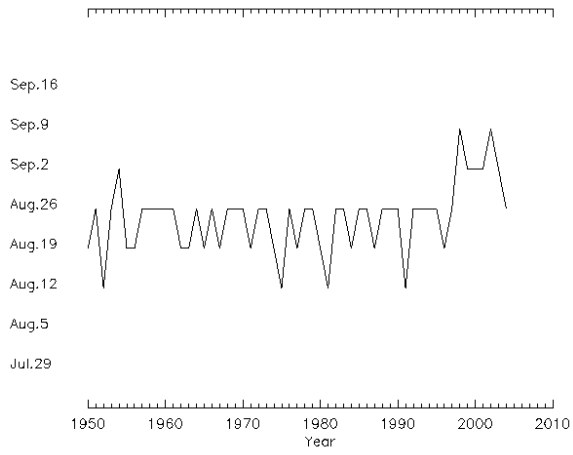

Figure 4.10: Time-series of the week of simulated minimum ice cover

Regional inter-annual variability

Observed regional inter-annual variability of ice cover within the CAA is attributed to large scale atmospheric patterns, which affect air temperatures and ice advection. The simulated sea-ice response also varies regionally (Fig. 4.11), but none of the regions have any significant trends in sea-ice from 1950-2004. However, sea-ice cover and thickness decreases slightly in the eastern regions (ie. Nares-Jones and QEI regions), and increases in the western regions of Amundsen-Lancaster and M'Clure Strait. The central regions (M'Clure and QEI) are mostly covered with perennial ice, which responds slower than seasonal ice to changes in atmospheric forcing. For

example, trends of ice area for the central regions are less than for the outer regions (Amundsen-Lancaster and Nares-Jones) with seasonal ice cover.

The regions display different patterns of inter-annual variability. The Amundsen-Lancaster region exhibits the largest variability in minimum ice area, ranging from ice-free to 30% ice covered. The remaining regions maintain a more consistent ice cover. The maximum ice thickness is also consistently maintained, but does vary in some years by up to 0.5 m.

The ice thickness in all of the regions, excepting the Nares-Jones region, display a sudden drop in minimum ice area (Fig. 4.11) and minimum ice thickness (not shown) in 1998. The maximum ice thickness also decreases, although the response is not seen immediately in the central regions. This event is connected to unusually high air temperatures from 1998 to 2002 (Fig. 4.12). After this time, the air temperatures and the ice thicknesses return back to 'normal'.

In all regions, air temperatures have been steadily increasing since 1950. Warming has occurred at a faster rate in the QEI and M'Clure Strait regions. Due to other factors influencing the ice thickness, a clear response is not seen in the ice thickness trends.

Due to the intensification of northerlies over the CAA region during positive AO conditions (e.g. 1990-1996), it is expected that the CAA air temperature would be cooler. This change in air temperature is not seen in the forcing data (Fig. 4.12), and thus associated effects on the ice is not expected.

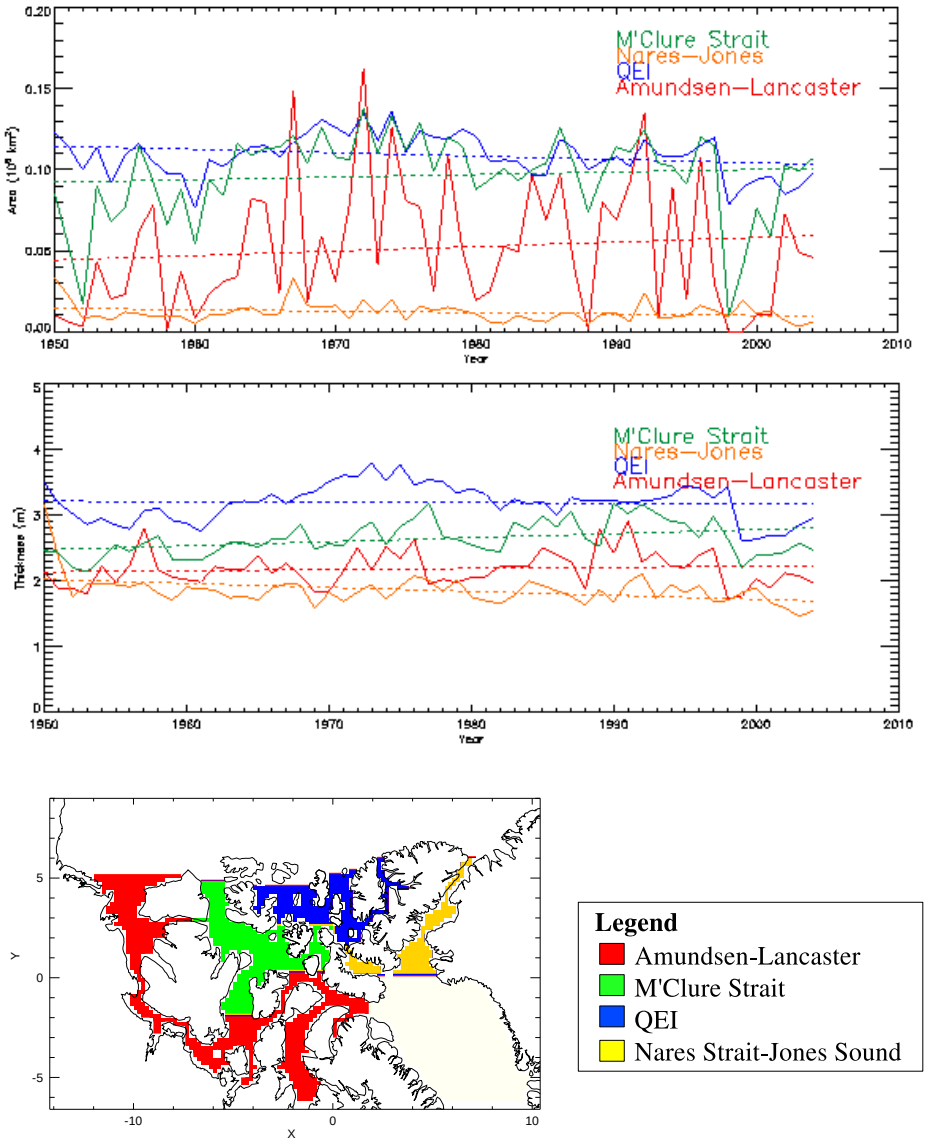

Figure 4.11: Time-series of modelled minimum ice area (upper panel) and maximum ice thickness (middle panel) for four regions. The regions are shown in the lower panel. The total area for each region (in 10^6 km^2) is: 0.43 for Amundsen-Lancaster, 0.21 for M'Clure, 0.17 for QEI, and 0.11 for Nares-Jones.

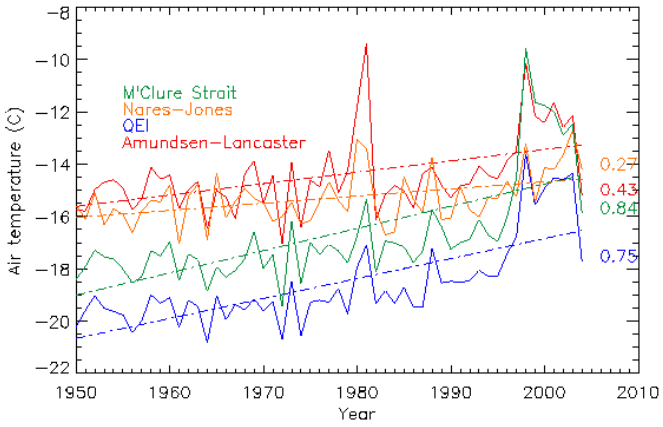

Figure 4.12: Time-series of annually averaged (forcing) air temperature for each region, as defined in Fig. 4.11. The trend in air temperature (per decade) is included.

4.2.4 Ice volume evolution: thermodynamics and advection

Advective and thermodynamic processes modify the ice cover and its associated volume. Identifying the contribution of each process provides insights into the sources of ice variability. In the model simulation, the CAA study region (as shown in grey in Fig. 4.14) experiences net (annually averaged) export and thermodynamic growth, which generally balance. Averaged over 55 years (1950-2004), the net export (-116 $km^3\ yr^{-1}$) is slightly larger than net growth (108 $km^3\ yr^{-1}$). Thermodynamic growth is anti-correlated with export in this model, with a correlation coefficient of -0.7 (statistically significant at the 99.9% level). Growth and export are inter-dependent; the export of ice results in increased ice growth to replace ice, while ice growth results in more ice available for export.

Large changes in ice volume occur during years where there is an imbalance of advection and thermodynamic growth. This occurred in 1998, when export was dominant, and in 1989, when growth was dominant. It also happens when there is net import and growth (e.g. 1974) or net export and melt (which does not happen in this annually averaged time-series). The net volume change from year to year is gradual, with the exception of the mid 1970's and the 1990's. During these times, there is higher inter-annual variability, with an unusual number of net 'import and melt' years alternating with 'export and growth' years.

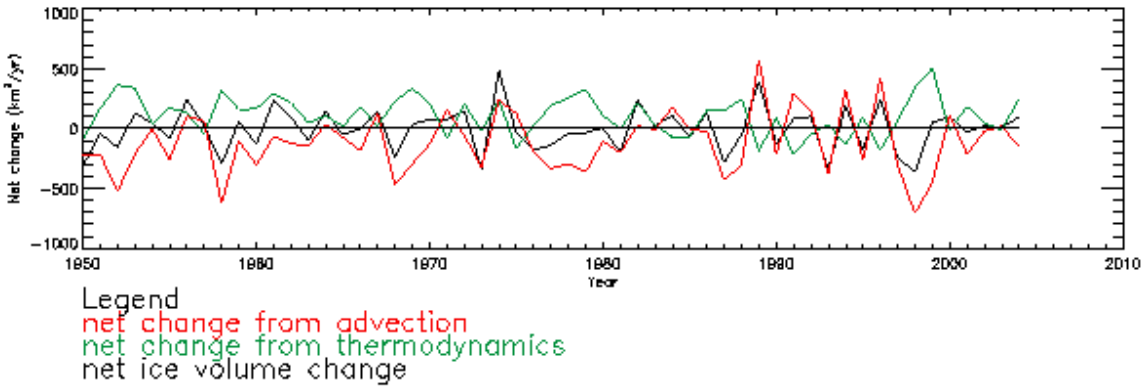

Figure 4.13: Change in modelled (annually averaged) ice volume: balance between thermodynamics and advection

4.2.5 Ice fluxes

Results

Ice fluxes through key channels (Fig. 4.14) are considered to assess the regional variability and magnitude in ice advection, and to identify channels dominating total ice volume changes. The ice volume flux through the northern boundary has very high inter-annual variability, compared to the southern boundary (Fig. 4.15). Its variability strongly effects the ice volume of CAA study region. Annually averaged, the flux through Amundsen Gulf dominates the northern boundary variability. The high import (1989) and export (1998) years shown in Fig. 4.13 are evident in the volume transport through Amundsen Gulf. The increase in alternating net import and export years of in the 1990's is also seen.

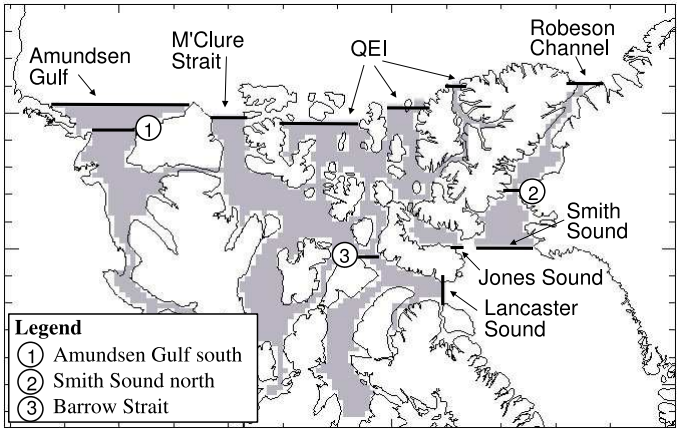

Figure 4.14: Location of gates used for model ice flux diagnostics. Grey represents the CAA study region.

Since the 1990's, there has been a slight increase in import through the QEI and M'Clure Strait, possibly indicating more open water and increased ice mobility. This may also explain the high inter-annual variability of ice through Amundsen Gulf in the 1990's.

The net fluxes averaged over the simulation run (from 1950-2004) show that, even though the ice fluxes of the Amundsen Gulf gate has large annual transports, the

Gates	Ice volume flux	Ice area flux	Ice thickness	Ice velocity
	(km^3 yr^{-1})	(10^3 km^2 yr^{-1})	(m)	(km day^{-1})
Amundsen Gulf	-40.9	-84.4	2.4	5.9
MClure Strait	78.2	19.1	3.1	2.3
Queen Elizabeth Islands	48.6	13.0	3.6	0.3
Robeson Channel	0.1	-0.1	3.2	0.1
Northern boundary	86.0	-52.5	3.1	2.2
Smith Sound	-170.0	-201.1	0.7	10.7
Jones Sound	-2.7	-3.4	1.1	0.8
Lancaster Sound	-33.0	-34.4	1.0	4.7
Southern boundary	-205.8	-238.9	0.9	5.4
Amundsen Gulf south	-6.0	-34.5	1.8	-0.1
Smith Sound north	-8.5	-10.8	0.7	-0.0
Barrow Strait	-9.4	-9.9	1.4	-0.0

Table 4.1: 55 year annually averaged ice volume and area fluxes through gates pictured in Fig. 4.14, as well as associated estimates of thickness and ice velocity. Positive (negative) values indicate import (export) into the CAA region.

years of export and import events nearly balance (Table 4.1). Hence, the averaged volume flux through Amundsen Gulf is more similar to transports through M'Clure Strait and the QEI. The M'Clure Strait and QEI experience a net import of ice, and when combined, is larger than the export from Amundsen Gulf. The simulated flux through Robeson Channel is positive, but very near zero. The resulting net flux through the northern boundary is 86 km^3 yr^{-1} (import).

Compared to northern boundary, the ice volume flux through the southern boundary is much larger (-206 km^3 yr^{-1}), mostly due to ice transport through Smith Sound. Also, all of the southern gates consistently export ice. More ice is exported from the southern boundary than is imported in from the north; hence, the CAA is a region of net ice production. This result is in agreement with *Agnew et al.* (2006).

Additional gates are included within the CAA study region (numbered in Fig. 4.14) to assess the advective contribution of three polynya regions: Lancaster Sound, the NOW region (Smith Sound) and Bathurst Polynya (Amundsen Gulf). It is expected

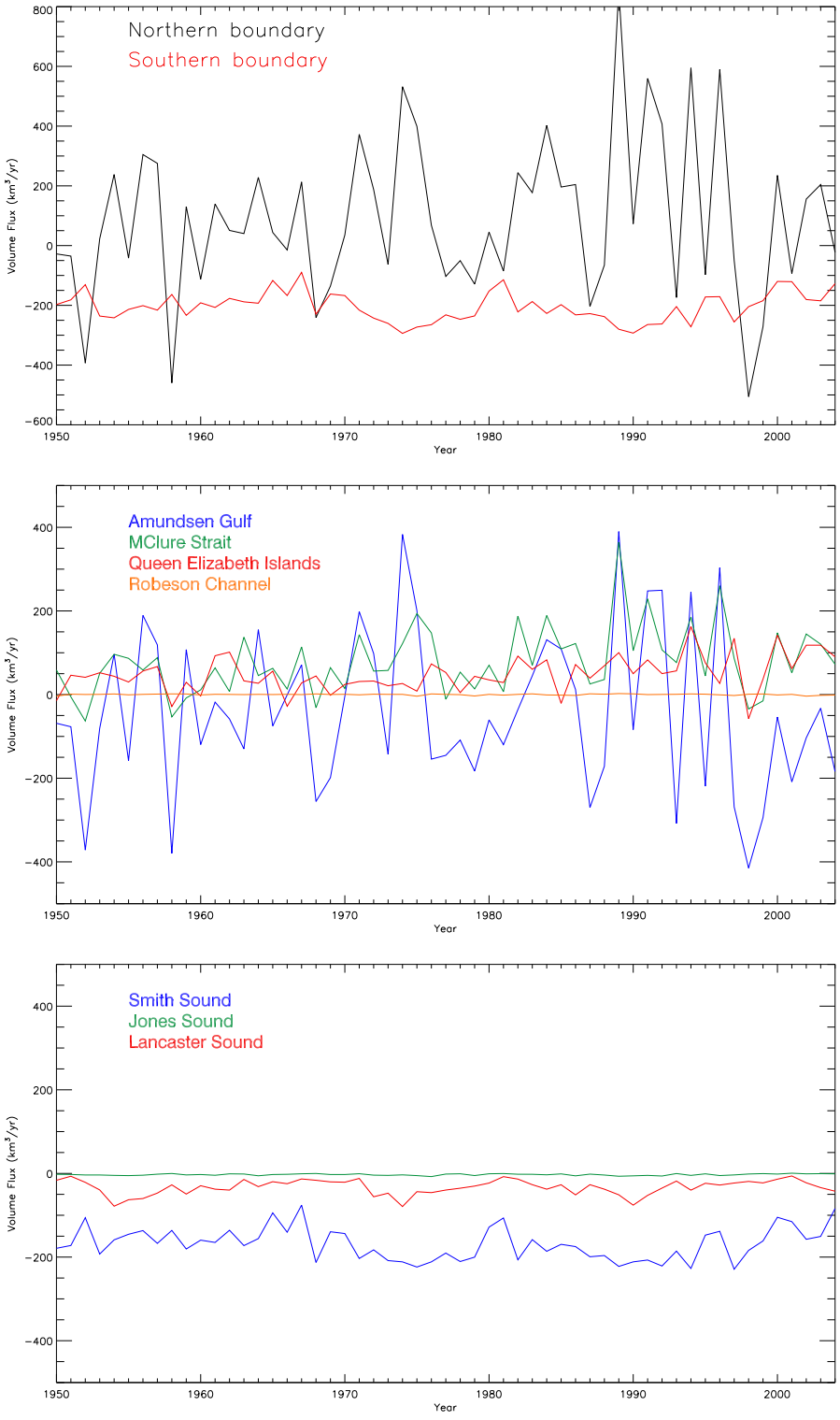

Figure 4.15: Annually averaged ice advection through gates: net northern and southern gates (upper panel), individual northern gates (middle panel), and individual southern gates (lower panel). Positive values represent import and negative values represent export from the CAA study region.

that the polynyas will be regions of high ice production, as is observed. For example, observed ice fluxes through the gates at Barrow Strait and eastern Lancaster Sound indicate that Lancaster Sound is a region of ice production. An ice bridge forms at Barrow Strait in the fall, and ice grows to replace the ice flowing out of Lancaster Sound, which remains mobile in winter. The simulated ice regime is similar, with more ice advected out of the eastern Lancaster Sound gate than in through the Barrow Strait gate. The observed net (wintertime) area flux through Lancaster Sound was 24x10^3 km^2 (*Agnew and Vandeweghe* 2005). The comparable modelled flux is 30x10^3 km^2 yr^{-1}.

Net ice production is also simulated in the NOW and Bathurst polynya regions. The volume flux through southern gate of Smith Sound is -170 km^3 yr^{-1}, and includes ice that is formed and recirculated in the NOW polynya. The northern Smith Sound gate represents the ice flow through Nares Strait, and has a much lower flux (-8.5 km^3 yr^{-1}). The situation is similar in the Bathurst polynya region. More ice is exported through the northern Amundsen Gulf gate (-41 km^3 yr^{-1}) than through the southern gate (-6 km^3 yr^{-1}). The northern gate represents polynya conditions, as well as the mobile Arctic Ocean ice pack, while the southern gate represents a landfast ice region. Consequently, the choice of gate location is very important in regions that have different ice regimes. The ice volume flux through other regions where the ice conditions are more homogeneous, such as M'Clure Strait and QEI, are less sensitive to the location of the gates.

The simulated fluxes indicate that most of the ice exported from the CAA region, into the Beaufort Sea and Baffin Bay, is generated in the polynya regions. When these polynya regions are excluded from the CAA study region, the resulting fluxes within the CAA are relatively small. Consequently, the changes in annual ice volume (Fig. 4.13) are dominated by the polynya regions, especially in Amundsen Gulf.

Dey (1981) also found that the polynya regions play a significant role in modifying

ice fluxes. The estimated ice volume flux into northern Baffin Bay, via Smith, Jones and Lancaster Sounds, was 655 km^3 yr^{-1}. This rate is much larger than the transport through the interior CAA region; the estimated net flux through Robeson Channel, Fram Sound (QEI), and Barrow Strait was 201 km^3 yr^{-1}.

Estimated ice volume fluxes

Currently, observations of ice transport are limited to area fluxes. Volume fluxes are normally estimated using the observed ice area flux, and a representational ice thickness. The skill of this method is assessed using data from the model simulation: ice area flux, ice volume fluxes, and ice thickness. It is found that the method fails under certain conditions. One example is when ice direction commonly reverses, and ice thicknesses through a gate are systematically thicker in one direction. The net ice volume may be significant, but the ice area flux nets to zero. At gates that experience large variability in ice thickness, applying a representation ice thickness will not be accurate. For example, during a warm year when ice is unusually mobile and the area flux is high, the ice will likely be thinner than usual; applying the mean ice thickness (averaged over several years) will result in overestimating the ice volume flux.

In the simulation, these problematic conditions occur at the Amundsen Gulf gate. The ice direction commonly reverses and there is high inter-annual variability in ice area and thickness. Hence, the method's skill is poor. The estimated volume flux, using the simulated ice area flux and simulated ice thickness is 203 km^3 yr^{-1}. The actual modelled ice volume flux is very different (-41 km^3 yr^{-1}). The discrepancy between area and volume fluxes (and the weighting by thickness) is also seen in the total flux through the northern boundary, where there is net export in area flux, but net import in volume flux (Table 4.1). However, in the case of the QEI, where the direction (and thickness) is more consistent, the simulated ice volume (49 km^3 yr^{-1}) is well represented by the estimated (47 km^3 yr^{-1}). The weaknesses of this method to represent ice volume fluxes is an important consideration when comparing and

assessing estimated ice fluxes in the CAA.

Daily variability in ice volume flux

Daily (simulated) ice volume fluxes illustrate the short-term ice behaviour. Advective events are sudden and intense, with many reversals in direction (Fig. 4.16). The modelled ice volume flux in Amundsen Gulf has the largest daily transports (10,000 km^3 yr^{-1}) and inter-annual variability of all the gates. It experiences perennial ice in some summers but not others, it is landfast some winters but not others, and the ice direction often reverses. The ice at Amundsen Gulf gate remains mobile during most years. M'Clure Strait experiences less daily transport (20,000 km^3 yr^{-1}) but has a similar advective pattern. Ice at the QEI, Robeson Channel and Jones Sound gates is landfast during winter, while ice at Lancaster Sound gates remains mobile. Barrow Strait (not shown) is similar to Jones Sound, in terms of magnitude and mobility, but experiences more import events.

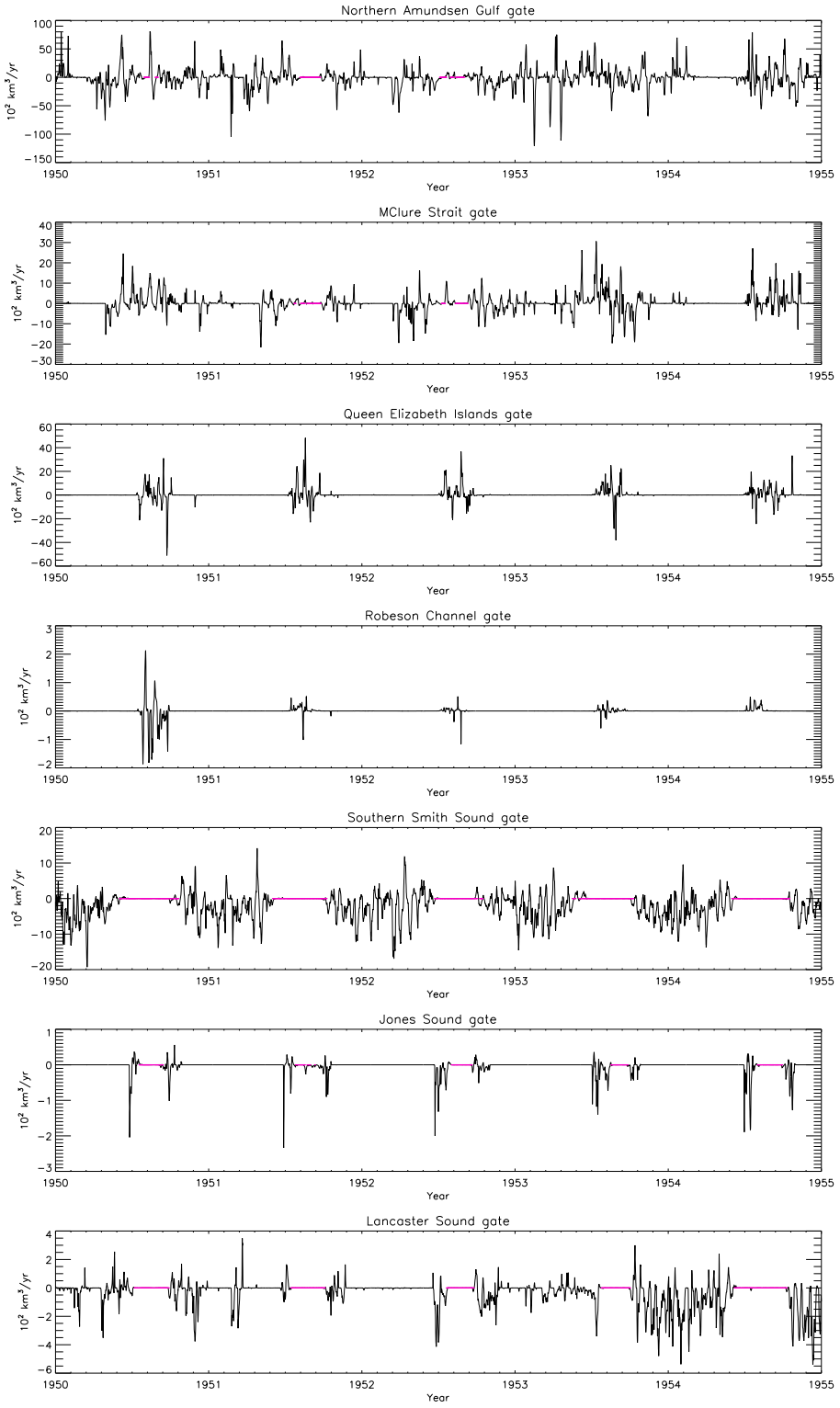

Figure 4.16: Daily ice volume flux through selected gates, 1950-1955. Pink represents open water conditions.

Source	*Kwok* (2006)			Model		
	Volume	Area	Thickness	Volume	Area	Thickness
	$km^3\ yr^{-1}$	$10^3\ km^2\ yr^{-1}$	m	$km^3\ yr^{-1}$	$10^3\ km^2\ yr^{-1}$	m
Amundsen south	-85	-85	1.0	-97	-130	1.1
M'Clure north	-80	-20	4.0	54	2	2.0
QEI north	27	8	3.4	72	11	3.6
NET	-138	-97		29	-117	

Table 4.2: Modelled and observed ice fluxes through the northern gates, 1998-2002. The ice volume flux from *Kwok* (2006) is estimated, using the observed ice area flux and an average (representational) thickness, as shown.

Comparison to observations

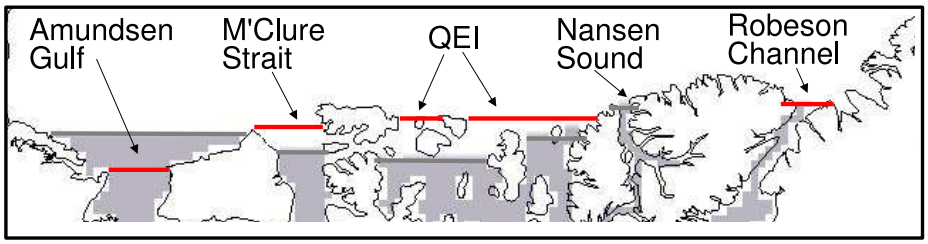

Figure 4.17: Location of gates used for model-observation comparison. Red gates are used for comparison. Grey gates define the northern edge of the CAA study domain.

Northern Channels

Simulated ice area fluxes through the northern boundary (Fig. 4.17 compare well to observations (*Kwok* 2006), in terms of the magnitude and the net flux (Table 4.2). The model does particularly well in the QEI channel. However, the simulated ice area flux through Amundsen Gulf is larger than observed, and M'Clure Strait flux is positive (import) instead of negative. Considering that the northern boundary ice fluxes experiences large variability, in both the observations and the model, discrepancies are not unexpected.

Observed inter-annual variability for 1998-2002 (*Kwok* 2006), as well as winter-time estimates for 2003-2004 (*Agnew et al.* 2006), are compared in Fig. 4.18 (top panel). The simulated ice area flux has a similar range of variability and timing of extreme years. The model captures the import conditions at QEI, export conditions

at Amundsen Gulf and reversals at M'Clure Strait. It also simulates increased export in 1998 (although overestimated) and decreased export in 2000.

The volume fluxes[3] reflect the area flux variability (middle panel, Fig. 4.18) but the modelled volume flux tends to overestimate the (observationally based) estimated import. This discrepancy is attributed to poor representation of the fluxes by the model, but also to the assumptions used to estimate the volume fluxes.

To demonstrate the ability of the estimated ice volume flux to represent the actual flux, an estimated flux is calculated (with the simulated ice area and the representational ice thickness, as used previously). The estimated flux is compared to the simulated ice volume flux (Fig. 4.18, lower panel). A similar bias exists. The simulated import is larger than estimated, suggesting limited skill in representing volume fluxes using this method. It also shows that the representational ice thickness is more accurate in some years (e.g. 1998) than others (2002).

The simulated ice area flux in northern Nares Strait (Robeson Channel) is near zero (net export of -0.2 x10^3 km^2 yr^{-1}, 1996-2002), and is too low compared to estimates (16 to 48x10^3 km^2 yr^{-1}) by *Kwok* (2005). The discrepancy in ice movement is attributed to the coarse wind forcing, which is mostly northward over the channel. In addition, the ice velocities are much weaker than observed, and the very narrow strait is poorly resolved in the model.

[3]The observed volume fluxes are calculated using the observed area flux and a representation ice thickness. The representational ice thicknesses are taken from *Agnew et al.* (2006), and are 1.0 m for Amundsen Gulf, 2.0 m for M'Clure Strait and 3.4 m for QEI. The same values are used by *Kwok* (2006), except he adopts 4.0 m for M'Clure Strait.

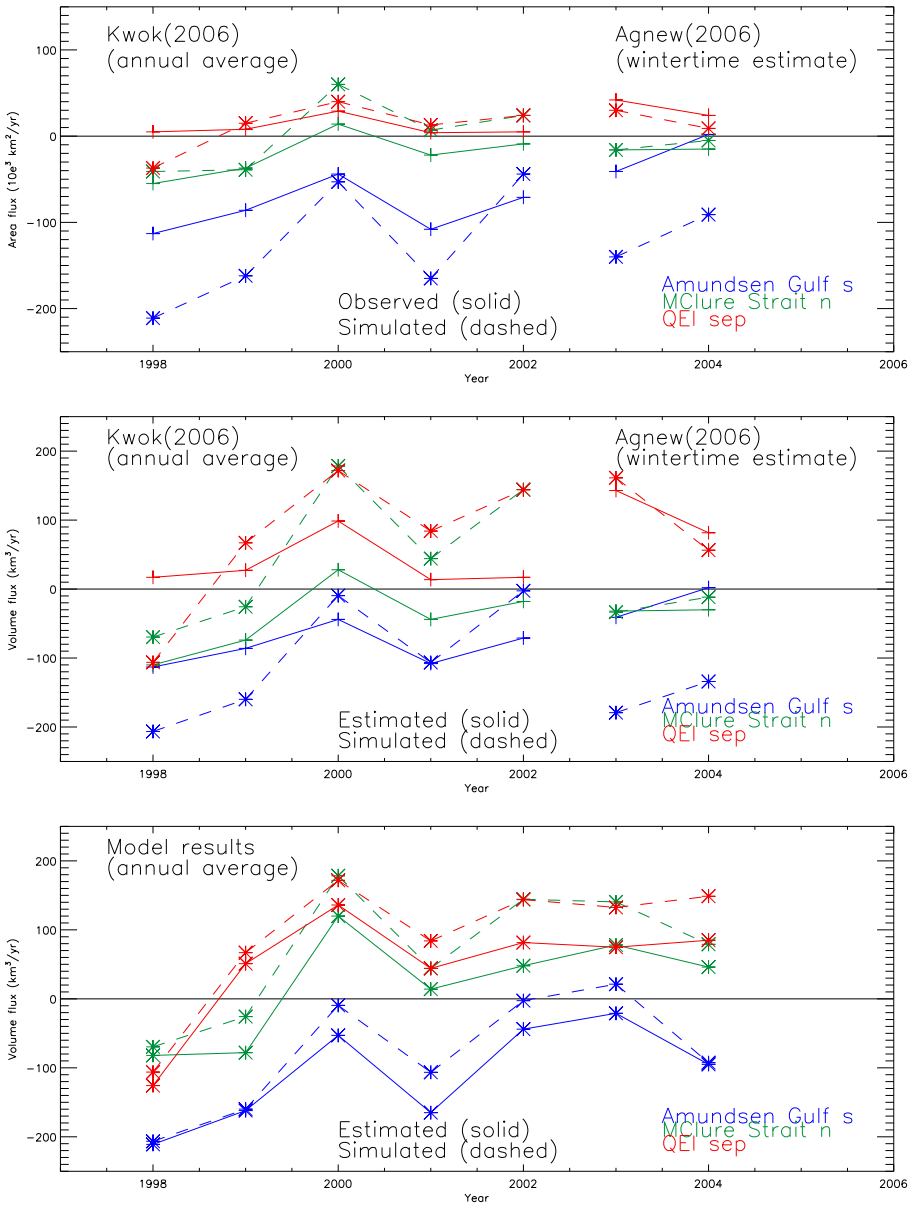

Figure 4.18: A model-observation comparison of ice fluxes through three northern gates: ice area fluxes (top panel), and ice volume fluxes (middle panel). The simulated ice volume flux is compared to an estimated volume flux, described in the text (lower panel).

Southern Channels

Simultaneous year-round observations of ice flux through the southern channels of the CAA do not exist. Estimates were made using ship, aircraft or satellite-based data, and range from 655 km^3 yr^{-1} (*Dey* 1981) to 220 km^3 yr^{-1} (*Sadler* 1976). *Dey* (1981) estimated 126 km^3 yr^{-1} through Smith Sound, 47 km^3 yr^{-1} through Jones Sound and 482 km^3 yr^{-1} via Lancaster Sound. *Sadler* (1976) estimated the flux in Lancaster Sound to be 110 km^3 yr^{-1} and made the assumption that flow through Lancaster Sound represented half of the flux into Baffin Bay. *Dunbar* (1973) estimated the ice flux through Smith Sound to be 75 km^3 yr^{-1}.

In comparison, the simulated net ice volume flux is 202 km^3 yr^{-1} (for 1950-2004). The average flux through Smith Sound is 168 km^3 yr^{-1}, through Jones Sound is 3 km^3 yr^{-1} and through Lancaster Sound is 33 km^3 yr^{-1}. Other than Smith Sound, ice volume transport is under-represented by the model. Simulated ice flux through narrow straits (such as Jones and Lancaster Sound) may be unrealistically limited by inadequate model resolution or coarse wind forcing. The discrepancy between the observations and the models can also be attributed to inter-annual variability. During the observational time period of the mid-1970's, the simulated flux in Lancaster Sound was 80 km^3 yr^{-1} (in 1974) and in Smith Sound was 76 km^3 yr^{-1} (in 1967). Also, transport rates are dependent on the exact gate location.

More recently, *Agnew et al.* (2006) estimated wintertime fluxes during 2002-2003 (Table 4.3), and these are compared to the model results. The area flux for Lancaster Sound is nearly the same, but the model overestimates the flux through Smith Sound (north) and underestimates the flow through Jones Sound. As seen in the comparison with the *Kwok* (2006) fluxes, the model is in better agreement with the area fluxes than the volume fluxes. The representational ice thicknesses may be too thick, as the model's ice thickness for 2003-2004 (annually averaged) is less than 0.8m.

The winter ice of the CAA region is mostly immobile when the AO pattern is

Source	Model			Agnew(2006)		
	Volume	Area	Thickness	Volume	Area	Thickness
	$km^3\ yr^{-1}$	$10^3\ km^2\ yr^{-1}$	m	$km^3\ yr^{-1}$	$10^3\ km^2\ yr^{-1}$	m
Smith Sound north	-16.6	-21.0	0.5	-9.5	-9.5	1.0
Jones Sound	-0.7	-1.0	0.8	-17.2	-11.5	1.5
Lancaster Sound	-47.9	-52.5	0.6	-75	-50	1.5
Net	-32.0	-74.5		-101.7	-71.0	

Table 4.3: Modelled and observed ice fluxes through southern gates, 2002-2003

the most dominant. However, it is expected that the mobile ice (both in winter and summer) is influenced by the changes in atmospheric circulation. Simulated ice flux variability is found to be correlated with the AO index. Annually averaged fluxes from 1950-2004 at all gate locations except Robeson Channel are positively correlated with the AO index and have R values greater than 0.35. The correlation is time-dependent, with higher correlations after 1977. There is very little discussion in the literature regarding the dependence of CAA ice fluxes on atmospheric variability, but observations and modelled ice fluxes through Fram Strait are also more correlated with the NAO after 1978 (*Mysak et al.* 2005).

4.2.6 Site comparison

The ability of the model to represent specific locations is also of interest in terms of assessing local climate change. Simulated ice at six coastal sites (Fig. 4.19) is compared to CIS data and 1-d model results (*Dumas et al.* 2006a) for 1970-1989. The observations and 1-d model represent landfast sea-ice at coastal locations. The CAA model, on the other hand, does not resolve the coastal landfast ice that forms in small bays; so, a direct comparison is not possible. However, the simulated ice does represent the mid-channel ice, most of which is also landfast in winter. It is expected that the coastal and mid-channel landfast ice would have similar seasonal cycles and maximum ice thicknesses; the differences will be more evident in summer. The coastal landfast ice would be thinner and experience a longer summer duration.

Consequently, the 1-d model results will be more like observations because the model represents the coastal landfast ice, is forced with observed atmospheric data from each site, and does not include ice dynamics.

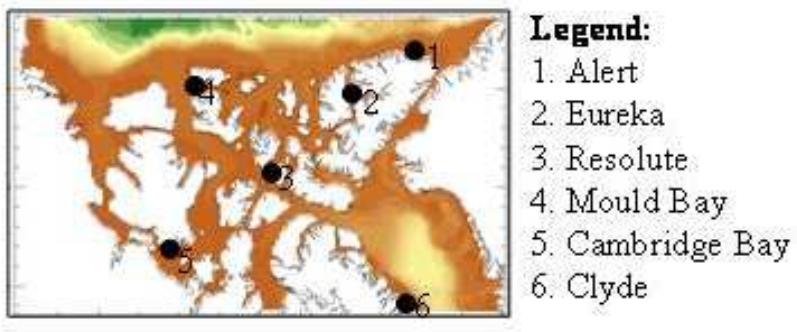

Figure 4.19: Location of coastal stations chosen for comparison with the CAA model

The CAA model does well in reproducing the seasonal cycle (Fig. 4.20), except at the Alert and Mould Bay sites. Alert is located within a small bay that is not resolved by the model. The simulated ice thickness represents the adjacent offshore pack ice, which is thicker all year. A similar situation exists at the Mould Bay site. In addition, the simulated ice thickness at the Mould Bay site experiences a second maximum in late summer, caused by ice import. While seasonal ice is observed the coastal sites, the simulated ice is perennial. The simulated maximum ice thickness (at Alert and Mould Bay) has a higher inter-annual variability than the observations (Table 4.4), as the maximum ice thickness varies from 2-4m.

At the remaining four sites, the simulated wintertime ice thickness compares well to observations and the 1-d model results. In summer, ice-free conditions are observed at all of the sites. In the model, Clyde and Cambridge Bay are ice-free in the summer, but ice remains at Eureka and Resolute. It is possible that the adjusted air temperature forcing remains too cold, or that the model represents the mid-channel conditions accurately. At Cambridge Bay, the model does very well in simulating the seasonal cycle and open water duration. As expected, the 1-d model generally

Stations	Observed		CAAmodel		1d-model	
	(m)	(σ)	(m)	(σ)	(m)	(σ)
Alert*	1.95	0.22	3.71	0.62	2.13	0.16
Eureka	2.30	0.18	2.44	0.11	2.42	0.17
Mould Bay	2.04	0.17	3.27	0.72	2.03	0.19
Resolute	2.06	0.21	2.27	0.08	2.09	0.25
Clyde	1.76	0.23	1.78	0.31	1.96	0.24
Cambridge Bay	2.15	0.19	2.10	0.10	2.33	0.10

Table 4.4: Observed and simulated maximum ice thickness and standard deviation (σ) for 1970-89. (* Observed data is not available for year 1988).

performs better than the CAA model.

Simulated snow thickness (not shown) compares well to observations at Alert and Cambridge Bay, but is underestimated (by half) at the other sites. At all of the sites, the snow inter-annual variability is low; this is expected as the regional model is forced with climatological precipitation. However, snow cover is also dependent on air temperature and ice advection. For example, the simulated snow cover at the Mould Bay site is anomalously light due to the high ice velocities and warm air temperatures of 1998.

The pattern of seasonal ice movement varies at each site (Fig. 4.21) and represents different ice regimes. In the model, the sites within the CAA islands experience landfast ice conditions in winter. Alert is landfast nearly all year. Eureka, Mould Bay and Resolute have longer periods of ice movement with faster velocities. Cambridge Bay experiences mobile ice during summer and fall, with open water in August. In Baffin Bay, ice at Clyde is mobile all year.

The timing of simulated break up and freeze up[4], and the associated summer duration, is also compared to observations. Break up and freeze up is observed at all of the selected sites. In the CAA model, most of the stations experience break up and freeze up during 1970-1989, except for Alert and Mould Bay[5]. There is a

[4]Break up occurs when ice thickness becomes less than 0.5 m and freeze up occurs when ice becomes greater than 0.3 m thick.

[5]Mould Bay does experience break and freeze up in the model at other times.

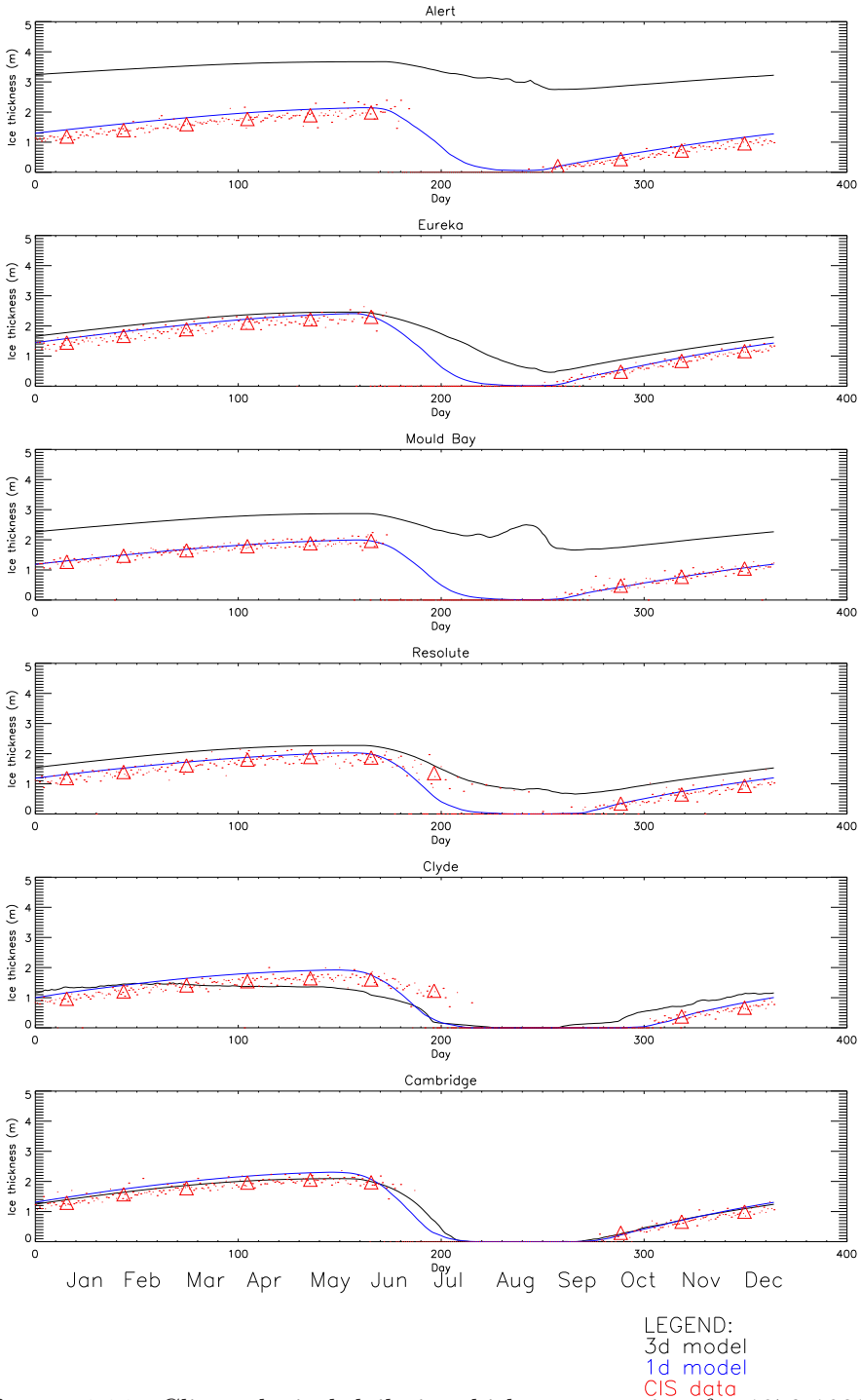

Figure 4.20: Climatological daily ice thicknesses at sites for 1970-1989

Stations	Observed			CAAmodel			1d-model		
	days	σ	years	days	σ	years	days	σ	years
Alert	70	20	13	0	0	0	63	11	17
Eureka	103	9	17	31	10	10	69	9	19
Mould Bay	94	18	12	0	0	0	76	11	19
Resolute	104	15	14	14	18	3	87	11	19
Clyde	150	18	17	96	15	20	123	14	19
Cambridge Bay	122	16	20	91	7	20	100	9	19

Table 4.5: Observed and simulated mean summer duration, standard deviation (σ) and the number of years break up and freeze up occurred during 1970-89.

large range in dates, but the break up and freeze up 'seasons' are clearly defined (Fig. 4.22). The models do a fair job representing the freeze up dates, but simulated break up is delayed. Simulating break-up is difficult. Break-up is dominated by wind and associated ice advection off shore. The CAA model does not resolve the coastal landfast ice region; it is also forced with coarse wind and air temperatures. Although the 1-d model is forced with observed daily forcing, it is missing ice dynamics and so cannot represent either wind-forced break-up, or the replenishment of ice from offshore. Also, observations will be biased towards earlier break up dates as ice melts first along the shore, and its break up does not represent off-shore conditions, which retain ice longer into the season and are being modelled here. It is therefore not unexpected that simulated break-up is delayed, in comparison to observations, in both models. Also, because of transport of ice from offshore, break up (and freeze up) occurs less often in the CAA model, than in observations or the 1-d model. Hence, the simulated summer duration is under-estimated in the CAA model (Table 4.5).

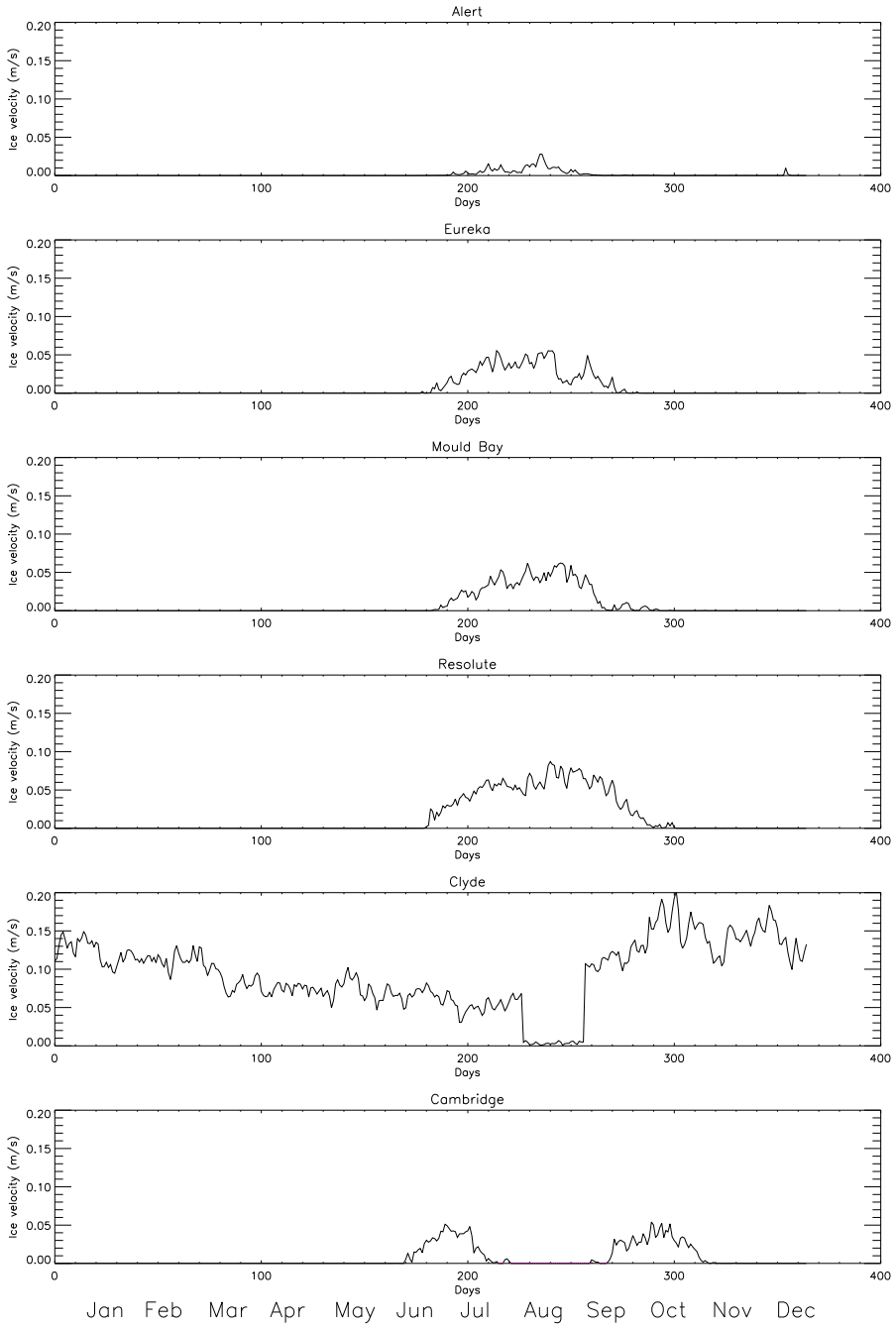

Figure 4.21: Climatological daily ice velocities at select sites. Ice velocities for ice with zero thickness are set to zero.

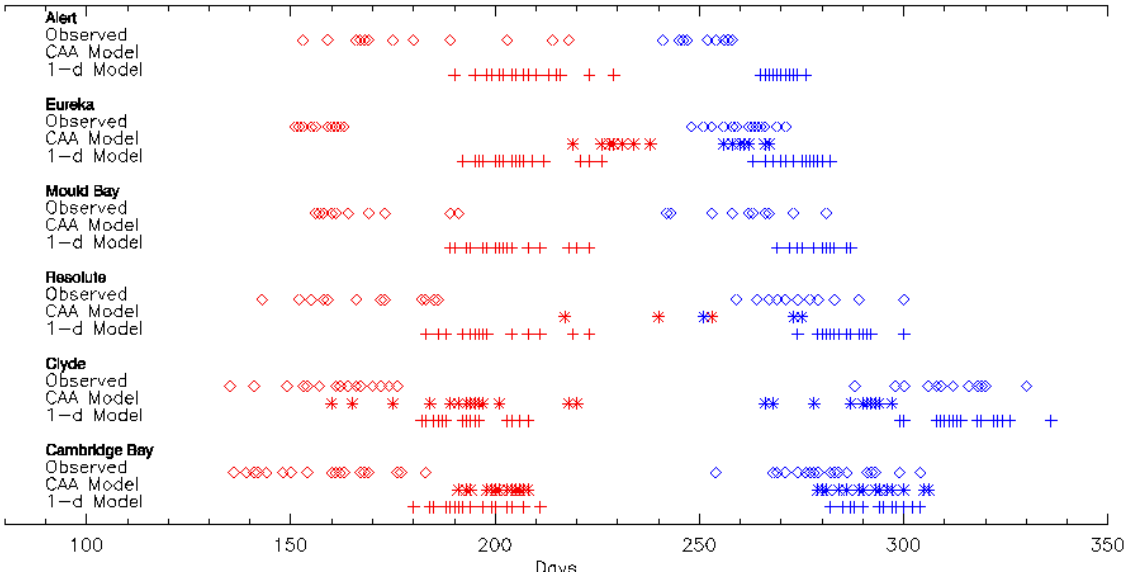

Figure 4.22: Dates of break up (red) and freeze up (blue) for each site (1972-1990), comparing observations (diamonds), CAA regional model (asterix) and 1-d model (plus).

Chapter 5

Modelled results, 2041-2060

5.1 Anticipated future CAA ice conditions

Before considering the model results, speculation of the sea-ice behaviour in a warmer climate can be made based on the current understanding of the CAA ice processes. The northern ice plugs will likely weaken, permitting more heavily ridged multi-year ice to enter the CAA from the Arctic Ocean. The ice can be expected to transit more quickly through the QEI, resulting in less melt time and stronger, thicker ice entering Parry Channel or Jones Sound. Encounters with such ice would make navigation through the Northwest Passage more hazardous than now (*Melling* 2002). This may continue until the Arctic ice retreats and the influx of multi-year ice into the western channels of the CAA ceases (*Howell et al.* 2007). However, observations of ice fluxes from 1997-2002 showed an export of ice into the Arctic (from M'Clure Strait and Amundsen Gulf) (*Kwok* 2006). This suggests that the clearing of ice from these channels could occur sooner, depending on the future wind regime. Lastly, the impact of increasing ice melt on the freshwater budgets of Baffin Bay is considered minimal. The total freshwater export would remain the same, although the ratio of ice to oceanic freshwater would change (*Melling* 2002).

Although most global climate models (GCMs) do not resolve the channels of the CAA region, they can provide a sense of possible ice conditions. Generally, GCMs

project enhanced high latitude warming with decreased ice cover in the Arctic. Even though projections of ice cover vary among models, the CAA region consistently remains ice covered in the simulations. *Walsh and Timlin* (2003) compared results from five models for 2070-90. The modelled March ice extent for the Arctic Ocean remained similar to ice cover observed today, while the simulated September ice extent ranged from the present-day ice extent to an ice free Arctic. Three of the models retained ice cover in summer along the CAA coast (above Ellesmere Island). All of the models showed a significant retreat of ice in the western CAA, indicating navigational possibilities through the Northwest Passage (*Walsh and Timlin* 2003). A multi-model mean for 2080-2100 (*IPCC* 2007) shows September sea-ice in the central Arctic Ocean and along the CAA coast, with more ice cover than those models compared by *Walsh and Timlin* (2003). In a model which loses most of its summer ice cover by 2040-49 (*Holland et al.* 2006), the persistence of ice in the CAA region is evident; it was the only region to retain September ice cover. Ice is persistent in the north of the CAA region because future Arctic Ocean atmospheric circulation patterns in the GCM's remain similar to present day (*ACIA* 2005), where ice is pushed up against the northern coast of the CAA and Greenland, and continues to supply ice to the CAA region. Continental affects, including the predominance of land in the CAA and the nearby glaciers and ice sheets, may also play a role in retaining a cold and ice-favourable climate into the future.

GCMs also predict thinner ice in the CAA region; in another study, three of the four models considered showed that ice near the CAA region was thinner (by up to 1 m) in 2041-2060 from 1971-1990 (*IPCC* 2001). Although dynamics modifies ice thickness and influences interannual variability, future thinning in GCM's is attributed to thermodynamic processes (*Holland and Bitz* 2003).

Considering the GCM results, and the observed tendency of the CAA to retain ice, it is expected that ice will be present, albeit thinner, in the future run of the

CAA regional model. This chapter describes the climatological change in simulated ice cover from 1970-89 (hereafter referred to as the 'past') compared to the 2041-2060 ('future') time-period.

5.2 Simulated changes in the future CAA ice

5.2.1 Seasonal ice cover

Ice concentration

Future wintertime ice concentrations are similar to the past conditions, but differences are evident in the spring when the simulated ice opens up earlier in the Amundsen Gulf, Beaufort Sea and Baffin Bay regions (Fig. 5.1). The July future ice concentrations are less throughout the CAA interior (not shown), and in September, there is more open water in Parry Channel and around Ellesmere Island, compared to the past (Fig. 5.2). Also, the Alaskan coast (southern Beaufort Sea) is ice free where ice existed in the past. Regions of 10/10 ice concentrations, which represent possible ice plug conditions, still exist north of the QEI and Nares Strait in summer but are not as widespread as in the past.

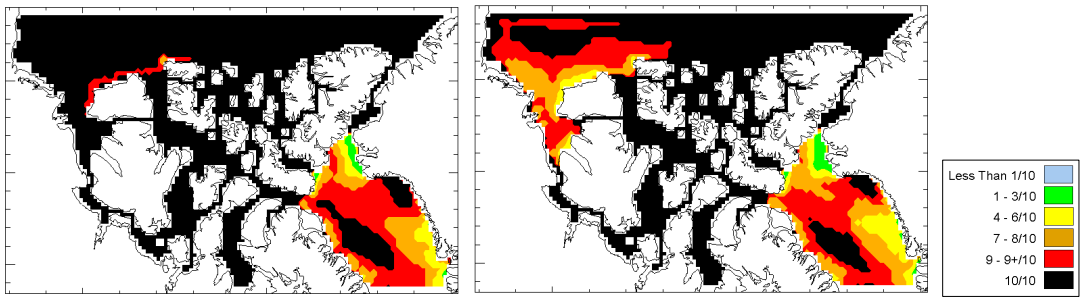

Figure 5.1: Median ice concentration for the week of May 15, past (left panel) and future (right panel).

Changes in seasonal ice cover are also evident in the monthly ice extent (Fig. 5.3). The wintertime ice extents are basically unchanged; the region remains completely ice covered from December to May. However, the future ice cover retreats faster in June and remains more open in October. The summertime ice extent is also reduced,

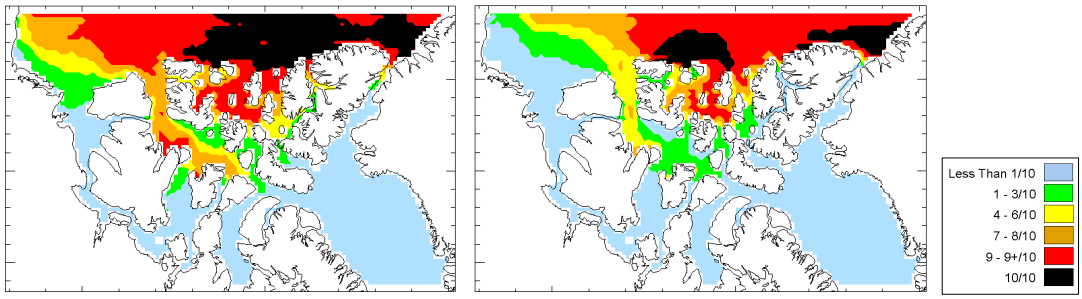

Figure 5.2: Median ice concentration for the week of Sept 10, past (left panel) and future (right panel).

up to 30% in August and 50% in September. Hence, the month of minimum ice cover shifts from August to September.

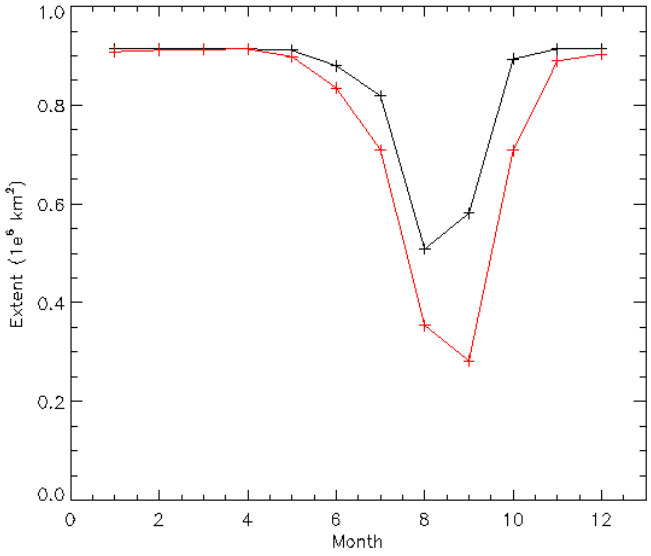

Figure 5.3: Seasonal ice extent, past (black) and future (red).

Ice thickness and velocity

In May, the future ice thickness is reduced by more than 1.0 m in M'Clure Strait, Viscount Melville Sound and the QEI regions, while ice thickness in Amundsen Gulf and Barrow Strait decreases by 0.5 m. The most dramatic loss of ice occurs north of the CAA, where ice thins by 2-4 m. Most of the CAA region remains landfast in winter, so the ice velocity patterns are unchanged, but there is increased ice movement in Baffin Bay and the Beaufort Sea. Ice velocities in the Beaufort Sea region increases by 0.3 m s^{-1} due to thinner ice and changes in the wind forcing (Fig. 5.4).

The simulated September ice thickness shows a similar pattern of thinning as seen in the winter, with the most reduction in ice thickness occurring at the north of the CAA region and within the QEI and Parry Strait (Fig. 5.5). Future ice retreat is evident in Beaufort Sea, Barrow Strait and around Ellesmere Island (also seen in ice concentrations). Summertime ice velocities are larger in the future, and are especially evident north of and within the QEI, suggesting an increase of ice import.

Regional changes in ice thickness and normalized ice coverage

Regional changes in ice thickness and normalized ice coverage are provided in Table 5.1. In winter, all of the regions remain completely ice covered and show little change in the future run, but ice thickness is reduced, by 6-20%. The regionally-averaged maximum ice thickness drops from 2.49 to 2.05 m. Future ice loss is more evident in summer. The M'Clure Strait and QEI regions experience the most decrease. The M'Clure Strait region switches from half ice covered to dominantly ice free (with ice coverage of .26), and the normalized ice coverage in the QEI drops from .69 to .54. In comparison, the Nares Strait and Amundsen Gulf regions were mostly ice free in the past and become more so in the future run. Ice thickness in the regions, except Nares Strait, decrease by 34-49%. During 1970-1989, the ice thickness in Nares Strait is relatively thin (0.45 m) and changes little in the future run (0.40 m.). Averaged over all the regions, the minimum ice coverage is reduced by 46% and the minimim ice thickness decreases by 36%.

5.2.2 Summer duration

In the future run, break up occurs earlier and freeze up starts later[1]. The largest differences in break up dates (Fig. 5.6) occurs in regions that did not open up in the past but experience ice retreat in the future, e.g. the southern Beaufort Sea, northern Barrow Strait and off the western coast of Ellesmere Island. In the future, ice in these

[1]Break up occurs the week the median ice concentrations are less than 1/10, and freeze up occurs the week the concentrations are greater than 1/10.

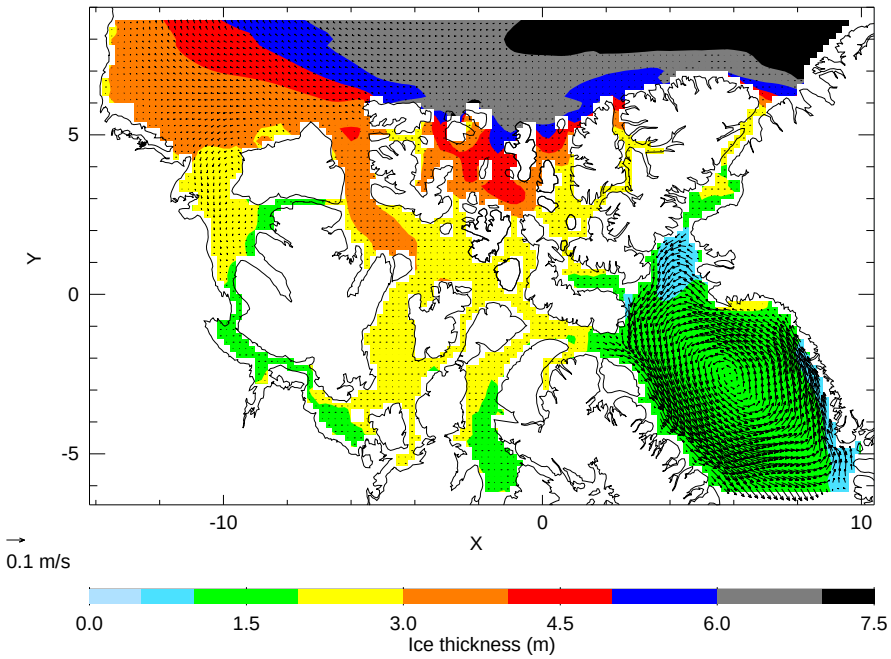

(a) Past

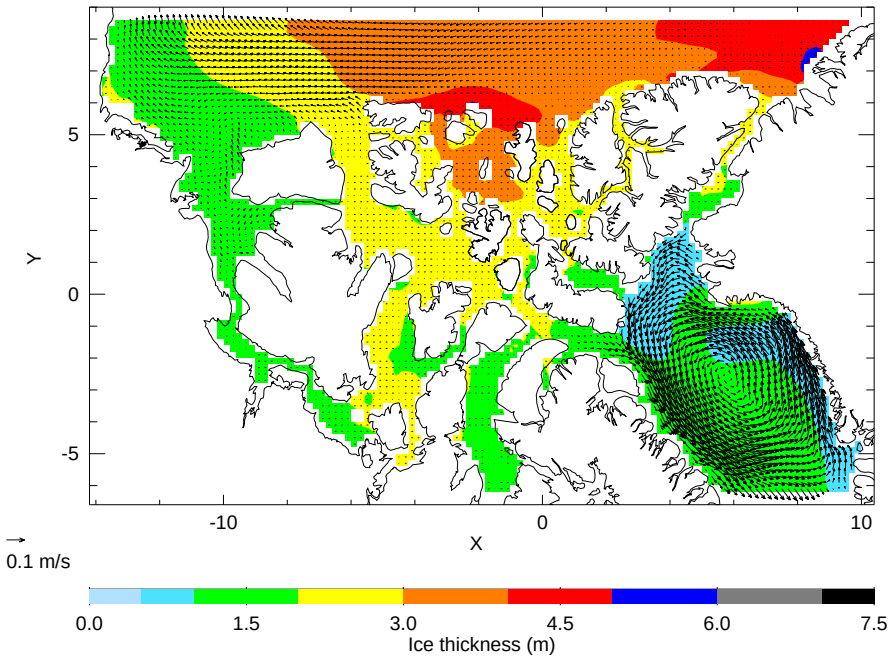

(b) Future

Figure 5.4: Average ice thickness and velocity for the week of May 15.

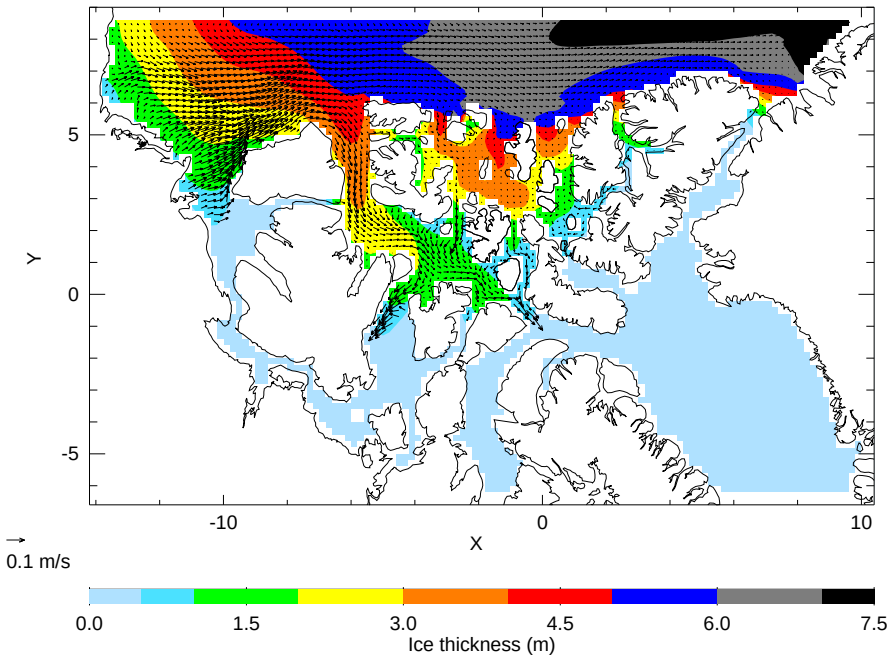

(a) Past

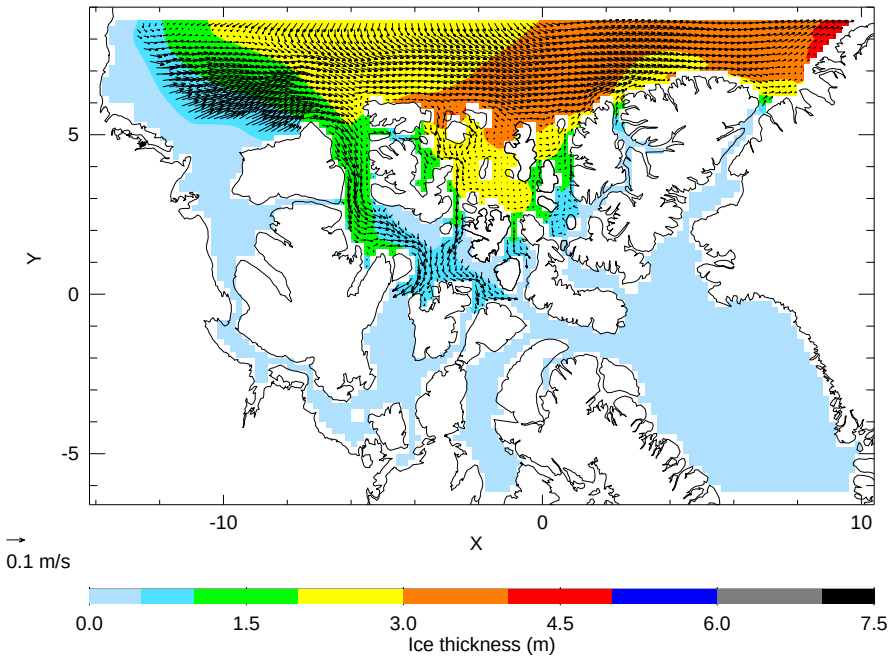

(b) Future

Figure 5.5: Average ice thickness and velocity for the week of September 10.

	Past		Future		Change	
	Coverage	Thickness	Coverage	Thickness	Coverage	Thickness
		(m)		(m)	(%)	(%)
Minimum						
Amundsen-Lancaster	.15	0.75	.04	0.38	-78	-49
QEI	.69	2.28	.54	1.49	-22	-35
Nares Strait	.10	0.45	.04	0.40	-60	-11
M'Clure Strait	.50	1.65	.26	0.80	-48	-48
For all regions	.34	1.23	.18	0.77	-46	-36
Maximum						
Amundsen-Lancaster	1.00	2.23	.98	1.86	-1	-16
QEI	1.00	3.39	1.00	2.67	0	-21
Nares Strait	.96	1.84	.96	1.73	0	-6
M'Clure Strait	1.00	2.74	1.00	2.21	-0	-20
For all regions	.99	2.49	.98	2.06	-1	-17

Table 5.1: Past and future normalized ice coverage and thickness for four regions. Regional locations are shown in Fig. 4.11.

regions breaks up as early as June. Northern Baffin Bay, Nares Strait and Amundsen Gulf open up 2-5 weeks earlier, while M'Clintock Channel and the Gulf of Boothia open up 1-2 weeks earlier than in the past. The timing of break up in Coronation Gulf is unchanged. Freeze up generally occurs about 2-4 weeks later, and is delayed the most in the Amundsen Gulf and the NOW regions (Fig. 5.7).

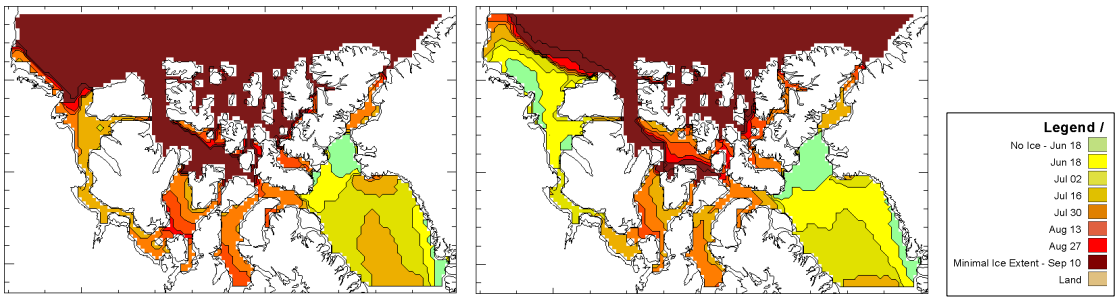

Figure 5.6: Break up dates for past (left panel) and future (right panel), based on median ice concentration of 1/10.

Consequently, the resulting length of summer duration [2] increases the most in the southern Beaufort Sea region (5 months longer) and Amundsen Gulf (2 months

[2]Summer duration is dependent on median ice concentrations of less than 1/10.

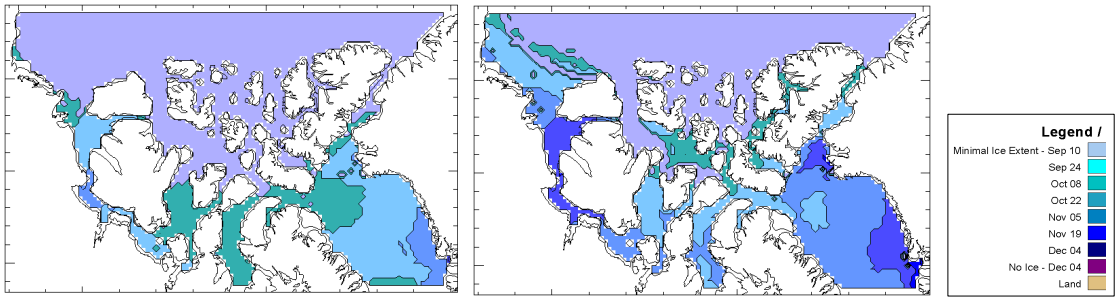

Figure 5.7: Freeze up dates for past (left panel) and future (right panel), as based on median ice concentration of 1/10.

longer), as well as around Ellesmere Island (1 month longer). The NOW region is open 5-6 months, a month longer than in the past. The remaining regions of seasonal ice-cover generally experience 3-5 more weeks of 'summer' (Fig. 5.8), shifting from 1-3 months to 2-4 months of summer duration.

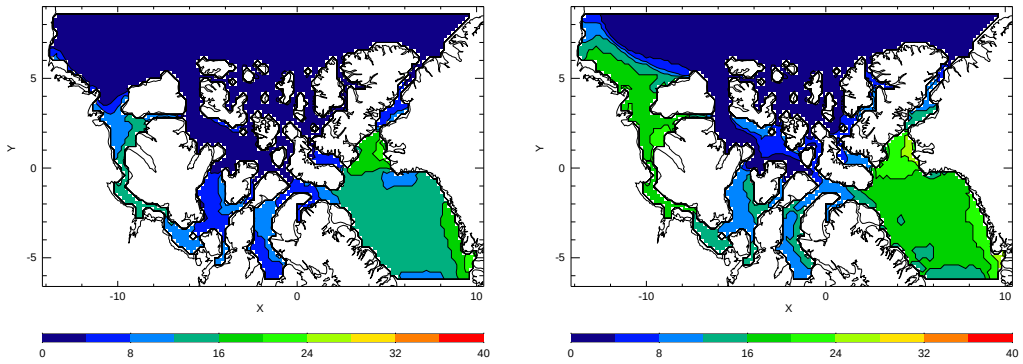

Figure 5.8: Summer duration (in number of weeks) for past (left panel) and future (right panel), as based on median ice concentration less than 1/10.

Two other definitions of summer duration are considered. Firstly, summer duration is calculated using the length of time ice thickness is less than 0.5 m. While the patterns of change remain similar, the duration is generally longer than in the previous definition (not shown). Changes in Baffin Bay are most dramatic, with the NOW region being open 7-8 months in the future compared to 4-5 months in the past. Also, ice along the Greenland coast is more open. The simulated ice tends to thin faster than it retreats, so that the duration of summer, as defined by ice thickness, will be more sensitive than that based on ice concentration.

Secondly, summer duration is calculated using the length of time ice velocities are greater than 0.005 m s^{-1}. The simulated future ice within the CAA region is generally mobile a month longer. The northern CAA region (e.g. QEI) experiences the largest changes, and is mobile for up to 5 months longer (Fig. 5.9). This means that the duration of landfast ice in the CAA region decreases in the future run.

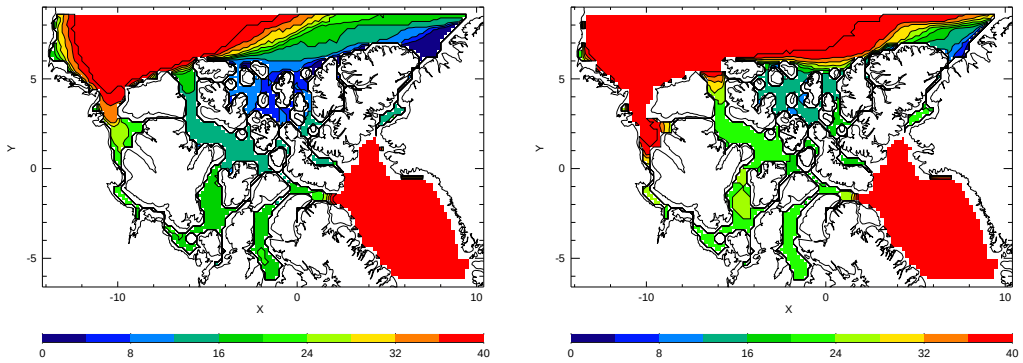

Figure 5.9: Summer duration (in number of weeks) for past (left panel) and future (right panel), based on median ice velocity of more than 0.005 m s^{-1}.

Northwest Passage

Summer duration can also be defined in terms of ice severity, related to accessibility for shipping. Ice retreat that would allow navigation through the Northwest Passage (NWP) is a matter of current political and economic interest. The ability to navigate through ice covered waters depends on many factors; e.g. the ship's ability to withstand ice pressure, requirements for draft, and the experience of the crew. Although there is a wide range of allowable conditions, commercial ships can generally withstand ice concentrations up to 60% with ice thickness less than 1.0 m (H. Melling, Pers. Comm). These criteria[3] are used to define 'good shipping conditions'. Channels are considered 'accessible' if these conditions exist for a minimum of 8 weeks a year. It is assumed a channel would need to be accessible more than 60-70% of the time (i.e. years) to be economically feasible. If so, a channel is considered

[3]Strength of the ice is also important, but is not considered here.

'open' for passage.

The NWP consists of two main routes: a shallow water route through Queen Maud Gulf (south of Victoria Island), and a deep water route through Viscount Melville Sound and out through Prince of Wales Strait (north of Victoria Island). The shallow water route has several access points, e.g. Prince Regent Inlet (through Bellot Sound) or Peel Sound. A plot of the frequency of past 'good shipping years' from 1970-1989 (Fig. 5.11) indicates that the deep water route is 'closed' in the past simulation run. The shallow water route is more accessible - 'good shipping conditions' occur 50-60% of the years- but is effectively 'closed' for commercial use. Baffin Bay is completely open, but access to the Beaufort Sea is blocked by ice along the Alaskan coast. Summertime ice along the Alaskan coast is not observed.

In the future simulation, the shallow NWP route through Prince Regent Inlet and Bellot Strait is 'open' every year. Passage through Peel Sound and the deep water route remains limited by ice in Barrow Strait, which is accessible 60% of the years. For opportunistic shipping (e.g. for tourism or research), which is not as dependent on year-to-year consistency, all of the NWP routes are 'open'. Even Viscount Melville Sound is accessible 30-40% of the years. In the future run, the Alaskan coast is clear of ice.

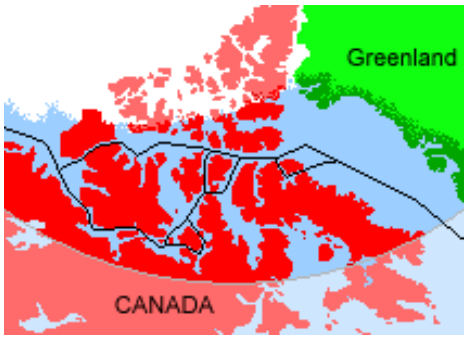

Figure 5.10: Routes through the Northwest Passage (www.athropolis.com).

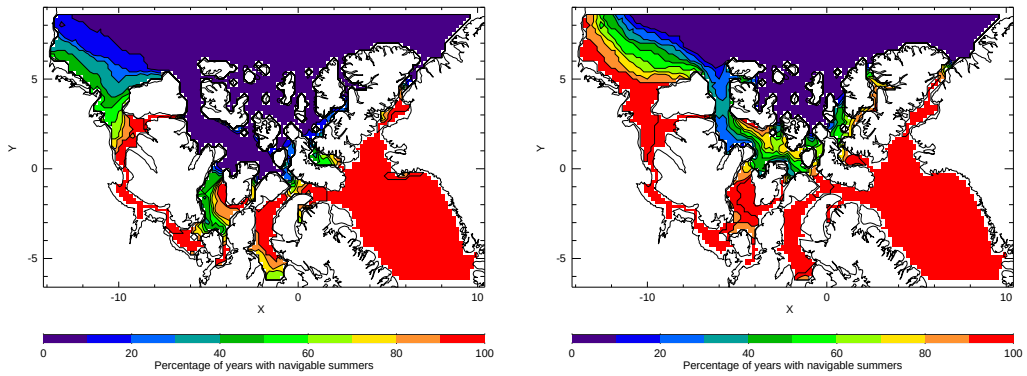

Figure 5.11: Frequency of accessible years with 'good shipping conditions' (defined in text), for the past (left panel) and future (right panel).

5.2.3 Inter-annual variability

The future inter-annual variability of simulated sea-ice is very similar to the historical run (1970-1989) due to the method used to calculate the future atmospheric forcing. However, the ice area and thickness do shift to a new equilibrium, with overall less ice (Fig. 5.12).

Although the future simulation suggests that the CAA region is more accessible in most years, knowledge of ice cover in extreme years is also important. In a heavy ice year, most of the northern CAA region is covered by compact ice, including the northern channels of the NWP. In a light ice year, most of the NWP region is ice free (Fig. 5.13).

5.2.4 Ice fluxes

The future ice volume fluxes of the northern boundary experience a significant reduction compared to the past fluxes and drop by 60%. The flux through the southern boundary also decreases, but only by 20% (Table 5.2). Due to the unequal change in ice volume fluxes, less ice enters the CAA region (via the northern boundary), and the volume of ice exported from the region increases (from 78 to 114 km^3 $yr-1$). The northern ice volume flux is modified the most by the reduction of ice thickness, as the average thickness drops from 3.3 to 1.9 m. There is little change in the ice area

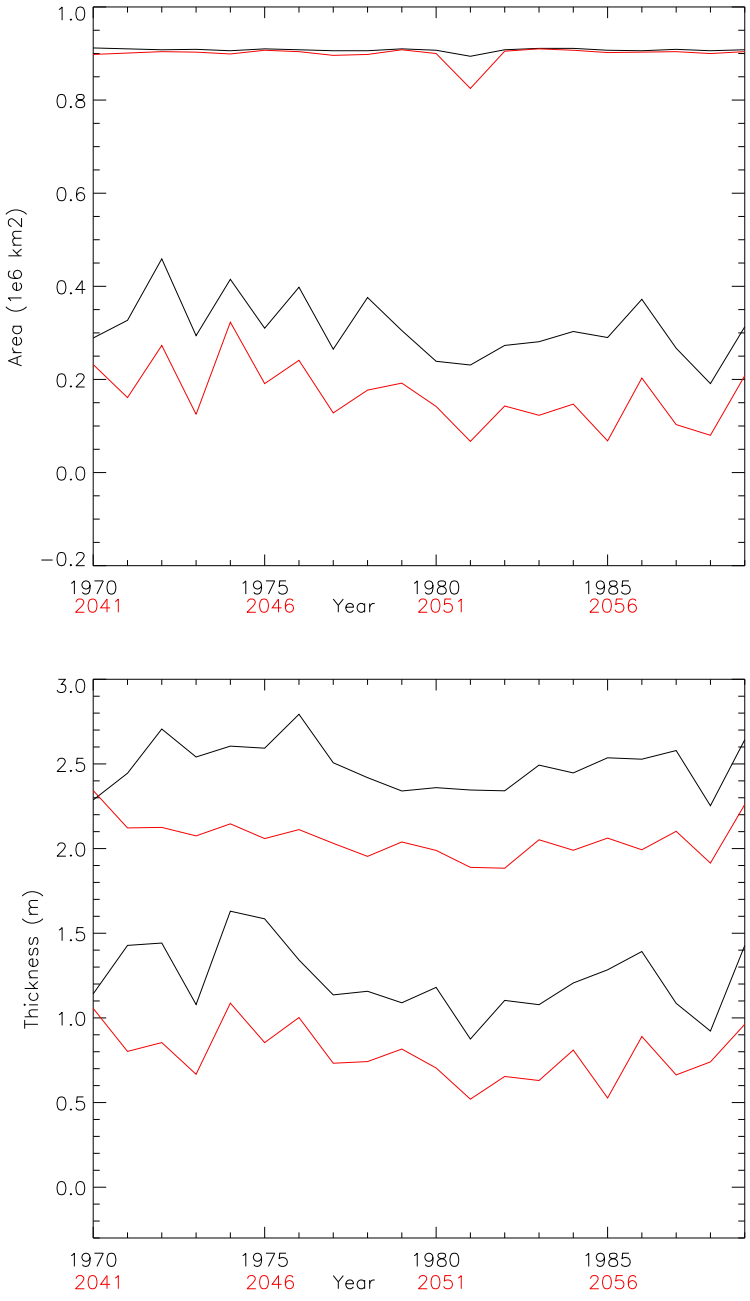

Figure 5.12: Past (black) and future (red) ice area and thickness: Maximum and minimum ice area (upper panel) and maximum and minimum ice thickness (lower panel).

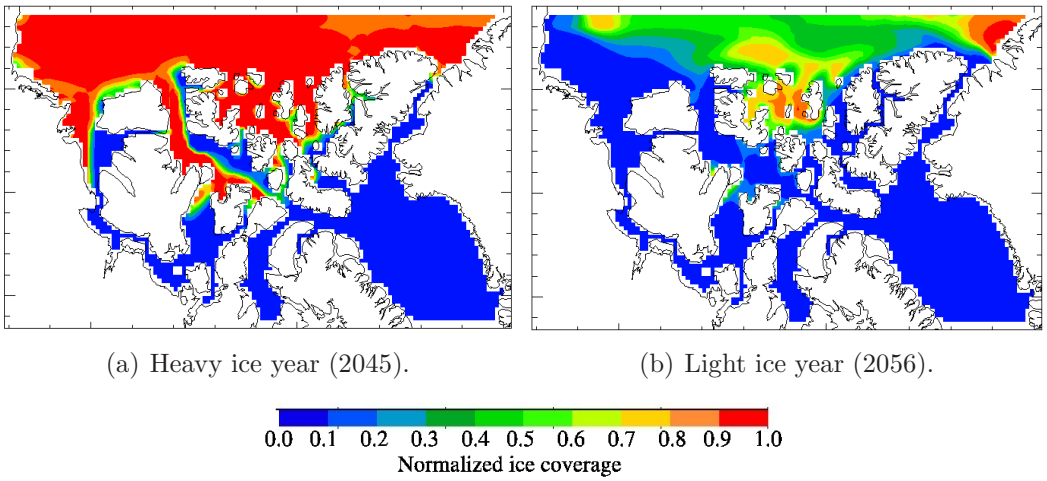

(a) Heavy ice year (2045). (b) Light ice year (2056).

Figure 5.13: An example of extreme ice years from the future run (week of September 10).

	Volume flux		Area flux	Thickness	Velocity
	(km^3 yr^{-1})	(mSv)	(10^3 $km^2 yr^{-1}$)	(m)	(km day^{-1})
Past, 1970-1989					
North boundary	149	5	-11	3.3	2.0
South boundary	-227	-7	-257	1.0	5.5
Net import to the CAA region	-78	-2	-268		
Future, 2041-2060					
North boundary	63	2	-14	1.9	4.1
South boundary	-177	-6	-234	0.8	6.2
Net import to the CAA region	-114	-4	-248		

Table 5.2: Simulated ice advection through gates for the past and future time-periods.

fluxes; reduced ice concentrations are compensated by faster ice velocities, especially through the northern boundary. The southern boundary experiences less change in ice thickness and velocity than the northern boundary.

Freshwater fluxes through the CAA are also considered, albeit briefly (Table 5.3). In the past and future time-periods, the CAA experiences a net freshening from oceanic transport. The oceanic flux outweighs the loss of freshwater from ice transports. In the future simulation, the region is freshening at a faster rate (137 km^3 yr^{-1}) than in the past (86 km^3 yr^{-1}). These rates are small relative to the oceanic freshwater fluxes, but are comparable to the ice fluxes.

Channel	Oceanic		Ice		Total
	Net	σ	Net	σ	Net
	$km^3\ yr^{-1}$		$km^3\ yr^{-1}$		$km^3\ yr^{-1}$
Past, 1970-1989					
North boundary	1603	396	122	213	1725
South boundary	-1457	376	-182	36	-1638
Net import to CAA region	146	294	-60	201	86
Future, 2041-2060					
North boundary	1396	432	52	229	1448
South boundary	-1170	267	-141	27	-1311
Net import to CAA region	226	370	-89	217	137

Table 5.3: Simulated net freshwater fluxes from oceanic and ice transports for the past and future time-periods, assuming ice salinity of 4.0 ppt and ocean salinity of 34.80 ppt.

5.2.5 Site comparison

To demonstrate changes in local ice cover between the past and future time-periods, ice thickness and summer duration are compared at six sites (locations shown in Fig. 4.19).

Ice thickness

Generally, the future maximum ice thicknesses are less than in the past, and the ice thins by about 1.0 m to 0.2 m, depending on the site (Table 5.4). The decrease in ice thickness is proportional to their initial thickness: that is, stations with thicker ice (i.e. Alert and Mould Bay) lose the most. The ice response at Clyde is unexpected; the future ice is slightly thicker, resulting from ice advection. The average change in ice thickness for the six sites is -0.34 m, similar to the value of -0.32 m reported by *Dumas et al.* (2006a).

Changes in climatogical ice thickness are shown in Fig. 5.14. The loss in wintertime ice thickness in the CAA model is similar to the 1-d model, although the 1-d model has thinner ice in the past and future timeperiods. However, the summer time ice thicknesses are different; the CAA model sites retain thicker ice at Alert, Eureka, Mould Bay and Resolute and, in the climatological mean, do not experience break

Stations	CAA model			1d-model		
Stations	Past	Future	Difference	Past	Future	Difference
Alert*	3.71	2.73	-0.98	2.13	1.72	-0.41
Eureka	2.44	2.28	-0.16	2.42	2.06	-0.36
Mould Bay	3.27	2.37	-0.90	2.03	1.65	-0.38
Resolute	2.27	2.20	-0.17	2.09	1.86	-0.23
Clyde	1.78	1.82	0.04	1.96	1.69	-0.27
Cambridge Bay	2.10	1.91	-0.19	2.33	2.07	-0.26

Table 5.4: Past and future maximum ice thickness at sites, for both the CAA regional model and the 1-d model (*Dumas et al.* 2006a).

up. The 1-d model experiences break up and freeze up at all of the sites, and in the future, break up shifts to an earlier date and freeze up occurs later. A shift in break up is not as evident in the CAA model at Clyde and Cambridge Bay (the two sites that experience break up and freeze up), but freeze up does occur later. The CAA model is not as sensitive to changes in break up, partially due to its ice dynamics. Models that include ice dynamics are less sensitive to climate changes than thermodynamic-only models (*Saenko et al.* 2002) and the advective processes within the 3-d model act to compensate for thermodynamically-driven changes.

Summer duration

In the historical run, there were sites that did not experience break up or freeze up[4] in any of the years (i.e. Alert and Mould Bay), or only occasionally (i.e. Eureka and Resolute). In the future run, break up and freeze up occurs occassionally at Alert and Mould Bay, and more often at Eureka and Resolute (Table 5.5). The remaining two stations, Clyde and Cambridge Bay, open up every year in both the past and future time-periods. All of the sites in the 1-d model opened up every year, except for Alert (which did not break up in two of the years in the past).

For the sites that experienced 'summer' in both the past and future time-periods (i.e. Eureka, Resolute, Clyde and Cambridge Bay), summer duration increases more

[4]Break up occurs when ice thickness is less than 0.3 m and freeze up occurs when ice thickness is greater than 0.5 m.

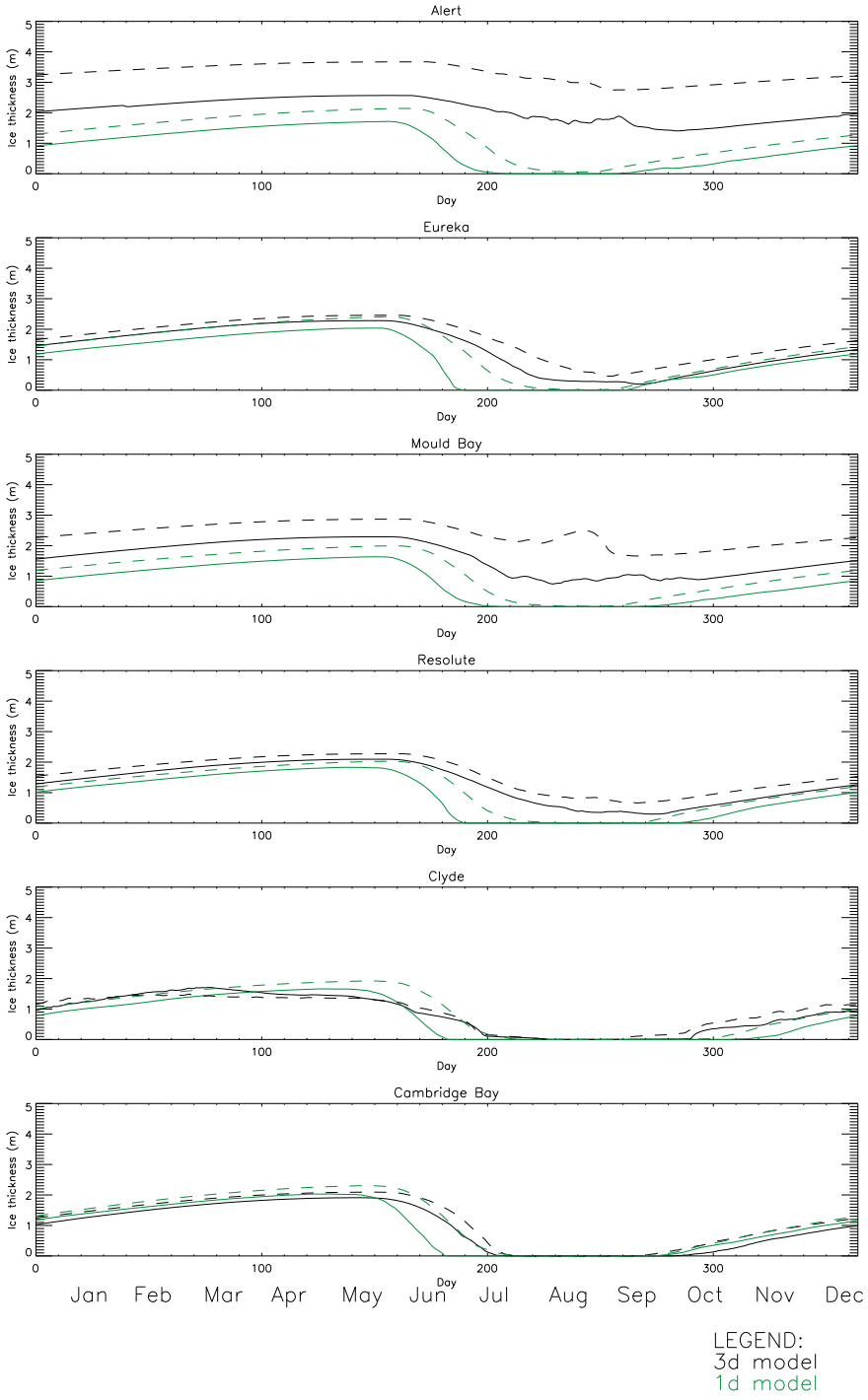

Figure 5.14: Climatological daily ice thickness at sites, past (dashed line) and future (solid line).

	CAA model					1d-model				
Stations	Past		Future		Diff	Past		Future		Diff
	days	(yrs)	days	(yrs)	days	days	(yrs)	days	(yrs)	days
Alert	0	(0)	6	(4)	6	63	(18)	111	(20)	48
Eureka	31	(9)	70	(15)	39	69	(20)	97	(20)	28
Mould Bay	0	(0)	44	(10)	44	76	(20)	121	(20)	44
Resolute	14	(3)	53	(12)	39	87	(20)	126	(20)	39
Clyde	98	(20)	110	(20)	12	123	(20)	164	(20)	41
Cambridge Bay	91	(20)	118	(20)	27	100	(20)	124	(20)	24

Table 5.5: Simulated summer duration, for the CAA regional model and the 1-d model (*Dumas et al.* 2006a). The number of years in which break up and freeze up occurred is included in brackets.

from a later freeze up (an average a 19 days) than an earlier breakup (8 days)[5]. Break up occurs earlier at all of the sites except Clyde, which retains its break up date to within a day. The shift in freeze up dates was more uniform among the 3-d model sites. The resulting future average summer duration is extended by 27 days. In comparison, the shift in the average freeze up date in the 1-d model is similar (18 days later), but the break up date was much earlier (20 days) than in the CAA model. The ice in the 1-d model had longer summer durations overall and experienced a greater lengthening of summer conditions (by 38 days).

Change in snow cover

In the future run, snow cover is reduced, both in duration and thickness. On average, the loss of snow cover occurs 7 days earlier, but the timing of fall snow cover occurs some 69 days later in the future run. Snow thickness is reduced by half.

[5]I include only the years that experienced break up and freeze up when I calculate the average change in dates.

Chapter 6

Conclusions

In the context of recently observed global climate change, associated with warmer air temperatures and exceptional summertime ice retreat in the Arctic, the fate of sea-ice in the Canadian Arctic Archipelago (CAA) region is of concern. Currently, the CAA region is maintaining its sea-ice cover, and trends of observed ice thickness and area are statistically insignificant. However, further warming is predicted by global climate models. Ice loss in the CAA would have a huge impact on the culture of the indigenous people as well as the survival of ice-dependent species, such as polar bears and bowhead whales. It would mean the loss of a northern ecosystem.

Negative impacts on polar bear health is already being felt in the Hudson Bay area, where ice is retreating sooner and freezing up later. Bears have less time to hunt before fasting on land during the summer (*Stirling and Parkinson* 2006). Although the habits of the CAA polar bears are different (CAA bears graze all year), the loss of summertime ice may prove fatal (*Derocher et al.* 2004). In addition to impacts on wildlife, indigenous people of the CAA are facing unprecedented shifts in climate, resulting in less predictable ice conditions (*ACIA* 2005). Changes in ice cover also has political implications. The anticipated increase in international commercial shipping through the Northwest Passage has challenged Canadian sovereignty, which is partially dependent on ice in defining its northern territory (*Huebert* 2001).

In this thesis, an ice-ocean coupled model is developed on a 0.2° horizontal grid, with open boundaries along both its northern and southern boundary, and is forced with historical atmospheric data taken from observationally-based data (e.g. NCEP/NCAR Reanalysis). The forcing for the lateral boundaries is provided by a basin-wide (Arctic Ocean) model, which was set up for this purpose and run offline for the same experiments as the regional CAA model.

In the process of setting up the models, it was found that the NCEP/NCAR air temperatures over the CAA region were systematically too cold compared to in-situ observations; the resulting simulated ice thicknesses were much larger (up to 15 m) than observed. This is important knowledge for interpreting results from models that employ the NCEP/NCAR Reanalysis atmospheric data. Air temperatures from the ERA-15 Reanalysis had similar problems. For this study, the NCEP/NCAR air temperatures are adjusted to remove most of this bias.

The model does reasonably well in representing the historical sea-ice from 1950-2004. Spatial patterns of ice thickness and area are as expected, including the polynyas in Amundsen Gulf and Smith Sound. The patterns of break-up and freeze-up are similar to observations, except along the Alaskan coast and in southern channels of Gulf of Boothia and M'Clintock Channel. Compared to observations, the model retains too much ice along the Alaskan coast, and not enough ice in the southern channels. Hence, the model under-estimates summertime ice cover, simulating ice-free conditions in the southern channels and lower ice concentrations in M'Clure Strait. The seasonal cycle of ice extent agrees well with observations, with the CAA region being completely covered with sea-ice from November to May, but the timing of the minimum ice cover occurs several weeks too early. Even so, the model captures the inter-annual variability in summertime ice cover, as well as the unusually light ice year of 1998.

Simulated ice volume changes in the CAA region are attributed to thermodynamic

and advective processes. These processes are found to be anti-correlated: the export of ice results in increased growth of replacement ice, and ice growth results in more ice available for export. In the model, the advection and thermodynamic changes in ice volume nearly balance, and the region experiences net export and growth in most years. However, the pattern of variability changes during the 1990's when years of 'export and growth' alternate with years of 'import and melt'. This change may be correlated with the AO index, but more study is required to understand the model's response.

The inter-annual variability of ice advection, as evident in the simulated ice volume changes, are due to fluxes in the Amundsen Gulf region. The northern Amundsen Gulf region experiences very high inter-annual variability, alternating between net export and import, with large transports in ice volume. In addition, it is found that the polynyas (e.g. Amundsen Gulf, Smith Sound and Lancaster Sound) are regions of high ice-production. Ice fluxes within the interior CAA region are much smaller in comparison. Hence, most of the sea-ice exported from the CAA region (to the Beaufort Sea or Baffin Bay) is generated within these polynya regions, and does not originate from within the CAA.

Simulated ice area fluxes at selected 'gates' compare well with observations but ice volume fluxes do not. This discrepancy is partially due to the method used to estimate ice volume fluxes from observations[1]. This method is assessed using simulated data from the CAA regional model. It is found that it fails in regions of high variability (i.e. in ice direction or thickness), and resulting estimates should be viewed with caution.

The future atmospheric forcing for the regional CAA model represents the projected climate during the mid 21^{st} century, under the SRES A2 scenario. The data is

[1]Ice area fluxes are observed by satellite, but associated ice thickness data is not available. Ice volume fluxes are normally estimated by applying a representational ice thickness to the ice area flux.

taken from the CGCM2 model, and is derived by applying the climatological monthly change, simulated by CGCM2, between 1970-1989 and 2041-2060, to the historical forcing. Generally, the future forcing has higher air temperatures and precipitation than in the past.

While global climate models project overall summertime ice retreat in the NH between 2050-2100, they reflect a persistence of sea-ice in the CAA region (and central Arctic). Results from this study agree: the CAA region remains ice covered from 2041-2060, with little change in wintertime ice extent or ice concentrations. Ice retreat is more evident in summer; ice concentrations decrease by 46%. Ice thickness is also reduced, by 17% in the winter, and by 36% in the summer. In spite of this future ice retreat, perennial ice is retained in the Queen Elizabeth Islands (QEI). This agrees with the ice-extent proxy data for the Holocene (*Dyke et al.* 1996), which showed a consistent ice cover in the QEI. Generally, ice is more mobile in the future run, especially in the northern channels.

The accessibility of the Northwest Passage for commercial shipping is of major interest. Is it 'open for business' by 2041-2060? A simple index is used to estimate the frequency of accessible years[2], and it is arbitrarily decided that, in order to be commercially viable, the region must be accessible for 60-70% of the years. In the past run, from 1970-89, the shallow water route through the Queen Maud Gulf is only accessible 50-60% of the years, and the route through Viscount Melville Sound is 'closed' every year. In the future simulation, access through Barrow Strait and Viscount Melville Sound increases to 30-50% of the years, but the deep water route remains effectively 'closed'. The shallow water route is 'open' in every year from 2041 to 2060. Results from this model suggest that a completely ice-free CAA is unlikely by the year 2050, but the region may be able to support commercial shipping.

[2]An accessible year is defined as having ice with less than 60% concentration and 1.0 m thickness for a minimum of 8 weeks

Bibliography

Aagaard, K., and E. Carmack (1989), The role of sea ice and other fresh water in the Arctic circulation, *Journal of Geophysical Research*, *94*(C10), 14,485–14,498.

ACIA (2005), *Arctic Climate Impact Assessment*, 1042 pp., Cambridge University Press.

Agnew, T., and J. Vandeweghe (2005), Report on estimating sea-ice tranport into the North Atlantic using the Advanced Microwave Scanning Radiometer (AMSR-E), *Tech. rep.*, Environment Canada unpublished report, pp21, Environment Canada, Toronto, Canada.

Agnew, T., B. Alt, R. D. Abreu, and S. Jeffers (2001), The loss of decade old sea ice plugs in the Canadian Arctic Islands, *Extended abstracts: Polar Meterology and Oceanography Conference, AMS, San Diego, May14-18*.

Agnew, T., J. Vandeweghe, and A. Lambe (2006), Estimating sea-ice area fluxes across the Canadian Arctic Archipelago using AMSR-E, *Tech. rep.*, Environment Canada unpublished report, pp20, Environment Canada, Toronto, Canada.

Barber, D., and J. Hanesiak (2004), Meteorological forcing of sea ice concentrations in the southern Beaufort Sea over the period 1979 to 2000, *Journal of Geophysical Research*, *109*, doi:10.1029/2003JC002027.

Becker, P. (1995), The effect of Arctic river hydrological cycles on Arctic Ocean circulation, Ph.D. thesis, Old Dominion University.

Belchansky, G., D. Douglas, and N. Platonov (2004), Duration of the Arctic sea ice melt season: regional and interannual variability, 1979-2001, *Journal of Climate*, *17*, 67–80.

Bitz, C., and G. Roe (2004), A mechanism for the high rate of sea ice thinning in the Arctic Ocean, *Journal of Climate*, *17*, 3623–3632.

Bourke, R. H., and R. Garrett (1987), Sea ice thickness distribution in the Arctic region, *Cold Regional Science Technology*, *13*, 259–280.

Brohan, P., J. Kennedy, I.Harris, S. Tett, and P. Jones (2006), Uncertainty estimates in region and global observed temperature changes: a new data set from 1850, *Journal of Geophysical Research*, *111*, doi:10.1029/2005JD006548.

Bromwich, D., R. Fogt, K. Hodges, and J. Walsh (2007), A tropospheric assessment of the ERA-40, NCEP, and JRA-25 global reanalyses in the polar regions, *Journal of Geophysical Research*, *112*, doi:10.1029/2006JD007859.

Brown, R., and B. Alt (2001), Executive Summary, in chapter ii:11 of the state of the Arctic cryosphere during the extreme warm summer of 1998: documenting cryospheric variability in the Canadian Arctic, CCAF summer 1998 project team, *CCAF Final Report*.

Brown, R., and P. Cote (1992), Interannual variability of landfast ice thickness in the Canadian High Arctic, 1950-89, *Arctic*, *45*(3), 273–284.

Brown, R., B. Brasnett, and D. Robinson (2003), Gridded North American monthly snow depth and snow water equivalend for GCM evaluation, *Appl. Opt.*, *41*(1), 1–14.

Bryan, K. (1969), A numerical method for the study of the circulation of the world ocean, *Jouirnal of Computational Physics*, *4*, 347–376.

CIS (2002), *Sea Ice Climatic Atlas- Northern Canadian Waters: 1971-2000*, Ministry of Public Works and Government Services of Canada.

Comiso, J. (2002), A rapidly declining perennial sea ice cover in the Arctic, *Geophysical Research Letters*, *29*(21), doi:10.1029/2002GLO015650.

Comiso, J. (2003), Warming trends in the Arctic from clear sky satellite observations, *Journal of Climate*, *16*, 3498–3510.

Crocker, G., T. Carrieres, R. Chagnon, S. McCourt, T. Agnew, and J. Lewis (2005), Analysis of the Canadian Ice Service digital charts database for ice climate trends in Canadian waters.

Curry, J., J. Schramm, A. Alam, R. Reeder, and T. Arbetter (2002), Evaluation of data sets used to force sea-ice models in the Arctic Ocean, *Journal of Geophysical Research*, *107*, doi:10.1029/2000JC000466.

Derocher, A., N. Lunn, and I. Stirling (2004), Polar bears in a warming climate, *Integr. Comp. Biol*, *44*, 163–176.

Dey, B. (1981), Monitering winter sea ice dynamics in the Canadian Arctic with NOAA-TIR images, *Journal of Geophysical Research*, *86*, 3223–3235.

Dumas, J., G. Flato, and R. Brown (2006a), Future projections of landfast ice thickness and duration in the Canadian Arctic, *Journal of Climate*, *19*(20), 5175–5189.

Dumas, J., H. Melling, and G. Flato (2006b), Late summer pack ice in the Canadian Archipelago : thickness observations from a ship in transit, submitted.

Dunbar, M. (1973), Ice regime and ice transport in Nares Strait, *Arctic*, *23*, 282–291.

Dunphy, M., F. Dupont, C. Hannah, and D. Greenberg (2005), Validation of a modelling system for tides in the Canadian Arctic Archipelago, *Tech. rep.*, Can. Tech. Pre. Hydrogr. Ocean Sci. 243:vi +70p.

Dyke, A., J.Hooper, and J. Savelle (1996), A history of sea ice in the Canadian Arctic Archipelago based on postglacial remains of the bowhead whale (Balaena mysticetus), *Arctic*, *49*, 235–255.

Eby, M., and G. Holloway (1994), Grid tranformation for incorporating the Arctic in a Global Ocean Model, *Climate Dynamics*, *10*, 241–247.

Falkingham, J., R. Chagnon, and S. McCourt (2002), Trends in sea ice in the Canadian Arctic, *Paper presented at 16th International Symposium on ice, Int. Assoc. for Hydrogr. Res., Dunedin, New Zealand*.

Fissel, D., J. Birch, H.Melling, and R. Lake (1998), Non-tidal flows in the Northwest Passage, *Tech. rep.*, Canadian Technical Report of Hydrography and Ocean Sciences, No 98, Institute of Ocean Sciences, Sidney, Canada, V8L 4B2, 142 pp.

Flato, G. M., and G. Boer (2001), Warming asymmetry in climate change simulations, *Geophysical Research Letters*, *28*(1), 195–198.

Flato, G. M., and R. D. Brown (1996), Variability and climate sensitivity of landfast Arctic sea ice, *Journal of Geophysical Research*, *101*(C10), 25,767–25,777.

Hibler, W. (1979), A dynamic thermodynamic sea ice model, *Journal of Physical Oceanography*, *9*, 815–846.

Holland, D. (2000), Merged IBCAO/ETOPO5 Global Topographic Data Product, *Tech. rep.*, National Geophysical Data Centre (NGDC), Boulder Colorado:: http://www.ngdc.noaa.gov/mgg/bathymetry/arctic/ibcaorelatedsites.html.

Holland, M., and C. Bitz (2003), Polar amplification of climate change in coupled models, *Climate Dynamics*, *21*, 221–232.

Holland, M., C. Bitz, and A. Weaver (2001), The influence of sea ice physics on

simulations of climate change, *Journal of Geophysical Research*, *106*(C9), 19,639–19,655.

Holland, M., C. Bitz, and B. Tremblay (2006), Future abrupt reductions in the summer Arctic sea ice, *Geophysical Research Letters*, *33*, doi:10.1029/2006GL028024.

Holloway, G. (1992), Representing topographic stress for large-scale ocean models, *Journal of Physical Oceanography*, *22*, 1033–1046.

Holloway, G., and T. Sou (2002), Has Arctic sea ice rapidly thinned?, *Journal of Climate*, *15*, 1691–1701.

Howell, S., A. Tivy, J. Yackel, and S. McCourt (2007), Are perennial sea ice conditions in the Northwest Passage changing?, submitted.

Huebert, R. (2001), Climate change and Canadian sovereignty in the Northwest Passage, *Isuma: Canadian Journal of Policy Research*, *2*(4), 86–94.

Hulme, M., E. Barrow, N. Arnell, P. Harrison, T. Johns, and T. Downing (1999), Relative impacts of human-induced climate change and natural climate variability, *Nature*, *397*, 688–691.

Hurrell, J. (1995), Decadal trends in the North Atlantic Oscillation: regional temperatures and precipitation, *Science*, *269*, 676–697.

IPCC (2000), *Special Report on Emission Scenarios: a special report of Working Group III of the Intergovernmental Panel on Climate Change*, Cambridge University Press.

IPCC (2001), *Climate change 2001: the scientific basis*, 1042 pp., Cambridge University Press.

IPCC (2007), *Climate change 2007: the physical scientific basis. Contribution of Working Group I to the Fourth Assessment Report of the Intergovernmental Panel on Climate Change*, Cambridge University Press.

Johannessen, O., et al. (2004), Arctic climate change: observed and modelled temperature and sea-ice variability, *Telus*, *56A*(4), 328–341.

Jones, P., and A. Moberg (2003), Hemispheric and large-scale surface air temperature variations: an extensive revision and update to 2001, *Journal of Climate*, *16*, 206–223.

Kalnay, E., et al. (1996), The NCEP/NCAR 40-year Reanalysis Project, *Bulleton of the American Metereological Society*, *77*, 437–470.

Kim, S.-J., G. Flato, G. Boer, and N. McFarlane (2002), A coupled climate model simulation of the last glacial maximum: part 1, transient response, *Climate Dynamics*, *19*, 515–537.

Kliem, N., and D. Greenberg (2003), Diagnostic simulations of the summer circulation in the Canadian Arctic Archipelago, *Atmosphere Ocean*, *41*(4), 273–289.

Komuro, Y., and H. Hasumi (2005), Intensification of the Atlantic deep circulation by the Canadian Archipelago throughflow, *Journal of Physical Oceanography*, *35*, 775–789.

Kreyscher, M., M. Harder, P. Lemke, and G. Flato (2000), Results of the sea ice model intercomparison project: evaluation of sea ice rheology schemes for use in climate simulations, *Journal of Geophysical Research*, *105*, 11,299–11,320.

Kwok, R. (2005), Variability of Nares Strait ice flux, *Geophys. Res. Lett*, *32*, doi: 10.1029/2005GL024768.

Kwok, R. (2006), Exchange of sea ice between the Arctic Ocean and the Canadian Arctic Archipelago, *Geophys. Res. Lett*, *33*, doi:10.1029/2006GL027094.

Lammers, R., A. Shiklomanov, C. Vorosmarty, B. Fekete, and B. Peterson (2001), Assessment of contemporary Arctic river runoff based on observational discharge records, *Journal of Geophysical Research*, *106*, 3321–3334.

Lindsay, R., and J. Zhang (2005), The thinning of Arctic sea ice, 1988-2003: have we passed a tipping point?, *Journal of Climate*, *18*, 4879–4894.

Mantua, N., S. Hare, Y. Zhang, J. Wallace, and R. Francis (1997), A Pacific interdecal climate oscillation with impacts on salmon production, *Bull. Amer. Meteor. Soc*, *78*, 1069–1079.

Maslowski, W., and W. Lipscomb (2003), High-resolution simulations of Arctic sea ice during 1979-1993, *Polar Research*, *22*, 67–74.

Maxwell, J. (1981), Climatic regions of the Canadian Arctic Islands, *Arctic*, *34*(3), 225–240.

McLaughlin, F., E. Carmack, R. Macdonald, A. Weaver, and J. Smith (2002), The Canada Basin, 1989-1995: upstream events and far-field effects of the Barents Sea, *Journal of Geophysical Research*, *107*(C7), doi:10.1029/2001JC000904.

Melling, H. (2000), Exchanges of freshwater through the shallow straits of the North American Arctic, in *The freshwater budget of the Arctic Ocean*, Kluwer Academic Publisher, Drodrecht and Boston and London.

Melling, H. (2001), Is the extent or thickness of arctic sea ice declining?, *in Chapter II:11 of The state of the Arctic cryosphere during the extreme warm summer of 1998: documenting cryospheric variability in the Canadian Arctic, CCAF summer 1998 Project Team, CCAF Final Report.*

Melling, H. (2002), Sea ice of the northern Canadian Arctic Archipelago, *Journal of Geophysical Research*, *107*(C11), 2–1, doi:10.1029/2001JC001102.

Merryfield, W., and G. Holloway (2003), Application of an accurate advection algorithm to sea-ice modelling, *Ocean Modelling*, *5*, 1–15.

Moritz, R., C. Bitz, and E. Steig (2002), Dynamics of recent climate change in the Arctic, *Science*, *297*, 1497–1502, doi:10.1126/science.1076522.

Mueller, D., W. Vincent, and M. Jeffries (2003), Break-up of the largest Arctic ice shelf and associated loss of an epishelf lake, *Geophysical Research Letters*, *30*, doi: 10.1029/2003GL017931.

Munoz, E. (1995), Canadian rivers data set: digital media, *Tech. rep.*, Boulder, Colorado: National Snow and Ice data centre.

Myers, P. (2005), Impact of freshwater from the Canadian Arctic Archipelago on Labrador Sea Water formation, *Geophysical Research Letters*, *32*, doi: 10.1029/2004GL022082.

Mysak, L., K. Wright, J. Sedlacek, and M. Eby (2005), Simulation of sea ice and ocean variability in the Arctic during 1955-2002 with an Intermediate Complexity Model, *Appl. Opt.*, *1*, 101–118.

Nazarenko, L., G. Holloway, and N. Tausnev (1998), Dynamics of transport of 'Atlantic Signature' in the Arctic Ocean, *Journal of Geophysical Research*, *103*, 31,003–31,015.

Pacanowski, R. (1995), MOM2 documentation, user's guide and reference manual. GFDL Ocean Tech. Rep 3, *Tech. rep.*, Geophysics Fluid Dynamics Lab., NOAA, Princeton Univ., Princeton, N.J.

Padman, L., and S. Erofeeva (2004), A barotropic inverse tidal model for the Arctic Ocean, *Geophysical Research Letters*, *31*, doi:10:1029/2003GL019003.

Parkinson, C. (2000), Recent trend reversals in Arctic sea ice extents: possible connections to the North Atlantic Oscillation, *Polar Geography*, *24*(1), 1–12.

Parkinson, C., and D. Cavalieri (2002), A 21 year record of Arctic sea-ice extents and their regional, seasonal and monthly variability and trends, *Annals of Glaciology*, *34*, 441–446.

Parkinson, C., and W. Washington (1979), A large scale numerical model of sea ice, *Journal of Geophysical Research*, *84*, 311–337.

Parkinson, C., D. Cavalieri, P. Gloersen, H. Zwally, and J. Comiso (1999), Arctic sea ice extents, areas, and trends, 1978-1996, *Journal of Geophysical Research*, *104*(C9), 20,837–20,856.

Polyakov, I., G. Alekseev, R. Bekryaev, U. Bhatt, R. Colony, M. Johnson, V. Karklin, D. Walsh, and A. Yulin (2003a), Long-term ice variability in Arctic marginal seas, *Journal of Climate*, *16*, 2078–2085.

Polyakov, I., R. Bekryaev, G. Alekseev, U. Bhatt, R. Colony, M. Johnson, A. Makshtas, and D. Walsh (2003b), Variability and trends of air temperature and pressure in the maritime Arctic, 1875-2000, *Journal of Climate*, *16*, 2067–2077.

Prather, M. (1996), Numerical advection by conservation of second-order moments, *Journal of Geophysical Research*, *91*, 6671–6681.

Prinsenberg, S., and J. Hamilton (2005), Monitering the volume, freshwater and heat fluxes passing through Lancaster Sound in the Canadian Arctic Archipelago, *Appl. Opt.*, *43*, 1–22.

Rigor, I., R. Colony, and S. Martin (2000), Variations in surface air temperature observations in the Arctic, 1979-97, *Journal of Climate*, *13*, 896–914.

Rigor, I., J. Wallace, and R. Colony (2002), Response of sea ice to the Arctic Oscillation, *Journal of Climate*, *15*, 2648–2663.

Rosati, A., and K. Miyakoda (1998), A general circulation model for upper ocean simulation, *Journal of Physical Oceanography*, *18*, 1601–1626.

Rothrock, D., and J. Zhang (2005), Arctic Ocean sea ice volume: what explains its recent depletion?, *Journal of Geophysical Research*, *110*, doi:10.1029/2004JC002282.

Rothrock, D., Y.Yu, and G. Maykut (1999), Thinning of the Arctic sea-ice cover, *Geophysical Research Letters*, *26*(23), 3469–3472.

Sadler, H. (1976), Water, heat and salt transports through Nares Strait, Ellesmere Island, *Fisheries Research Board of Canada*, *33*, 2286–2295.

Saenko, O. (2006), Influence of global warming on baroclinic rossby radius in the ocean: a model intercomparison, *Journal of Climate*, *19*, 1354–1360.

Saenko, O., G. Flato, and A. Weaver (2002), Improved representation of sea-ice processes in climate models, *Atmosphere-Ocean*, *40*(1), 21–43.

Samelson, R., T. Agnew, H. Melling, and A. Munchow (2006), Evidence for atmospheric control of sea-ice motion through Nares Strait, *Geophysical Research Letters*, *33*, doi:10.1029/2005GL025016.

Sanderson, T. (1988), *Ice Mechanics: Risks to Offshore Structures*, Graham and Trotman.

Serreze, M., and C. Hurst (2000), Representation of mean Arctic precipitation from NCEP-NCAR and ERA Re-analyses, *Journal of Climate*, *13*, 182–201.

Serreze, M., M. Clark, and D. Bromwich (2003), Monitoring precipitation over the Arctic terrestrial drainage system: data requirements, shortcomings, and applications of atmospheric reanalysis, *Journal of Hydrometeorology*, *4*(2), 387–407.

Serreze, M., et al. (2006), The large-scale freshwater cycle of the Arctic, *Journal of Geophysical Research*, *111*, doi:10.1029/2005JC003424.

Smith, S., R. Muench, and C. Pease (1990), Polynyas and leads: an overview of physical processes and environment, *Journal of Geophysical Research*, *95*(C6), 9461–9479.

Steele, M., R. Morley, and W. Ermold (2001), A global ocean hydrography with a high quality Arctic Ocean, *Journal of Climate*, *14*, 2079–2087.

Steiner, N., T. Sou, and G. Holloway (2003), Estimation of Arctic wind speeds and stresses with impacts on ocean-ice-snow modeling, *Journal of Marine Systems*, *39*, 129–151.

Stirling, I. (1981), Introduction: Polynyas in the Canadian Arctic, *Tech. rep.*, Occassional Paper Number 46, Canadian Wildlife Service, pp.7-19.

Stirling, I., and C. Parkinson (2006), Possible effects of climate warming of selected populations of polar bears (Ursus maritimus) in the Canadian Arctic, *Arctic*, *59*(3), 261–275.

Stone, R., D. Douglas, G. Belchansky, S. Drobot, and J. Harris (2005), Cause and effect of variations in western Arctic snow and sea ice cover, *Preprints, Eighth Conf. on Polar Meterology and Oceanography, San Diego, C.A., AMS, 8.3.*

Stroeve, J., M. Serreze, F. Fetterer, T. Arbetter, W. Meier, and J. Maslanik (2005), Tracking the Arctic's shrinking ice cover: another extreme September minimum in 2004, *Geophysical Research Letters*, *32*, doi:10.1029/2004GL021810.

Stroeve, J., M. Holland, W. Meier, T. Scambos, and M. Serreze (2007), Arctic sea ice decline: faster than forecast, *Geophysical Research Letters*, *34*, doi: 10.1029/200i7Gl029703.

Thompson, D., and J. Wallace (1998), The Arctic Oscillation signature in the wintertime geopotential height and temperature fields, *Geophysical Research Letters*, *25*, 1297–1300.

Thorndike, A., and R. Colony (1992), Sea ice motion in response to geostrophic winds, *Journal of Geophysical Research*, *87*(C8), 5845–5852.

Tivy, A., T. Sou, T. Carrieres, G. Flato, and G. Holloway (2004), Critical aspects of changes in sea ice cover on energy production, *Tech. rep.*, Canadian Ice Service, Ottawa.

Uppala, S., et al. (2005), The ERA-40 Re-analysis, *Quart. J. Roy. Meteor. Soc.*, *131*, 2961–3012.

Vinnikov, K., D. Cavalieri, and C. Parkinson (2006), A model assessment of satellite observed trends in polar sea ice extents, *Geophysical Research Letters*, *33*, doi: 10.1029/2005GL025282.

Wadhams, P., and N. Davis (2000), Future evidence of ice thinning in the Arctic Ocean, *Geophysical Research Letters*, *27*(24), 3973–3975.

Walsh, J., and M. Timlin (2003), Northern hemisphere sea ice simulations by global climate models, *Polar Research*, *22*(1), 75–82.

Walsh, J., W. Hibler, and B. Ross (1985), Numerical simulation of Northern Hemisphere sea ice variability, *Journal of Geophysical Research*, *90*(C3), 4847–4865.

Williams, C. (2004), The circulation and fluxes from the Arctic into the North Atlantic Ocean: 1979-2002 model results, Master's thesis, Naval Postgraduate School, Monterey, California.

Yao, T., and C. Tang (2003), The formation and maintenance of the North Water Polynya, *Atmosphere-Ocean*, *41*(3), 187–201.

Yu, Y., H. Stern, C. Fowler, and F. Fetterer (2006), Decline of Arctic landfast ice between 1976 and 2004, *Geophysical Research Letters*, submitted.

Zhang, X., and J. Walsh (2006), Toward a seasonally ice-covered Arctic Ocean: Scenarios from the IPCC AR4 model simulations, *Journal of Climate*, *19*, 1730–1747.

Appendix A

Description of the Arctic Ocean model

Output from an Arctic Ocean model is used to provide lateral forcing information for the CAA regional model's open boundary. The setup and forcing of the Arctic Ocean model is as similar to the CAA regional model as possible. The following describes the parts unique to the Arctic Ocean model.

The Arctic Ocean model (Fig. A.1) has a 0.5 ° horizontal grid, with 29 fixed ocean levels. It is run with slightly higher horizontal viscosity (4 x 10^4 m^2 s^{-1}). The tracer time-step is half a day (12 hours). The ice advection scheme is SOM (second-order moment) method after (*Prather* 1996). This SOM scheme was implemented into the *Hibler* (1979) ice model by *Merryfield and Holloway* (2003), and has minimal amount of numerical diffusion and dispersion.

The river runoff data for the Arctic Ocean is monthly climatology from *Becker* (1995) and *Munoz* (1995). River data for the Hudson Bay is from R-ARCTICNET (*Lammers et al.* 2001). Unlike the CAA model which is forced with daily wind-stress, the Arctic Ocean model is forced with monthly wind-stress and wind-speed derived as done in *Steiner et al.* (2003).

The open boundaries for the Arctic Ocean model exist at Bering Strait and the North Atlantic. Ice data is not supplied at the open boundaries. At the North Atlantic boundary, a free outflow condition exists so that outflowing ice is not modified. At the

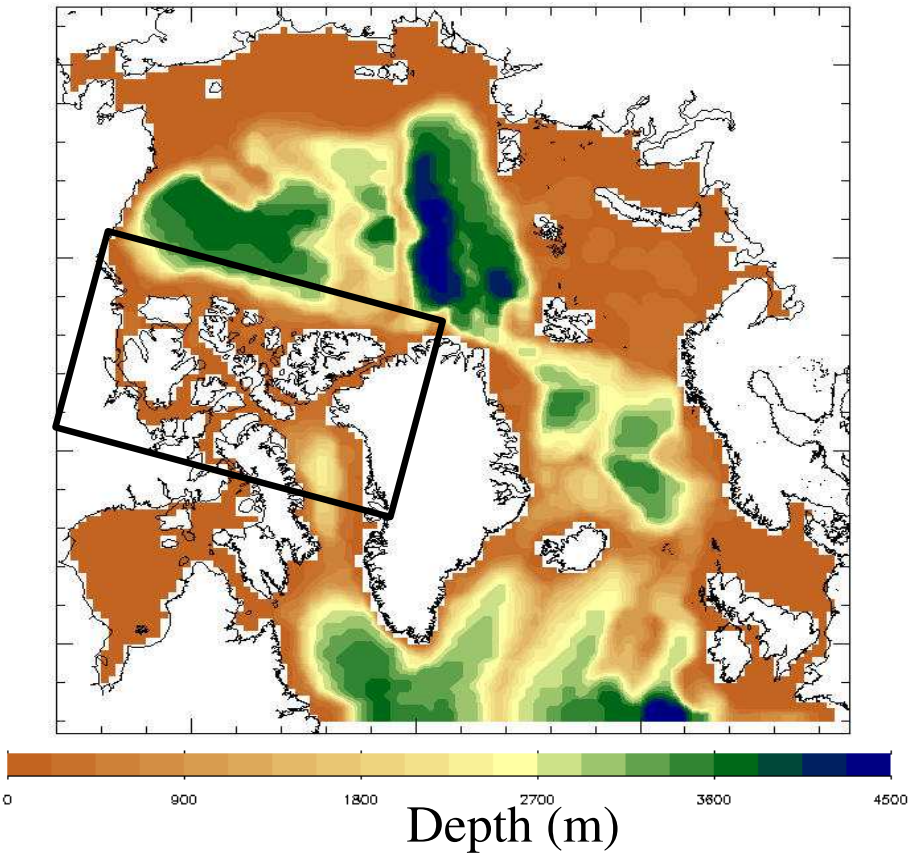

Figure A.1: Arctic Ocean bathymetry and domain with CAA model domain overplotted

Bering Strait boundary, ice grows quickly to enter the model domain. The ocean open boundary temperature and salinity data are taken from monthly climatological values from PHC (*Steele et al.* 2001), and are applied in the case of inflow. A free outflow condition exists for oceanic tracers. The net oceanic volume transport through the model is set to be 1.0 Sv, and represents the flow through Bering Strait. Annually averaged streamfunction and baroclinic velocities are taken from a global model, which determines if a boundary point is outflow or inflow. The global model is run on a 1.8° horizontal grid in the southern hemisphere, and the resolution increases in the northern hemisphere towards the North pole. The North pole is rotated to lie over northern Greenland.